UNIVERSIDAD DE CANTABRIA

ESCUELA DE DOCTORADO DE LA UNIVERSIDAD DE CANTABRIA

DOCTORADO EN INGENIERÍA DE COSTAS, HIDROBIOLOGÍA Y GESTIÓN DE SISTEMAS ACUÁTICOS (IH2O)

TESIS DOCTORAL

TRANSPORTE Y DISTRIBUCIÓN DE RESIDUOS PLÁSTICOS EN ESTUARIOS DEBIDO A LA ASIMETRÍA MAREAL

PhD THESIS

TRANSPORT AND FATE OF PLASTIC DEBRIS DUE TO TIDAL ASYMMETRY IN ESTUARIES

Presentada por: **PAULA NÚÑEZ PÉREZ**

Dirigida por: **Dr. Raúl Medina Santamaría**

Dra. Sonia Castanedo Bárcena

Santander, febrero de 2021

A mi familia

Por el mismo motivo del viaje, viajar.
Fabrizio De André

Agradecimientos

Esta Tesis doctoral es el resultado de la colaboración de numerosas personas y diversas instituciones que han contribuido en diferentes modos y formas a su consecución final.

En primer lugar, quisiera agradecer a mis directores Raúl y Sonia por compartir conmigo sus conocimientos e ideas y por guiarme a lo largo de este complejo recorrido que, a pesar de sus idas y venidas, finalmente ha conseguido llegar a buen término. Sin ellos, sin su dedicación y sin su motivación, no hubiese sido posible la realización de esta Tesis. Sonia, gracias por creer en mí a lo largo de todo este tiempo, por recibirme siempre con una sonrisa y por apoyarme, tanto profesional como personalmente, cada vez que lo he necesitado. ¡Gracias por estar siempre ahí! Raúl, gracias por el gran apoyo que he recibido y sentido siempre, especialmente, cuando más lo he necesitado.

Desde un punto de vista más formal, me gustaría expresar mi agradecimiento al IHCantabria, por la oportunidad que me ha ofrecido al permitirme desarrollar un trabajo de investigación de estas características, y al centro de investigación IST-MARETEC de Portugal, en especial a Ramiro Neves, por encontrar el modo y permitirme trabajar con ellos aun cuando las condiciones de colaboración no eran las más favorables.

También quisiera expresar mi más sincero agradecimiento a mis compañeros de IHCantabria que de un modo u otro han contribuido al resultado final de esta Tesis. Gracias a Inés por generarme las inquietudes que han desencadenado el tema sobre el que finalmente versa esta investigación.

Agradezco también a José Juanes, por su interés continuo y por crear las herramientas necesarias que han favorecido la finalización del presente trabajo. En especial, agradezco a todos los integrantes del grupo OCÉANO, tanto a los actuales como a todos aquellos que han ido pasando por el grupo y han dejado un pedacito de su sabiduría plasmada en este trabajo. Gracias por todos los consejos y por la ayuda prestados. He aprendido mucho trabajando con vosotros. Sois increíbles. Miri, nunca antes me había podido divertir tanto trabajando bajo presión. Tama... sobran las palabras, no cambies nunca.

Al margen de las contribuciones directas, quiero expresar mi agradecimiento a mis amigos y compañeros de fatigas. Mi mención especial es para Vero, gracias por todo tu apoyo y por estar siempre ahí, en definitiva, gracias por ser como eres. A Elba, una gran amiga y mejor persona, gracias por tu ayuda incondicional y por ser capaz de transformar en sencillo lo complicado. Quiero agradecer también a mis chicas griegas, Natalia, Bea y Gadea; a José y a Mireya por todos los buenos y para nada *sobrevalorados* momentos; a Marta, Alexia, Cassia, Alejandra, Julio, Paula G., Cavi, Carol y a ti, Camilo, gracias por todo, gracias por tanta ayuda desinteresada. También quisiera agradecer a todos aquellos, como Laurita, Elenita, Óscar, Edurne o Mae, que han ido pasando por mi vida y que han dejado una huella tan importante que ni siquiera la distancia puede borrar. Tampoco me puedo olvidar de Mar, Iñigo y mucho menos de Erica, una persona que me lleva soportando no poco tiempo y a la que considero una de mis amigas más queridas. Gracias a todos por estar ahí siempre pase lo que pase. Gracias a todos por tantos y tan buenos momentos que espero que continúen en la era *pospandemia*.

Por último, quiero dedicar mi agradecimiento más especial a toda mi familia por haberme acompañado muy de cerca en este complejo camino. A mi padre y a mi mejor amiga y mi alma gemela, mi madre, por estar siempre a mi lado y ser mi ejemplo de esfuerzo y dedicación. A mi abuela, a mi "hermano" y a mis tíos, por haberme apoyado siempre en cada aspecto de mi vida. A Elisa e Seba, "grazie a entrambi per essere così incredibilmente buoni con me", ad Ale, "il mio migliore amico, il mio compagno di viaggio, il

mio amore, grazie per esserci sempre... per rendermi felice" y también, como no podía ser de otra manera, a mi *cicciottina*, por su "incondicional apoyo" durante las jornadas de teletrabajo que han contribuido a la culminación de la presente Tesis.

Contents

List of Figures

List of Tables

Resumen

De acuerdo con la Normativa de Gestión Académica de los Estudios de Doctorado regulados por el Real Decreto 99/2011, a continuación, se presenta un resumen en español que sintetiza los materiales y métodos empleados en las investigaciones abordadas en esta Tesis, los principales resultados obtenidos, las conclusiones extraídas, así como las futuras líneas de investigación que derivan de los estudios realizados. Para una descripción más detallada, se remite al lector a los capítulos de la Tesis redactados inglés.

R1. Introducción

R1.1. Antecedentes y motivación

La basura marina constituye una de las principales amenazas actuales para el medio marino, ocasionando importantes daños a nivel ecológico, económico y social (UNEP, 2005). En la actualidad, la basura marina se ha convertido en un tema prioritario en las agendas ambientales internacionales, como la Directiva Marco sobre la Estrategia Marina de la UE (DMEM) (Galgani et al., 2013). Con relación a su composición, aproximadamente el 80 % de los residuos marinos están constituidos por plásticos (Barnes et al., 2009, Derraik, 2002). En 2010, entre 4.8 y 12.7 millones de toneladas de desechos plásticos se acumularon en los océanos y se estima un aumento de un orden de magnitud para 2025 (Jambeck et al., 2015). Respecto a su procedencia, en torno al 80 % de los residuos que llegan al medio marino proceden de fuentes terrestres, principalmente de los ríos (Galgani

et al., 2015, Rech et al., 2014). Una parte significativa de estos residuos alcanzará mar abierto y el resto quedará retenida en el interior de los estuarios, que frecuentemente actúan como trampas de residuos marinos (Acha et al., 2003). Asimismo, la marea y las olas pueden colaborar en la introducción de residuos desde fuentes marinas (Hinojosa & Thiel, 2009).

Los estuarios son zonas de mezcla entre agua dulce y agua salada, sometidos a la acción de multitud de dinámicas, principalmente, la marea, el caudal fluvial y el oleaje, lo que les confiere unas características muy particulares. Se trata de zonas de elevada productividad biológica que constituyen el hábitat de numerosas especies de flora y fauna. Innumerables especies de peces, crustáceos y moluscos dependen de las aguas estuarinas como lugares seguros para su supervivencia. Además, los estuarios sirven de refugio para una amplia variedad de aves acuáticas ya sean autóctonas o exóticas. También destaca la importancia socioeconómica de los estuarios para el desarrollo de distintas actividades locales tales como la pesca, el marisqueo, la pequeña industria o el turismo entre otras, sin olvidar las funciones de protección costera y de captura de carbono (Barbier et al., 2011). Por lo tanto, la acumulación de residuos plásticos representa una amenaza importante para los hábitats estuarinos y para los servicios ecosistémicos que éstos ofrecen (Mazarrasa et al., 2019).

En consecuencia, surge la necesidad de abordar el problema mediante la definición de estrategias de prevención y limpieza. Las *medidas de prevención* son aquellas orientadas a bloquear y reducir la entrada de residuos en el medio marino y requieren inversiones para, por ejemplo, la instalación de dispositivos de retención en los aliviaderos de aguas pluviales o en los desagües de las redes de saneamiento (Gallo et al., 2018). Los costes directos de las *estrategias de limpieza* son aquellos asociados a los procesos de recolección, transporte y gestión de los residuos (Hall, 2000, OSPAR, 2009). El estudio de *hotspots* (zonas de mayor acumulación o de mayor riesgo) de basuras marinas permite focalizar los esfuerzos de limpieza en las áreas prioritarias y reducir así los costes asociados. La disponibilidad de este tipo de información en la escala de estuario es limitada, dificultando a los gestores

la organización y la logística de estas actividades. Por lo tanto, investigar sobre la distribución de los residuos plásticos en los estuarios y fomentar el desarrollo de metodologías y herramientas de apoyo para los gestores son aspectos claves para afrontar el problema.

Diversos estudios han destacado la *asimetría mareal* como parámetro fundamental que define el transporte y distribución de sustancias en el interior de los estuarios dominados por la marea (p.ej., Aubrey & Speer, 1985, Dronkers, 1986, Friedrichs & Aubrey, 1988). Otras dinámicas que pueden adoptar papeles relevantes junto con la marea son: el *caudal fluvial*, los *gradientes de temperatura* y *salinidad*, el *viento* en el interior de los grandes estuarios o junto con el *oleaje* en las playas adyacentes exteriores. Además, en el proceso de transporte también intervienen las *propiedades intrínsecas de los residuos plásticos* y las *características físicas de cada estuario* (Browne et al., 2010, Carson et al., 2013, Zhang, 2017). Las propiedades de los residuos, fundamentalmente la densidad, aunque también el tamaño y la forma, definen su flotabilidad y, por lo tanto, influyen en su modo de transporte. Estudios, como el de Mazarrasa et al. (2019) o el de Zhang (2017), han encontrado que los plásticos con mayor presencia en el medio marino son el polietileno, el polipropileno y el poliestireno, es decir, son residuos flotantes. Por último, las características físicas de las áreas que configuran los estuarios se asocian con diferentes capacidades de retención de residuos (propiedad definida en la literatura a través el parámetro *beaching*) e influyen en la disposición final de los mismos. Estudios, como el efectuado por Mazarrasa et al. (2019), han detectado elevadas concentraciones de residuos en las zonas de marisma alta de los estuarios que se hacen especialmente significativas en las zonas vegetadas.

Se han mencionado numerosos factores que intervienen en los procesos de transporte y acumulación de residuos plásticos en estuarios. Esta tesis aborda el estudio de estos procesos en estuarios dominados por la marea desde una perspectiva hidrodinámica, enfocándose fundamentalmente en la marea astronómica y su asimetría. Además, favorece la toma de decisiones en la definición de estrategias de prevención y limpieza con el desarrollo de

una metodología general para identificar los *hotspots* de residuos plásticos en estuarios.

R1.2. Estado del conocimiento

Esta sección presenta una revisión del estado del conocimiento de los tres componentes principales de la tesis: la asimetría mareal, su potencial efecto en el transporte y distribución de sustancias en estuarios dominados por la marea y las técnicas actuales para evaluar el transporte y distribución de residuos plásticos en el medio marino en general y en los estuarios en particular.

Asimetría mareal

La asimetría mareal es la distorsión que presenta la onda de marea por la cual la fase de llenante es más corta que la fase de vaciante, o viceversa. Dado que el prisma de marea ha de ser el mismo, esta asimetría se traduce en una diferencia entre la intensidad de las corrientes en ambas fases. Si la llenante es más corta, mostrará velocidades más intensas que la vaciante, y viceversa. Esta asimetría en las velocidades puede inducir un transporte neto hacia el interior o hacia el exterior del estuario, de forma que el estuario muestre una tendencia a importar o a exportar sustancias (p.ej., residuos), respectivamente (Aubrey & Speer, 1985, Dronkers, 1986, Friedrichs & Aubrey, 1988, Speer & Aubrey, 1985, Zhang, 2017).

La asimetría de la marea surge tanto de la interacción de las componentes mareales principales como de los armónicos generados al propagarse por aguas someras, estuarios y bahías. En océanos abiertos, la principal causa de asimetría es la combinación de las componentes O1/K1/M2, seguida por P1/K1/S2, K1/K2 y, por último, por Q1/K1/N2 (Song et al., 2011). Cuando la marea se propaga por aguas someras, se ve sometida a una deformación debida a la fricción del fondo y al efecto de los contornos costeros generando lo que se conoce como sobremareas (o componentes superarmónicas) y mareas compuestas, respectivamente. Las sobremareas son componentes cuya

velocidad angular es un múltiplo exacto de las componentes astronómicas que las generan. Su origen se debe a la diferencia de celeridad que se produce por efecto de la fricción entre las situaciones de pleamar y bajamar. Las mareas compuestas son aquellas cuya velocidad angular es igual a la suma o diferencia de las velocidades de dos o más componentes astronómicas y son debidas a la interacción no lineal entre componentes debida a la presencia de la costa. De los estudios existentes se ha concluido que la principal causa de asimetría mareal en aguas someras es la generación de la sobremarea M4 y su superposición a la componente M2 (Aubrey & Speer, 1985, Speer & Aubrey, 1985). No obstante, existen muchas otras combinaciones que pueden producir asimetría en la marea. En el caso de mareas semidiurnas se incluye también el efecto de la sobremarea M6 (M2/M4/M6) (Blanton et al., 2002) y/o el de las mareas compuestas MS4 y 2MS6 (M2/S2/M4/MS4 y M2/S2/M6/2MS6) (Byun & Cho, 2006). En regímenes mareales diurnos, destaca la influencia de las componentes O1, K1 y M2 (Hoitink et al., 2003, Ranasinghe & Pattiaratchi, 2000).

Para caracterizar la asimetría mareal, tradicionalmente se han empleado dos parámetros: (1) el cociente entre las amplitudes de dos componentes mareales (p.ej., a_{M4}/a_{M2}) para cuantificar el grado de distorsión y (2) la diferencia entre fases (p.ej., $2\phi_{M2} - \phi_{M4}$) para determinar su orientación (p.ej., Aubrey & Friedrichs, 1988). Esta parametrización armónica permite describir la asimetría derivada principalmente de dos constituyentes. Otros estudios han utilizado funciones de densidad de probabilidad (PDF) de elevaciones de marea, pues las PDF retienen más información y, por lo tanto, son más adecuadas para caracterizar las distribuciones mareales a largo plazo (Castanedo et al., 2007, Woodworth et al., 2005). Siguiendo esta línea, Nidzieko (2010) recomendó el uso de un parámetro relacionado con la forma PDF, el coeficiente de asimetría (γ_1), y aplicó este coeficiente a la derivada temporal de elevación de la marea, es decir, a un parámetro representativo de las velocidades de ascenso y descenso de la marea y, en consecuencia, de las corrientes de llenante y vaciante, respectivamente, en los estuarios. En resumen, los métodos del estado del conocimiento para cuantificar la

asimetría pueden utilizar enfoques armónicos o estadísticos, ambos efectivos y con ventajas complementarias. Guo et al. (2019) encontraron que los métodos armónicos son más adecuados para estudiar áreas caracterizadas por regímenes diurnos y semidiurnos, mientras que la aplicación de métodos estadísticos es relevante en regímenes de mareas mixtas.

Efecto de la asimetría mareal en los procesos de transporte estuarinos

A lo largo de los últimos 20 años, se han publicado algunas investigaciones que sugieren que el estudio del transporte residuos plásticos en los estuarios puede asimilarse a un transporte de sedimentos y, por consiguiente, puede asociarse con la *asimetría mareal* (Ballent et al., 2012, Browne et al., 2010, Costa et al., 2011, Eerkes-Medrano et al., 2015, Galgani et al., 2000). La mayor parte de las teorías y estudios publicados hasta el momento relacionan la asimetría mareal que surge con la propagación de la marea a través de los estuarios, con el transporte de sedimentos y la tendencia morfológica de estos ambientes (Aubrey & Speer, 1985, Dronkers, 1986, Friedrichs & Aubrey, 1988, Speer & Aubrey, 1985). A continuación, se resaltan algunos de los aspectos clave extraídos de estos estudios:

- La onda de marea se deforma en su propagación por los estuarios debido a la fricción con los contornos y el fondo. Esta deformación se traduce en una diferencia en las duraciones de las fases de llenante y vaciante.
- Estas diferencia en las duraciones de las fases implica una diferencia entre las intensidades de las corrientes de llenante y vaciante y, por consiguiente, un transporte neto en la dirección de las corrientes más intensas. Este aspecto determina la tendencia a la importación o exportación de sedimentos del estuario.
- Los estuarios donde los bajos mareales ocupan un pequeño área o presentan una fricción elevada tienden a desarrollar asimetrías positivas (menor duración y corrientes más intensas para la fase de llenante)

y una tendencia a la importación de sedimentos. Por el contrario, si cuentan con extensas llanuras mareales y fricciones más débiles, surgen las asimetrías mareales negativas y una tendencia a la exportación sedimentaria.

De los estudios anteriores, se concluye que las amplitudes mareales, las fricciones con el fondo y las paredes laterales del estuario y las geometrías estuarinas son factores que condicionan las asimetrías mareales y la tendencia a acumular o exportar sustancias, como pueden ser los sedimentos o los residuos plásticos.

Hasta este punto, los estudios habían relacionado el origen de las asimetrías mareales con las interacciones no lineales en aguas someras; sin embargo, como ya se ha mencionado, Hoitink et al. (2003) y Song et al. (2011) demostraron que la asimetría mareal también surge en el océano abierto a causa de interacciones entre algunas de las principales componentes mareales. Esta asimetría mareal presente en las desembocaduras de los estuarios presenta una gran influencia en la deformación generada con la propagación y, en consecuencia, en el transporte de sedimentos (Moore et al., 2009, Nidzieko, 2010, Ranasinghe & Pattiaratchi, 2000). Por extensión, merece la pena investigar sobre el hecho de que un estuario presente una asimetría inicial en su desembocadura y su efecto en el transporte de plásticos.

Técnicas para evaluar el transporte y destino de residuos plásticos en ambientes marinos

Considerando que el 80 % de la basura marina está constituida por plásticos y que aquellos de mayor presencia en el medio marino son los elementos con densidades inferiores a las del agua de mar, las teorías más extendidas asumen partículas genéricas esféricas y flotantes para sus estudios (Zhang, 2017). Se distinguen tres categorías de estudios según su escala espacial de análisis: global, regional y local.

La mayor parte de los estudios existentes que evalúan el transporte y distribución de residuos marinos realizan análisis *globales* (Law et al., 2010,

Lebreton et al., 2012, Maximenko et al., 2012, Van Sebille et al., 2012) y *regionales* en áreas confinadas, como son los Mares del Asia Oriental (Isobe et al., 2009, Kako et al., 2014, 2011, Yoon et al., 2010), las aguas próximas a las islas hawaianas (Carson et al., 2013, Kubota, 1994) o el Mar Mediterráneo (Zambianchi et al., 2014, 2017). Sin embargo, en la escala de estuario son mucho más escasos (Browne et al., 2010, Klein et al., 2015, Mazarrasa et al., 2019, Yonkos et al., 2014).

En el estado del conocimiento se utilizan dos tipos de técnicas para evaluar la distribución de residuos marinos en estuarios: observaciones en campo y modelado numérico y ambas presentan limitaciones. El principal inconveniente de las *observaciones de campo* es la dependencia entre los resultados obtenidos, el método de muestreo seleccionado y las particularidades de la zona en el momento en el que se efectuó la campaña. Por ejemplo, si la campaña se realizó tras un evento de avenida fluvial o después una actuación de limpieza, los resultados aparecerán alterados y no serán representativos de las condiciones de la zona. Las principales desventajas de aplicar *modelado numérico* son la alta resolución espacial requerida para los estudios a escala estuarina, el gran número de dinámicas involucradas en los procesos (marea, caudal fluvial, viento, oleaje, temperatura y salinidad) (Zhang, 2017) y la disponibilidad de series temporales de las variables metoceánicas suficientemente largas para utilizar como forzamientos climáticos y como condiciones de contorno. Los resultados conseguidos con estos enfoques no son fácilmente generalizables, ni pueden obtenerse en un tiempo adecuado para servir de apoyo a los gestores en la planificación de actividades de limpieza o de mitigación.

Teniendo en cuenta que muchos estudios identifican los aportes de los ríos como las principales fuentes de basura marina no solo en las playas (Rech et al., 2014), sino también en los océanos (Claessens et al., 2011, Galgani et al., 2015, Klein et al., 2015), promover el desarrollo de métodos y herramientas efectivos para investigar la distribución de basura marina a escala estuarina es un paso necesario para abordar el problema en su origen.

Conclusiones

El estado actual de los conocimientos científico-técnicos sobre la distribución de residuos plásticos en estuarios evidencia, por un lado, la escasez de estudios existentes en estas escalas espaciales tan reducidas, así como las limitaciones que presentan las técnicas utilizadas para tal fin: las observaciones en campo y el modelado numérico. Estas limitaciones, que pueden resumirse en la dependencia entre los resultados obtenidos y el método de muestreo seleccionado y en los altos costes computacionales asociados al modelado numérico, dificultan la aplicabilidad de estos enfoques en cualquier estuario del mundo.

Además, se ha comprobado que los factores que condicionan el transporte y distribución de residuos plásticos en el medio marino, en general, y en los estuarios, en particular, son la hidrodinámica (destacando el papel de la marea astronómica en estuarios dominados por la marea), la capacidad de atrapamiento costera y las propias características de los residuos. Todos ellos son aspectos insuficientemente explorados en la actualidad en la escala de estuario que requieren análisis paralelos en profundidad.

Esta tesis pretende contribuir a la mejora del conocimiento desde la perspectiva hidrodinámica, en concreto la hidrodinámica debida a la marea astronómica y a su asimetría, ya que se trata de una de las dinámicas más relevantes que generalmente condiciona el transporte de sustancias en el interior de los estuarios dominados por la marea. En este sentido, numerosos estudios evalúan la deformación que experimenta una onda de marea al propagarse por los estuarios, su relación con el transporte de sedimentos y con la evolución morfológica de los mismos. Sin embargo, hasta ahora no se ha analizado en detalle la influencia directa que la asimetría originada en océanos abiertos tiene, como condición de contorno, en la posterior deformación generada en aguas someras, ni tampoco su efecto en la distribución de sustancias, en concreto de sustancias plásticas, en los estuarios.

En consonancia con todo lo anterior, esta tesis busca cubrir algunas de las lagunas detectadas en el estado del conocimiento de las técnicas utilizadas para identificar zonas de acumulación de residuos plásticos en la escala de estuario. En concreto, pretende: (1) ampliar el conocimiento actual sobre la asimetría mareal en océanos abiertos y su efecto como condición de contorno en la distribución de residuos plásticos en ambientes estuarinos y (2) aplicar este conocimiento en el desarrollo de una metodología, de aplicación general, que permita identificar las zonas más probables de acumulación de residuos plásticos en ambientes estuarinos, reduciendo las limitaciones de las técnicas actuales utilizadas para tal fin.

R1.3. Objetivos

El objetivo general de esta Tesis es investigar la relación entre la hidrodinámica estuarina, profundizando en las corrientes debidas a la marea astronómica y a su asimetría, y la distribución de residuos plásticos en estuarios dominados por la marea. Dicho objetivo se desglosa en los siguientes objetivos específicos:

1. Caracterización de la asimetría mareal a escala global para conocer su efecto como condición de contorno en los estuarios.

2. Estudio de la evolución espacial de la asimetría mareal al propagarse en estuarios de distinta geometría y su efecto en la acumulación de residuos plásticos.

3. Desarrollo de una metodología para evaluar la probabilidad de acumulación de residuos plásticos en estuarios.

Para dar respuesta a cada uno de los objetivos, se plantean una serie de análisis cuyo desarrollo se presenta en las secciones posteriores.

R2. Caracterización de la asimetría y periodicidad de la marea astronómica a escala global [I]

R2.1. Introducción

La asimetría y la periodicidad de la marea astronómica en océanos abiertos son dos parámetros de gran relevancia en el estudio de los procesos estuarinos. La asimetría mareal presente en las desembocaduras de los estuarios influye en el intercambio de flujos estuario-océano, en la propia propagación de la marea y, en consecuencia, en los procesos de transporte interno. La periodicidad de la marea depende de la interacción no lineal entre componentes mareales diurnas y semidiurnas y, por lo tanto, está relacionado con la asimetría mareal y con el trasporte de sustancias.

En este apartado de la Tesis, se caracteriza la asimetría y periodicidad de la marea astronómica en las áreas costeras del mundo, antes de su propagación por los estuarios. Para ello, se aplican métodos estadísticos, técnicas de clasificación y aproximaciones armónicas a la solución global de marea barotrópica TPXO9-atlas, la solución más completa y de mayor resolución espacial hasta el momento. El propósito es obtener una guía gráfica que pueda aplicarse para el estudio del transporte y acumulación de residuos plásticos en cualquier estuario del mundo.

R2.2. Material y métodos

Los pasos seguidos para caracterizar la marea astronómica a escala global atendiendo a su asimetría y periodicidad han sido los siguientes: (1) análisis estadístico de la marea astronómica, (2) aplicación de técnicas avanzadas de clasificación, (3) selección de los tipos estadísticamente representativos

[I] Los resultados de este apartado han sido publicados en: Núñez, P., Castanedo, S., & Medina, R. (2020). A Global Classification of Astronomical Tide Asymmetry and Periodicity Using Statistical and Cluster Analysis. *Journal of Geophysical Research: Oceans, 125*(8), e2020JC016143.

de marea astronómica en el mundo e (4) identificación de las principales componentes mareales que contribuyen a la asimetría en cada tipo de marea presente en el globo.

A partir de la versión más reciente de TPXO Global Tidal Solutions (TPXO9-atlas) (Egbert & Erofeeva, 2002) (`https://www.tpxo.net`), se ha parametrizado la marea astronómica atendiendo a las propiedades que la relacionan con el transporte de sustancias en los estuarios: asimetría y periodicidad.

TPXO9-atlas es la solución de marea barotrópica más completa (15 componentes mareales) y de mayor resolución espacial (1/30°) disponible hasta el momento que permite describir las condiciones de marea en las proximidades de las áreas costeras. Con relación a los parámetros descriptivos de la marea, se han utilizado las funciones de densidad de probabilidad (PDFs), definidas por los coeficientes de asimetría (γ_1) y curtosis (g_2), de la variable "derivada temporal del nivel de marea" ($d\eta/dt$). Además, se ha incluido el análisis del régimen mareal, TR (semidiurno, S; mixto con predominancia semidiurna, MS; mixto con predominancia diurna, MD y diurno, D) para considerar la influencia de la periodicidad mareal en el transporte estuarino de sustancias (Lesser, 2009).

Como la única dinámica analizada en este estudio es la marea astronómica antes de su propagación por los estuarios, sin considerar ningún otro fenómeno adicional, la variable $d\eta/dt$ puede asociarse a las corrientes mareales de llenante y vaciante en los estuarios dominados por la marea y, en consecuencia, al transporte de sustancias (Hoitink et al., 2003). A pesar de la disponibilidad de çorrientes de marea barotrópicas"del TPXO9-atlas, se selecciona $d\eta/dt$ como variable de análisis debido a sus posibilidades de validación, pues, mientras los datos del nivel del mar están disponibles en los mareógrafos, los registros de corrientes de marea son escasos.

El segundo paso de la metodología ha consistido en aplicar el algoritmo K-medias (Hastie et al., 2001) a los parámetros anteriores (γ_1-g_2-TR) para agrupar las diferentes mareas astronómicas del mundo en tipos estadísticamente representativos (en adelante, *ATtypes*). El algoritmo

K-medias utiliza un proceso iterativo para dividir el conjunto inicial de datos en un determinado número de subconjuntos. Cada subconjunto está representado por un centroide o prototipo y está constituido por los datos que mejor representan dicho prototipo. En cada iteración, K-medias desplaza el centroide hasta que la varianza total intragrupo es mínima. En este análisis, K-medias ha sido inicializado con el algoritmo de máxima disimilitud (Camus et al., 2011b).

Por último, se han identificado los principales componentes mareales que influyen en el carácter asimétrico de cada *ATtype* siguiendo la metodología propuesta por Song et al. (2011). Para ello, se han calculado las contribuciones (β_i) de las diferentes combinaciones (pares o tripletes) de componentes mareales que pueden influir en la asimetría de cada *ATtype*. Estas combinaciones son aquellas para las cuales se cumplen las siguientes relaciones de frecuencia: $2\omega_1 = \omega_2$, o $\omega_1 + \omega_2 = \omega_3$. Este último paso de la metodología aporta un valor añadido a la guía gráfica generada, permitiendo abordar futuros estudios de mareas, no solo desde un enfoque estadístico sino también a través de métodos armónicos.

Los resultados han sido validados con datos de 757 mareógrafos distribuidos por todo el mundo que han sido seleccionados del conjunto de datos GESLA-2 (Woodworth et al., 2017). La excelente concordancia obtenida en el 97 % de los nodos en los que se compararon las PDFs y en el 87 % de los nodos en los que se contrastaron los regímenes mareales demuestra la calidad de la información proporcionada por la clasificación global de mareas efectuada en esta Tesis.

R2.3. Resultados

La Figura 1a muestra los centroides (C_i) de la clasificación ordenados de mayor a menor γ_1. Cada C_i se define en términos de la forma de su PDF de $d\eta/dt$ (es decir, a través de los coeficientes γ_1 y g_2) y de su régimen mareal (S, MS, MD y D) y representa un tipo de marea concreto (*ATtype*). La Figura 1b muestra la distribución geográfica de los 25 *ATtypes* identificados.

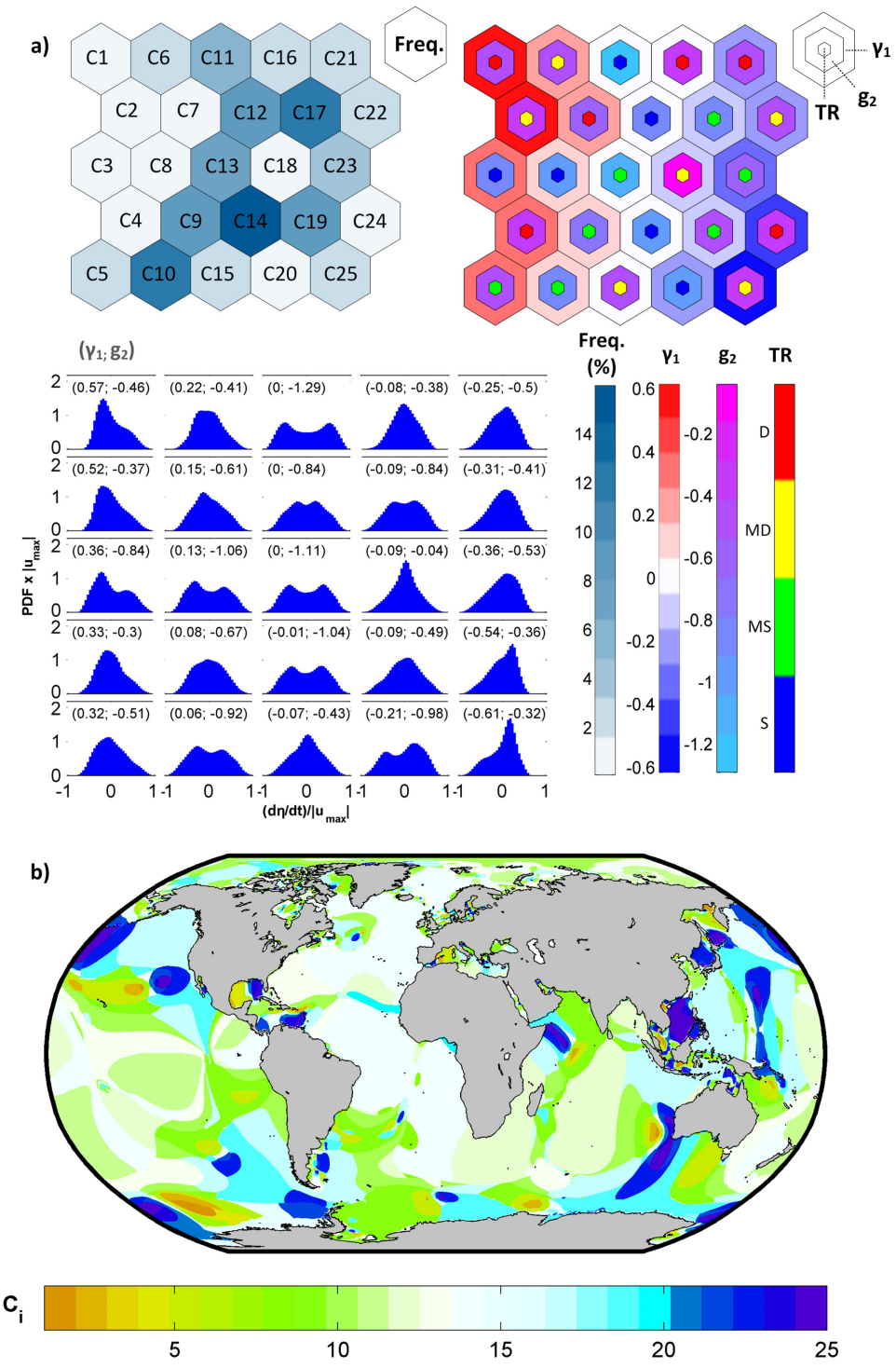

Figura 1: Tipos de marea astronómica resultantes de la clasificación (*ATtypes*): a) estadísticos de los centroides (C_i; $Freq$: frecuencia, γ_1: coeficiente de asimetría, g_2: curtosis, TR: régimen mareal, PDF: función de densidad de probabilidad) y b) distribución de C_i en el mundo.

Los resultados indican que las mareas simétricas ($|\gamma_1| < 0{,}1$; de C9 a C19) dominan el 85.3 % de la superficie oceánica del mundo, así como el 77.4 % de las áreas costeras y se corresponden principalmente con los regímenes mareales mixto semidiurno (MS) y semidiurno (S). Aproximadamente, el 60 % de las mareas simétricas presentes en los océanos cuentan con régimen MS y un 36 % con régimen S. Estos valores para las áreas costeras son 60 % y 30 %, respectivamente. Una parte significativa del Océano Atlántico, incluida la costa este de los EEUU, la costa occidental de España y grandes porcentajes de las costas brasileña y africana exhiben estos *ATtypes* (áreas representadas en colores claro en la Figura 1 b). Por el contrario, 14 *ATtypes* muestran un claro componente asimétrico ($|\gamma_1| > 0{,}1$), donde las mayores asimetrías ($|\gamma_1| > 0{,}5$) tienen lugar en los regímenes diurnos (D) y mixtos diurnos (MD) (C1, C2, C24 y C25).

Las asimetrías positivas (de C1 a C8) se encuentran en el 6.5 % de los océanos y constituyen el 11.3 % de las áreas costeras del mundo. La zona oeste del Golfo de México, el norte del Mar Caribe, la costa mediterránea francesa y parte de la española, así como la costa sur de Australia son buenos ejemplos de estos *ATtypes* (áreas representadas en colores cálidos en la Figura 1b). Los estuarios ubicados en estas áreas costeras muestran una predominancia de llenante en su desembocadura. Este es el caso del estuario del río Dee (Reino Unido), que muestra un predominio general de llenante, probablemente inducido por mareas oceánicas asimétricas positivas, que explica la acreción de gran escala a la que se ha visto sometido durante los últimos 2 siglos (Moore et al., 2009).

Las asimetrías negativas (de C20 a C25) cubren el 8.2 % de los océanos y el 11.3 % de las áreas costeras del mundo. El sur del Mar Caribe, la costa norte de Groenlandia, el Mar de China Meridional y la costa oeste de Australia son claros ejemplos de áreas con asimetrías mareales negativas. Los estuarios alojados en estas áreas exhiben una predominancia de vaciante en su zona más externa (áreas representadas en colores fríos en la Figura 1b). Algunos estuarios del mundo sometidos a este tipo de asimetrías son los estuarios del río Swan y Peel–Harvey (Australia Occidental) (Ranasinghe & Pattiaratchi,

2000), la bahía de Tomales y Elkhorn Slough (California, EEUU) (Nidzieko, 2010) y la laguna de Venecia (Italia) (Ferrarin et al., 2015, Finotello et al., 2019).

Figura 2 muestra los pares y tripletes de componentes mareales que contribuyen a la asimetría mareal, así como el valor de cada contribución (β_i), expresado como porcentaje, para cada *ATtype* (C_i). Las celdas de colores cálidos representan contribuciones con el mismo signo que la asimetría resultante, mientras que los colores fríos señalan contribuciones de signo opuesto. La suma de todas las contribuciones resulta en el γ_1 representativo.

Como muestra la figura, las mareas simétricas ($|\gamma_1| < 0{,}1$) cuentan con un mayor número de combinaciones de componentes mareales que contribuyen a la asimetría con un porcentaje similar, aunque con signo diferente, cancelándose entre sí y resultando en un γ_1 nulo. Por el contrario, las mareas con una clara componente asimétrica ($|\gamma_1| > 0{,}1$) presentan unas pocas contribuciones principales. En general, el triplete astronómico O1/K1/M2 domina los regímenes D, MD y MS, mientras que las combinaciones P1/K1/S2 y M2/M4 juegan un papel secundario o terciario en la asimetría. En el régimen S, la principal contribución proviene de M2/M4.

Entre el conjunto de combinaciones analizadas, se enmarca en gris el subconjunto de componentes mareales que mejor explica el par γ_1-g_2. De los análisis realizados puede concluirse que un número relativamente pequeño de componentes mareales es capaz de describir γ_1, sin embargo, es necesario un número mayor para caracterizar correctamente g_2. La Figura 2b muestra la buena concordancia entre la asimetría y el exceso de curtosis que resultan de la clasificación (γ_1-g_2) y los mismas estadísticos obtenidos de las componentes mareales más influyentes (γ_1'-g_2'), donde R^2 excede 0.9 en ambos casos.

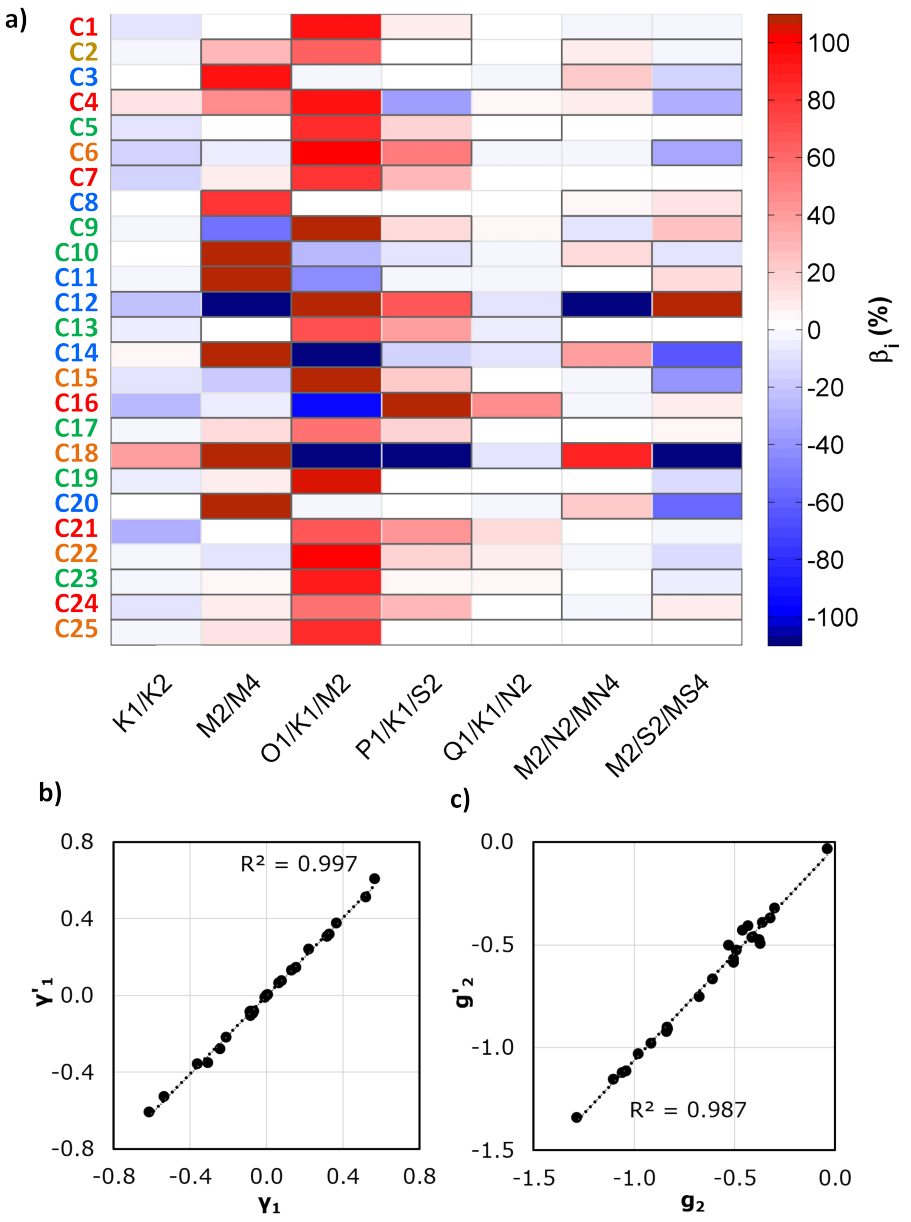

Figura 2: a) Contribuciones (β_i) al coeficiente de asimetría de los tipos representativos de marea astronómica (C_i) (las principales contribuciones que explican el par γ_1-g_2 aparecen remarcadas en gris); b) gráfico de dispersión de γ_1 (procedente de la clasificación)-γ_1' (resultante de las principales componentes mareales que explican la forma PDF) y c) gráfico de dispersión de g_2 (procedente de la clasificación)-g_2' (resultante de las principales componentes mareales que explican la forma PDF). Cada C_i en el *eje-y* se representa con un color asociado al régimen mareal: azul para S, verde para MS, amarillo para MD y rojo para D.

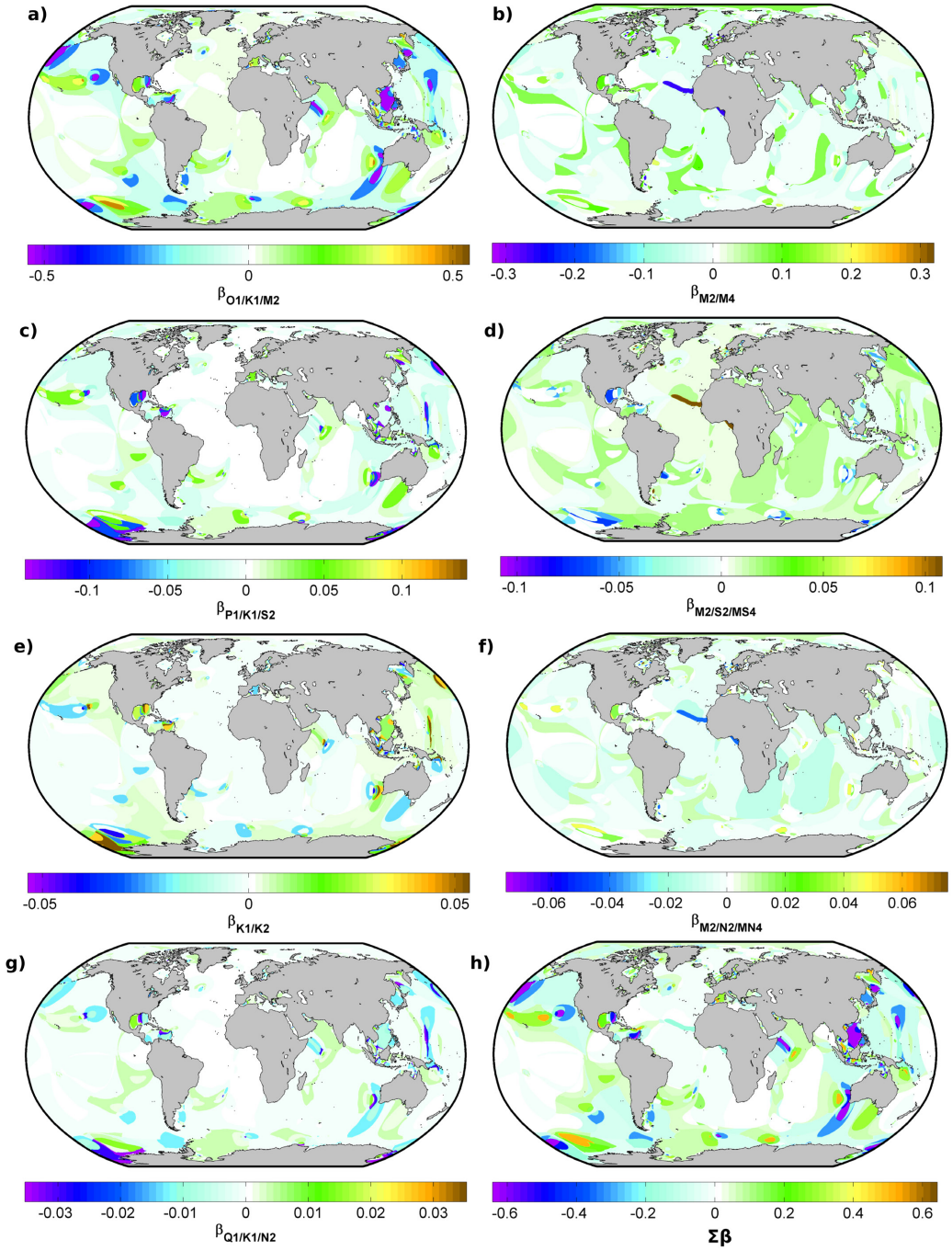

Figura 3: Distribución global de las contribuciones (β_i) responsables de la asimetría de los tipos de marea: a) O1/K1/M2, b) M2/M4, c) P1/K1/S2, d) M2/S2/MS4, e) K1/K2, f) M2/N2/MN4, h) Q1/K1/N2 y h) sumatorio de todas las contribuciones ($\sum \beta$). Nótense las diferencias en las escalas de colores.

Finalmente, la Figura 3 muestra las distribuciones globales de las contribuciones (β_i) de las componentes mareales responsables de la asimetría de cada uno de los *ATtypes* identificados. Se observa que las combinaciones O1/K1/M2 y M2/M4 contribuyen con las mayores intensidades. Las contribuciones de P1/K1/S2 y M2/S2/MS4 son entre 3 y 5 veces menos significativas y las contribuciones de K1/K2, M2/N2/MN4 y Q1/K1/N2 presentan un orden inferior de magnitud. Se estimó que las principales contribuciones de O1/K1/M2 y M2/M4 representan el 95 % y el 5 %, respectivamente, de las áreas oceánicas que muestran asimetrías. De hecho, los mapas de la Figura 3a ($\beta_{O1/K1/M2}$) y la Figura 3h ($\sum \beta$) son muy similares.

R2.4. Conclusiones

En esta investigación se ha clasificado la marea astronómica a escala global, aplicando el algoritmo K-medias a la solución TPXO9-atlas, cuya resolución espacial (1/30°) permite una adecuada caracterización de la marea astronómica en áreas costeras. De este modo, se han identificado veinticinco tipos representativos de la marea astronómica en el mundo. Además, se han identificado las principales componentes mareales que intervienen en la asimetría de cada tipo de marea. La clasificación ha sido validada con datos de 757 mareógrafos seleccionados estratégicamente para cubrir las áreas costeras del mundo. Los resultados mostraron que tanto los océanos como las áreas costeras del mundo están dominados por mareas simétricas (85.3 % y 77.4 %, respectivamente); las asimetrías negativas caracterizan el 8.2 % de los océanos y el 11.3 % de las áreas costeras y las asimetrías positivas cubren el 6.5 % de los océanos y el 11.3 % de las costas. En general, el triplete astronómico O1/K1/M2 controla las asimetrías mareales en los regímenes diurnos y mixtos, mientras que el par M2/M4 es la combinación que destaca en la mayoría de los regímenes semidiurnos.

La clasificación desarrollada representa un marco de referencia en cuanto a tipos de mareas astronómicas según su asimetría y periodicidad a escala mundial. Esta información puede servir como base para futuras investigaciones sobre el transporte de sustancias (por ejemplo, sedimentos,

nutrientes, residuos plásticos, derrames de petróleo y productos químicos) en los estuarios, ya que la asimetría impuesta en la desembocadura de un estuario puede influir en la mayoría de los procesos de transporte interno.

R3. Efecto de la asimetría de la marea oceánica y de la geometría estuarina en la acumualación de residuos plásticos en estuarios [II]

R3.1. Introducción

En esta sección se describe brevemente la relación existente entre la deformación que experimenta la onda de marea al propagarse por aguas someras, con la asimetría mareal inicial existente en las desembocaduras de los estuarios y las características morfológicas de estos ambientes. Además, se evalúa probabilísticamente el efecto de estas interacciones sobre la acumulación de residuos plásticos en el interior de estuarios dominados por la marea. Para lograr estos objetivos, se propone una serie de análisis basados en la aplicación de los módulos hidrodinámico y Lagrangiano del modelo numérico Delft3D a estuarios de diferente geometría. Los estuarios de estudio se definieron según los criterios de Speer & Aubrey (1985) y las condiciones de contorno de los modelos numéricos se construyeron a partir de la información de alta resolución (1/30°) proporcionada por la clasificación de la marea astronómica presentada en la sección anterior. El análisis probabilístico de los resultados numéricos permitió establecer algunas consideraciones generales sobre el papel de la asimetría de la marea oceánica y la morfología de los estuarios en las acumulaciones de residuos plásticos en el interior de los estuarios mareales.

[II] Los resultados de este apartado han sido enviados para su publicación a la revista *Estuarine, Coastal and Shelf Science*.

R3.2. Material y métodos

La metodología propuesta se basa en la aplicación de los módulos hidrodinámico (FLOW) y de transporte de partículas (PAR) del modelo numérico Delft3D (Hydraulics, 2018a,b, Roelvink & Van Banning, 1995) en estuarios de diferente geometría forzados con mareas asimétrica positiva, simétrica y asimétrica negativa. A continuación, se describen los estuarios de estudio, así como la configuración adoptada para los módulos FLOW y PAR.

Estuarios de estudio

Para la definición de los estuarios de estudio se han seguido los criterios de Speer & Aubrey (1985). Estos autores propusieron el estudio de estuarios poco profundos, bien mezclados y dominados por la marea, cuyas secciones transversales están constituidas por un canal principal de sección trapezoidal y, a partir de cierta elevación, aparecen los bajos mareales o marismas. En este estudio, se han definido cuatro casos particulares (EA, EB, EC y ED) con estas características, considerando cambios en la inclinación de las paredes laterales del canal, en la profundidad y en la anchura del mismo. La Figura 4 muestra las geometrías y dimensiones (longitud, L; anchura, b; profundidad, h; e inclinación de las paredes, N) de los estuarios de estudio. Todas las dimensiones pertenecen a los rangos evaluados por Speer & Aubrey (1985).

Módulo hidrodinámico

Dado que los estuarios de estudio son de escasa profundidad y están dominados por la marea, siendo ésta la única variable analizada, la aplicación de un modelo hidrodinámico bidimensional permite representar convenientemente las características del flujo. Las mallas numéricas para evaluar la hidrodinámica en los estuarios de estudio cuentan con 160000 elementos de cálculo y una resolución espacial media de 1 m, capaz de describir los procesos hidrodinámicos y de transporte de sustancias en estas escalas locales.

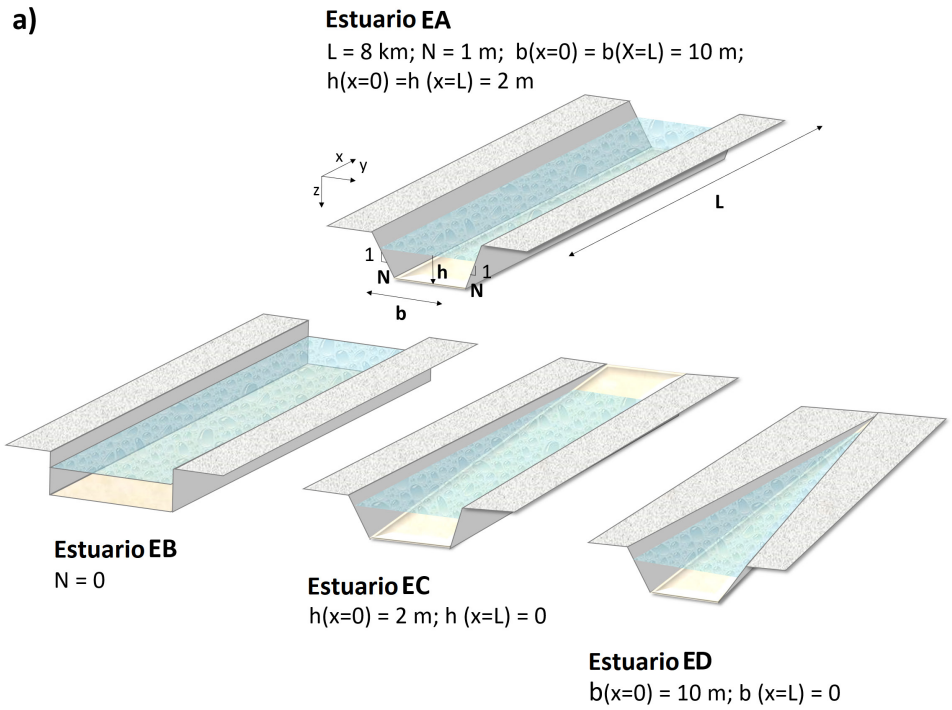

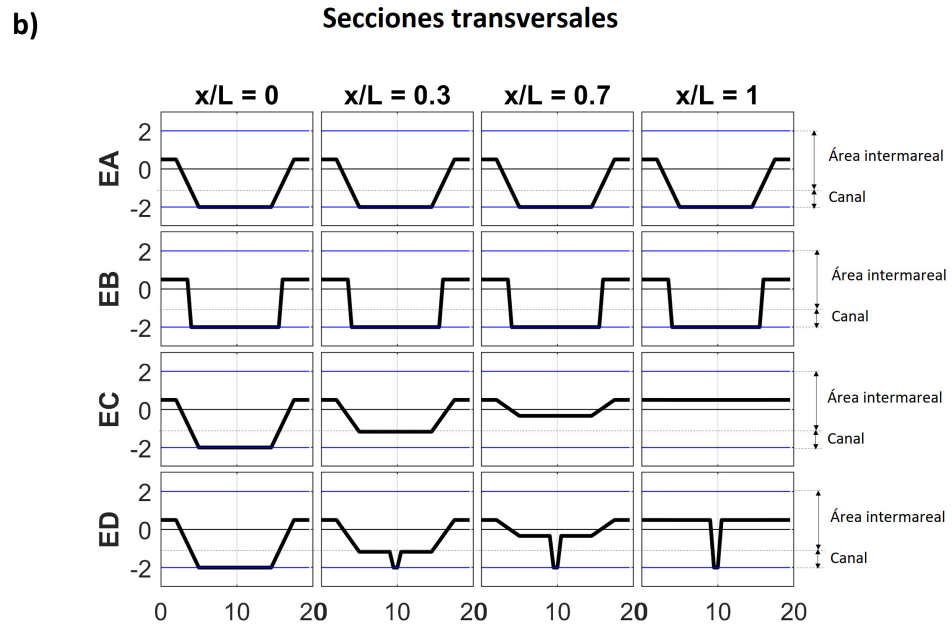

Figura 4: Geometría de los estuarios de estudio: a) esquemas con las dimensiones generales y b) detalle de diferentes secciones transversales (la desembocadura se ubica en $x/L = 0$ y el área más interna en $x/L = 1$).

Como período de análisis, se seleccionaron 15 días para contemplar el transporte residual originado durante un ciclo de mareas vivas-muertas.

Para definir las condiciones de contorno se utilizó la clasificación de la marea obtenida en el paso anterior. Teniendo en cuenta el objetivo perseguido, se seleccionaron los tres tipos de mareas más diferentes entre sí según su asimetría. En este caso se seleccionaron los tipos: $ATtype_1$ (γ_1=0.57; g_2=-0.46), $ATtype_{16}$ (γ_1=-0.08; g_2=-0.38) y $ATtype_{24}$ (γ_1=-0.54; g_2=-0.36). Además, se normalizaron las amplitudes máximas de las series temporales de marea, lo que permite analizar de forma exclusiva el efecto de la asimetría mareal y de la geometría estuarina, sin considerar la influencia que puede tener la existencia de diferentes rangos mareales máximos. Del mismo modo, en todos los casos se asume que los residuos llegan a los estuarios durante la bajamar de una carrera de marea de 1 m. Con esta hipótesis, se evita que los resultados de la distribución de residuos se vean influenciados por la llegada de residuos en diferentes fases mareales. Por lo tanto, las condiciones de contorno fueron las series temporales de marea astronómica de 15 días, con resolución temporal de 10 min, asociadas con los tipos de mareas mencionados ($ATtypes_i$, donde i = 1, 16 y 24).

Las condiciones iniciales de análisis para todos los casos evaluados se corresponden con el nivel que la marea astronómica adquiere 10 minutos después del nivel de bajamar, cuando el estuario comienza a inundarse.

El coeficiente de rugosidad (C) se ha definido variable con la profundidad de acuerdo con la rugosidad equivalente de Nikuradse (k_s). La viscosidad de remolino horizontal (ϵ) se ha definido variable con tamaño de celda en función de una constante de calibración (k). Teniendo en cuenta que tanto las geometrías como las dimensiones representativas de los estuarios de estudio pertenecen a los rangos evaluados por Speer & Aubrey (1985) y Bárcena et al. (2016), se ha fijado el valor de estos parámetros de forma consistente para todos los estuarios de estudio, adoptando un valor de 0.2 para k_s y 0.1 para k.

Aplicando el modelo con la configuración descrita, se obtuvieron las corrientes de llenante y vaciante asociadas a los tipos de marea astronómica

seleccionados (asimétrica positiva, simétrica y asimétrica negativa) y a los estuarios definidos para el estudio (EA, EB, EC y ED).

Módulo Lagrangiano

Las corrientes de llenante y vaciante de alta resolución obtenidas se utilizaron para alimentar al módulo Delft3D-PAR. Para simular el transporte de residuos plásticos incluyendo el efecto del atrapamiento costero, se seleccionó el modelo de hidrocarburos anulando los procesos de degradación (van Utenhove, 2019). Los únicos procesos considerados fueron el transporte advectivo debido a las corrientes mareales y el transporte difusivo. El coeficiente de difusión (D) se fijó en 1 m^2/s,adecuado para las áreas estuarinas (Abascal et al., 2012, 2017, Viikmäe et al., 2013).

Teniendo en cuenta que uno de los plásticos más comúnmente encontrados en el medio marino es el polipropileno (Mazarrasa et al., 2019, Zhang, 2017), este estudio representó residuos de polipropileno con partículas flotantes de 0.89 g/cm^3 de densidad. Se asumió que el origen de los desechos es marino y que éstos alcanzaban las desembocaduras de los estuarios durante la bajamar de una marea con un rango de 1 m para todos los escenarios evaluados. En cuanto al número de partículas, en la literatura existe una gran variabilidad en la selección del número óptimo en función de la extensión del área de estudio. Estudios, como Abascal et al. (2009a), Barker & Galt (2000), Díaz et al. (2008) o van Utenhove (2019), han demostrado que un orden de magnitud de miles de partículas puede ser suficiente para representar las en escalas espaciales regionales y locales. En este estudio, para asegurar la precisión y robustez de los análisis probabilísticos, se ha elegido un orden de magnitud 100 veces superior. Con respecto al paso de tiempo (Δt), se adoptaron 5 min para asegurar la estabilidad del modelo.

Como resultado de la aplicación del modelo de partículas con la configuración descrita, se obtuvieron las trayectorias asociadas a los cuatro estuarios de estudio forzados con los tres tipos de mareas.

Análisis probabilístico

El análisis probabilístico de las trayectorias de partículas obtenidas con Delft3D-PAR determinó los tramos más probables, definidos según su distancia a la desembocadura, para acumular residuos plásticos en el horizonte temporal seleccionado de 15 días. Para ello, el estuario se discretizó en veinte tramos de 400 m de longitud y, para cada tramo (j), se calculó la probabilidad media de presencia de partículas durante un ciclo de mareas vivas-muertas ($P_{mj} = n_j/N_T \times 100$), donde n_j es el número medio de partículas presentes en el tramo j durante un ciclo de mareas vivas-muertas y N_T es el número total de partículas evaluadas (100000).

R3.3. Resultados

Efectos de la asimetría mareal y la morfología estuarina en la propagación de la marea

La Figura 5 muestra la evolución de los coeficientes de asimetría (γ_1) y curtosis (g_2) de $d\eta/dt$ cuando se propagan las mareas asimétrica positiva, simétrica y asimétrica negativa por cada uno de los estuarios de estudio.

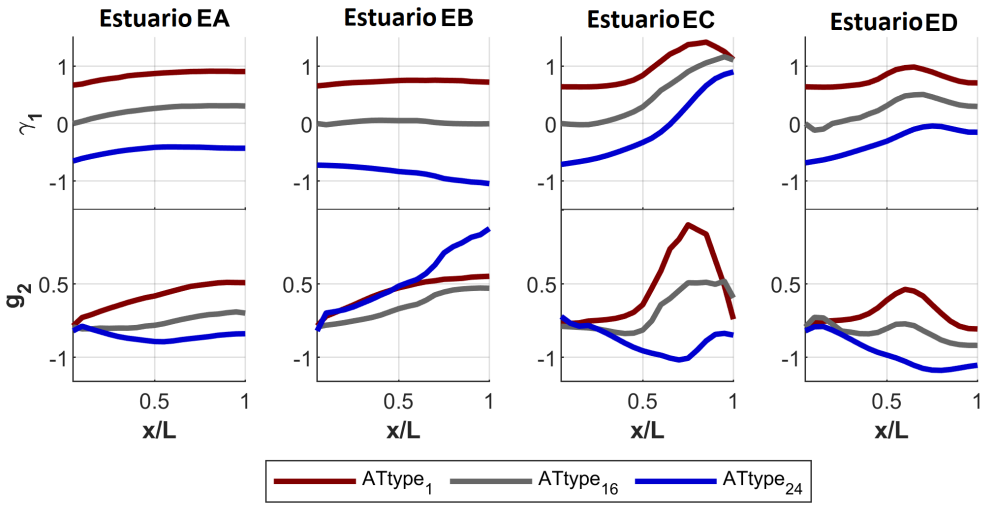

Figura 5: Coeficientes de asimetría (γ_1) y curtosis (g_2) para $ATtype_1$, $ATtype_{16}$ y $ATtype_{24}$ a lo largo de los estuarios EA, EB, EC y ED.

De la comparación de los resultados obtenidos en los estuarios EA y EB se deduce el efecto de la inclinación de las paredes laterales del canal en la propagación de la marea. Una mayor inclinación se traduce en una mayor fricción que se opone al flujo mareal. Esta oposición se hace más notable durante la bajamar que durante la pleamar y retrasa la salida de la marea, aumentando las asimetrías mareales positivas y reduciendo las negativas (aumento de γ_1) con la propagación. Sin embargo, el carácter asimétrico final de la marea, positivo o negativo, en las secciones más internas de los estuarios no queda determinado por este aspecto geométrico, sino por la naturaleza asimétrica inicial de la marea en sus desembocaduras. Con respecto a la curtosis, una mayor inclinación de las paredes laterales del canal se traduce en menores valores de g_2, lo que implica las mayores fricciones generan corrientes más intensas.

El efecto de la reducción de la profundidad sobre las mareas simétrica y asimétricas puede describirse a partir de las condiciones hidrodinámicas obtenidas para los estuarios EA y EC. La reducción de profundidad que caracteriza al estuario EC describe un doble comportamiento. Por un lado, en las zonas más exteriores donde la profundidad permite el pleno desarrollo de los rangos mareales, la reducción de la profundidad se traduce en un incremento de fricción que ralentiza la fase de vaciado de todas las mareas analizadas y conduce a una asimetría mareal positiva ($\gamma_1 > 0$) con independencia de la asimetría inicial en la bocana. Por otro lado, en las áreas interiores tienen lugar procesos de inundación-secado que favorecen el almacenamiento intermareal y establecen un límite en el crecimiento de la asimetría positiva. Asimismo, la evolución de la curtosis también se ve influenciada por la relación entre ambos aspectos (fricción con el fondo y almacenamiento intermareal). En la zona exterior, una mayor fricción con el fondo genera corrientes mareales más intensas (menores valores de g_2); mientras el almacenamiento de agua en las áreas más internas ralentiza las corrientes de inundación (crecimiento de g_2), reduciendo así el efecto de transporte inducido por el aumento positivo de la asimetría.

El efecto de la anchura de canal en la propagación de las mareas

asimétricas se explica contrastando los resultados obtenidos para los estuarios EA y ED. A diferencia del estuario EA, el estuario ED muestra una reducción lineal de la anchura de su canal hasta anularse en su parte más interna. El comportamiento de las mareas es similar en ambos estuarios hasta aproximadamente la mitad de sus longitudes. La inclinación a 45° de las paredes de sus respectivos canales frenan el vaciado de las mareas e inducen asimetrías positivas ($\gamma_1 > 0$). Sin embargo, comienzan a apreciarse diferencias de comportamiento en las mitades más internas de estos estuarios. Mientras que las asimetrías mareales se mantienen prácticamente constantes en la zona más interna del estuario EA, en el estuario ED se inducen asimetrías negativas ($\gamma_1 < 0$). Este hecho puede explicarse por dos motivos relacionados con la configuración física del estuario ED. Por un lado, el estrechamiento gradual de la sección reduce la inclinación de las paredes laterales del canal y, por consiguiente, el rozamiento. Por otro lado, el área de los bajos interiores aumenta en esta zona respecto a EA, favorece el almacenamiento del agua y contrarresta la deformación inducida por el canal. No obstante, como se observa en la figura, el valor de la asimetría en la zona interior de este estuario depende tanto del valor inicial de la asimetría como de la morfología estuarina. Con relación a g_2, los valores máximos alcanzados en el estuario ED para las tres mareas son siempre inferiores a los alcanzados en el estuario EA. Por lo tanto, se puede deducir que una reducción en la sección del canal provoca corrientes de marea más fuertes.

Un aspecto significativo para destacar de esta figura es que la tendencia a la dominancia de llenante o vaciante en las distintas partes de los estuarios EA, EB y ED dependen tanto de la geometría estuarina como de la asimetría impuesta en la bocana de los estuarios; sin embargo, la geometría juega el papel clave en el estuario EC. También destaca el papel regulador y corrector de la curtosis en el transporte inducido por la asimetría. Se observa que, a medida que una marea se vuelve más asimétrica (positiva o negativa) aumenta g_2 y, por lo tanto, disminuye la intensidad de las corrientes mareales, y viceversa.

Efectos de la asimetría mareal y la morfología de los estuarios en el destino de los residuos plásticos

La Figura 6 muestra, para cada estuario y para cada marea, la distribución de la probabilidad media de presencia de partículas durante un ciclo de mareas vivas-muertas (P_m). La Tabla 1 incluye la suma de estas probabilidades dentro de los estuarios del estudio.

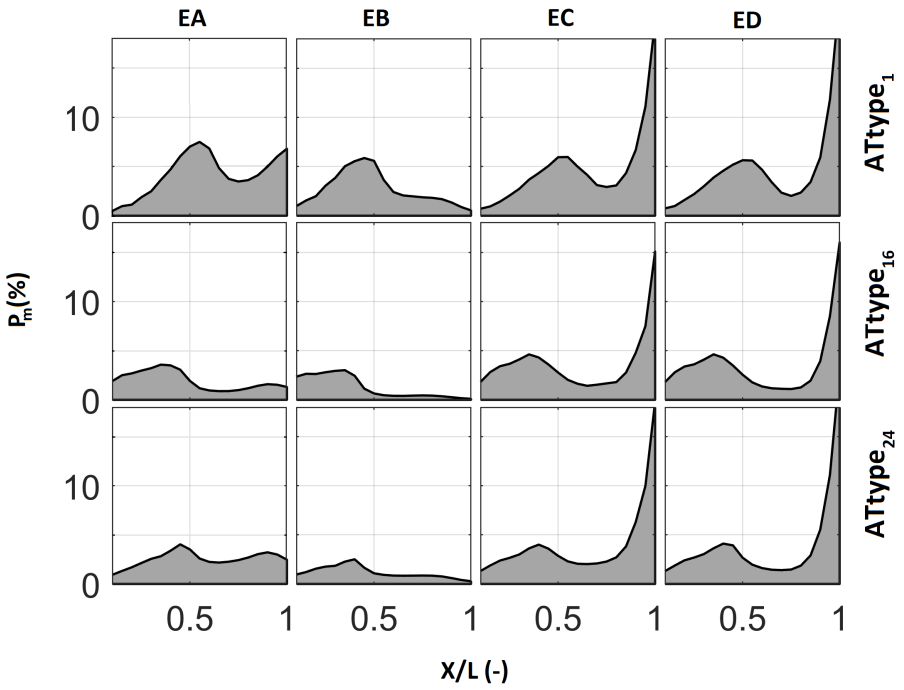

Figura 6: Probabilidad media de presencia de partículas P_m (%) en un ciclo de mareas vivas-muertas de $ATtype_1$, $ATtype_{16}$, $ATtype_{24}$ para los estuarios EA, EB, EC y ED.

	EA	EB	EC	ED
$ATtype_1$	81	52	93	92
$ATtype_{16}$	38	25	72	70
$ATtype_{24}$	49	23	78	78

Tabla 1: $\sum P_m(\%)$ dentro de los estuarios EA, EB, EC y ED para $ATtype_1$, $ATtype_{16}$ y $ATtype_{24}$.

Los resultados indican que la capacidad de importar residuos plásticos de los estuarios con geometría tipo canal, como el estuario EA, está significativamente condicionada por la asimetría mareal. Con la propagación de mareas asimétricas positivas, el estuario EA muestra una clara tendencia a la importación de flotantes ($\sum P_m^{ATtype_1} = 81\,\%$) y revela una mayor probabilidad de acumulaciones en las proximidades de los tramos medio y final del estuario ($P_m^{ATtype_1}$ en x/L próximo a 0.5 y 1 adquiere valores cercanos al 8 %). Esta distribución de probabilidades es equivalente para las mareas simétrica y asimétrica negativa, solo que en estos casos, los picos aparecen en posiciones ligeramente adelantadas y su magnitud se reduce significativamente ($P_m^{ATtype_{16}}$ y $P_m^{ATtype_{24}} < 4\,\%$ en los picos). En ambos casos, la capacidad de importación de residuos plásticos se reduce en aproximadamente un 38 % ($\sum P_m^{ATtype_{16}}$) y un 49 % ($\sum P_m^{ATtype_{24}}$), respectivamente.

Al igual que en el estuario EA, la acumulación de residuos plásticos dentro del estuario EB está fuertemente condicionada por la asimetría de la marea oceánica. Sin embargo, el estuario EB presenta una menor capacidad para importar residuos plásticos debido a las corrientes de llenante/vaciante. La probabilidad media de importación no supera el 52 % para la marea asimétrica positiva ($ATtype_1$), el 25 % para la marea simétrica ($ATtype_{16}$) y el 23 % para mareas asimétricas negativas ($ATtype_{24}$). Las distribuciones de P_m en la dirección longitudinal de estuario muestran patrones comunes que difieren en magnitud según el tipo de marea propagado. Así, se observa una tendencia acumulativa creciente entre la desembocadura y el tramo medio del estuario para todos los tipos de mareas analizados y, desde esta zona, se produce una reducción significativa en el valor de P_m.

Las geometrías EA y EB representan canales idealizados donde, como se deduce de los resultados, las probabilidades de acumulación dependen tanto de la asimetría de marea inicial presente en las desembocaduras como del rozamiento con los límites laterales de los canales.

Las geometrías de los estuarios EC y ED describen estuarios con configuraciones morfológicas más extendidas. Los resultados de las

acumulaciones muestran probabilidades de acumulación de residuos plásticos muy similares entre sí y demuestran que, con independencia de la asimetría que presenta la marea en la desembocadura, estas tipologías de estuarios sometidas a la acción de la marea actúan frecuentemente como trampas de residuos plásticos. Así, tanto el estuario EC como el ED, cuentan con una probabilidad media de acumular residuos superior al 90 % para la marea asimétrica positiva $ATtype_1$, en torno al 70 % para la marea simétrica $ATtype_{16}$ y cerca del 80 % para la marea asimétrica negativa $ATtype_{24}$. La distribución de P_m en estos estuarios presenta un pico relativo del 5 % en torno a la mitad de la longitud del estuario y un pico absoluto del 20 % en su parte final.

R3.4. Conclusiones

Esta investigación estudia el efecto de las asimetrías mareales oceánicas y de la morfología de los estuarios sobre la propagación de la marea y el destino de los residuos plásticos procedentes del océano en el interior de los estuarios dominados por la marea.

Se realizaron experimentos numéricos aplicando los módulos hidrodinámico y Lagrangiano del modelo numérico Delft3D a cuatro estuarios de estudio, definidos con diferentes secciones transversales y extensiones de bajos mareales. Como condiciones de contorno se utilizaron tres tipos de marea de diferente asimetría. Los parámetros de análisis describen, por un lado, la naturaleza de las mareas (los coeficientes de asimetría, que representa la diferencia entre la intensidad de las corrientes mareales de llenante y vaciante, y curtosis, referido a la frecuencia de las corrientes mareales más intensas, de la derivada temporal del nivel de marea) y, por otro, las morfología de los estuarios (inclinación de las paredes laterales, profundidad y anchura del canal principal). Los resultados confirman los resultados encontrados en estudios previos sobre la evolución de las mareas simétricas y proporcionan algunas conclusiones nuevas sobre la evolución de las mareas asimétricas, así como los efectos de ambas en las acumulaciones de residuos plásticos.

Los tipos simétricos de mareas evolucionan a asimétricos positivos con la propagación de las mareas a medida que aumenta la fricción con las paredes laterales y el lecho del canal. Por el contrario, la asimetría mareal puede experimentar una tendencia negativa si las fricciones son débiles o si las llanuras mareales cuentan con la extensión suficiente para contrarrestar el efecto del canal. Las mareas simétricas explican el comportamiento de los estuarios ubicados en el 77.4 % de las zonas costeras del mundo; sin embargo, en el 22.6 % restante, las mareas muestran asimetrías positivas o negativas. Al igual que ocurre con las mareas simétricas, las tendencias evolutivas de las mareas asimétricas están moduladas por la geometría del estuario y siguen el mismo patrón; sin embargo, el valor adoptado por la asimetría mareal dentro de los estuarios también está condicionado por su valor externo.

Del análisis de propagaciones de mareas asimétricas, se concluye que la asimetría inicial presente en las desembocaduras condiciona fuertemente la dominancia de llenante o vaciante y, por consiguiente, el grado de importación de residuos plásticos oceánicos en áreas estuarinas donde el canal principal presenta poca oposición al flujo y favorece la circulación mareal. En este tipo de geometrías, las mareas asimétrico-positivas muestran una capacidad de importación un 50 % superior a las de las mareas simétricas y asimétrico-negativas. Por el contrario, si hay una clara oposición al flujo o un área de almacenamiento intermareal importante, el papel relevante en la definición de la dominancia de llenante o vaciante lo juega la geometría del estuario, aunque también hay pequeñas influencias de la asimetría de las mareas externas. Así, las probabilidades de acumulación de residuos plásticos se sitúan en torno al 90 % para las mareas asimétrico-positivas y oscilan entre el 70-80 % para las mareas simétricas o asimétrico-negativas.

Sin embargo, la importación y distribución de residuos plásticos dentro de los estuarios no queda exclusivamente determinada por el valor positivo o negativo de la asimetría, sino también por el de la curtosis. Un aspecto relevante y novedoso que se deriva de este estudio es el papel regulador de la curtosis, que corrige la tendencia inducida por la asimetría en el destino de los plásticos dentro de los estuarios mareales. El valor de la curtosis aumenta

con el carácter asimétrico de la marea. Esto significa que las corrientes de llenante/vaciante van perdiendo intensidad para las mareas asimétricas positivas/negativas. En consecuencia, la capacidad de la marea astronómica para transportar, hacia el interior o hacia el exterior del estuario, residuos plásticos se puede describir de forma completa a través del conjunto de los coeficientes de asimetría y curtosis de la derivada temporal del nivel de marea.

R4. Metodología para evaluar la probabilidad de acumulación de residuos plásticos en estuarios [III]

R4.1. Introducción

Llegados a este punto en el desarrollo de la Tesis, cabe recordar que hasta el momento se ha caracterizado la asimetría mareal en la desembocadura de los estuarios de todo el mundo y se ha analizado su efecto sobre el transporte de residuos plásticos en las áreas interiores de estos ambientes. Sin embargo, como se ha indicado en el apartado de "Introducción", la marea astronómica no es la única dinámica involucrada en estos procesos, sino que también son relevantes los gradientes de temperatura y salinidad, las descargas fluviales, el viento o el oleaje. Además, destaca el papel relevante de la costa, con su capacidad de captura de los residuos (*beaching*) y las propiedades fisicoquímicas intrínsecas de los residuos plásticos que afectan a su flotabilidad, fundamentalmente, su densidad específica, tamaño y forma.

En este apartado se resumen los principales aspectos relacionados con el desarrollo de una metodología general, basada en modelado numérico y análisis estadístico, para identificar con unos recursos mínimos las principales áreas de acumulación (*hotspots*) de residuos plásticos en estuarios y, para cada

[III] Los resultados de este apartado han sido publicados en: Núñez, P., García, A., Mazarrasa, I., Juanes, J. A., Abascal, A. J., Méndez, F., Castanedo, S. & Medina, R. (2019). A methodology to assess the probability of marine litter accumulation in estuaries. *Marine Pollution Bulletin, 144*, 309-324.

una de estas áreas, el principal foco contaminante. Estos resultados reflejan información valiosa que, por un lado, faclilitaría la gestión y optimización de las actividades limpieza en estuarios, bahías y playas y, por otro, favorecería la definición de estrategias de mitigación. Así, por ejemplo, si en un estuario hay una o varias áreas significativamente afectadas por los residuos y se conoce(n) la(s) principal(es) fuente(s) contaminante(s), es posible plantear la instalación de filtros u otros dispositivos de retención en las propias fuentes para impedir o, en su defecto, reducir la entrada de residuos al medio.

R4.2. Marco metodológico

La metodología se basa en la aplicación combinada de técnicas estadísticas y modelado numérico para evaluar probabilísticamente la distribución de residuos plásticos dentro de estuarios y bahías. La Figura 7 presenta un esquema de la metodología propuesta que se estructura en los siguientes pasos: a) identificación de escenarios metoceánicos estadísticamente representativos; b) *downscaling* dinámico para obtener las dinámicas de alta resolución; c) modelado de potenciales trayectorias de residuos plásticos y d) análisis probabilístico de acumulación de residuos plásticos.

Como se muestra en el esquema de la Figura 7, el primer paso de la metodología es la identificación de los escenarios metoceánicos estadísticamente representativos del área de estudio. Para completar este paso, es necesario identificar las dinámicas dominantes (marea, caudal fluvial, oleaje, viento, temperatura y salinidad) y recopilar series temporales de dichas dinámicas suficientemente largas (años) para llevar a cabo análisis estadísticos. Estos datos pueden obtenerse de observaciones o simulaciones numéricas (reanálisis).

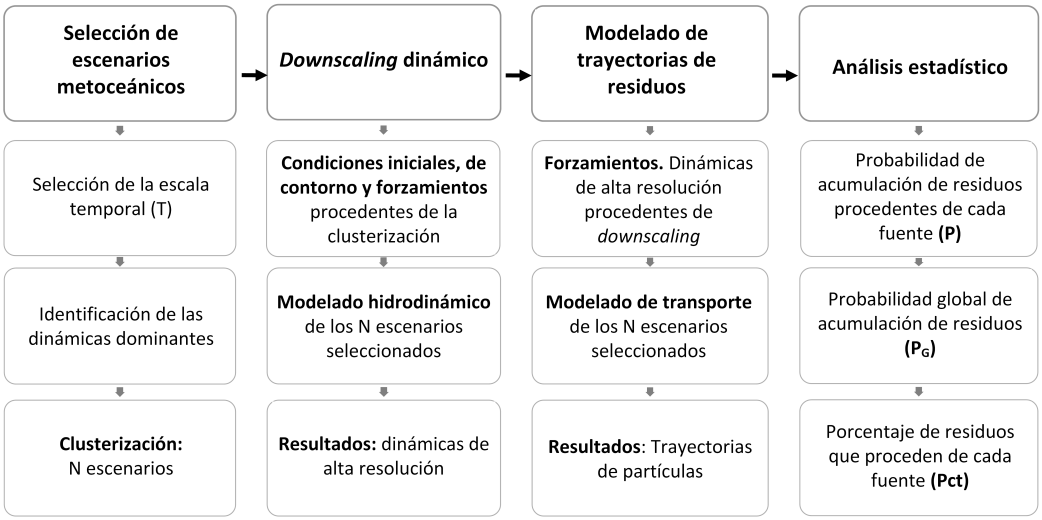

Figura 7: Metodología para identificar la acumulación de residuos plásticos en la escala de estuario.

Uno de los puntos clave de la metodología es la selección del horizonte temporal (T) más adecuado para realizar los análisis. Un valor adecuado de T es aquel que permite la consecución de la distribución de residuos plásticos más estable. En la escala de estuario, esta distribución se logra cuando una parte importante de los residuos alcanza las zonas costeras, donde pueden quedar retenidos durante años o incluso décadas (p.ej., Lebreton et al., 2012), o cuando los residuos plásticos llegan al océano abierto para ser transportados a las áreas de convergencia globales (Barnes et al., 2009, Cózar et al., 2014, Law et al., 2010). Para la selección de T, deben considerarse las escalas temporales hidrodinámicas, ya que las corrientes son determinantes en el transporte de cualquier sustancia (Hoitink et al., 2003) y, por lo tanto, en el tiempo que tardan los residuos plásticos en llegar a la costa o perderse en el océano. Sin embargo, la velocidad de la corriente no es la única variable involucrada. La distancia recorrida por los residuos plásticos desde su fuente y la capacidad de la costa para retenerlos también son aspectos de relevante consideración. Por ejemplo, en estuarios pequeños y lineales, es previsible que los residuos plásticos alcancen las áreas costeras más rápidamente que en las grandes bahías. Si además estos estuarios presentan una elevada densidad de vegetación, es probable que los residuos permanezcan retenidos

durante largos periodos de tiempo en sus áreas costeras. En consecuencia, las variables que influyen en la selección de T son tanto las escalas de tiempo hidrodinámicas, como aquellas variables relacionadas con la configuración física del estuario estudio, tales como la anchura, largura, sinuosidad costera, tipología sedimentológica y presencia/ausencia de vegetación (Zhang, 2017).

A partir de la información recopilada sobre las variables oceánicas y para la escala de tiempo T elegida, se seleccionan N escenarios con probabilidad de ocurrencia P_i, donde $i = 1, 2 \ldots N$, aplicando técnicas de clusterización (o agrupamiento). Una vez identificados los escenarios metoceánicos, se definen los forzamientos atmosféricos y las condiciones iniciales y de contorno del modelo numérico hidrodinámico. A continuación, se evalúa numéricamente cada escenario y se obtienen las condiciones hidrodinámicas de alta resolución con las que alimentar al modelo de transporte. La aplicación del modelo de transporte genera, para cada escenario, una base de datos de potenciales trayectorias de residuos plásticos procedentes de un conjunto de fuentes de residuos (*litter sources*, LS) previamente identificadas. El último paso consiste en analizar estadísticamente la base de datos de trayectorias generada para obtener diferentes tipos de resultados.

Considerando la probabilidad de ocurrencia de cada escenario metoceánico ($P[C, AT]$) e identificando presencias/ausencias de partículas en diferentes ubicaciones del área de estudio ($PA[0, 1]$), se obtiene un mapa de probabilidad de residuos plásticos por cada LS (P). Estos resultados permitirán a los responsables políticos y a los gestores elegir las áreas prioritarias de actuación si se conoce la fuente de un importante aporte de residuos en un momento dado. Considerando P y la probabilidad de cada fuente de generar residuos plásticos (P_{LS}), se calcula un mapa de probabilidad global (P_G) de distribución de residuos. Estos resultados serán de utilidad para definir medidas de limpieza generales en el estuario, cuando los residuos proceden de los aportes habituales y no hay ninguna fuente concreta conocida. Los mapas de los porcentajes de residuos plásticos (Pct) que llegan de cada fuente a cada ubicación del estuario de estudio pueden ayudar en la toma de decisiones para tratar de resolver el problema en el

origen. Esta información puede resultar de especial interés para implementar medidas de protección en áreas de interés turístico, que sirvan de refugio para las aves o que constituyan el hábitat de especies amenazadas.

La definición de un plan de limpieza para un período de tiempo específico, por ejemplo, antes de un evento deportivo o de un período vacacional, también puede resultar un aspecto interesante. Además de los valores medios anuales de los resultados mencionados anteriormente, una de las principales ventajas de estas técnicas es que permiten dar respuestas sobre la acumulación de residuos plásticos en diferentes intervalos de tiempo con un mínimo esfuerzo computacional. La metodología propuesta permite analizar periodos concretos con solo calcular la probabilidad de ocurrencia de cada escenario de transporte en el período requerido, por ejemplo, mensual, estacional o, incluso, para un mes o estación de un año concreto.

Para ilustrar el funcionamiento de la metodología propuesta, se ha descrito su aplicación en un estuario real. La Bahía de Santoña, un estuario localizado en la costa norte de España (véase la Figura 8) dominado por la marea, se ha seleccionado como estuario de estudio. El criterio de selección utilizado prioriza la posibilidad de recopilar datos de campo con fines de validación.

R4.3. Área de estudio

La Bahía de Santoña se localiza en la costa norte de España (Figura 8). Su configuración es compleja, distinguiéndose las rías de Boó, Argoños, Escalante, Rada, Limpias y Treto. Su longitud máxima es de unos 13,3 km y cuenta con una orientación N-S, desde la bocana del estuario hasta la desembocadura del río Asón (punto Q en la Figura 8). La Bahía de Santoña cuenta con extensas llanuras intermareales (aproximadamente el 65 % de su área total) ubicadas en su área occidental y dos playas adyacentes: Regatón (dentro del estuario) y Laredo (en la zona exterior). La profundidad media oscila entre 0,5 m y 4 m en las llanuras intermareales y en el canal principal, respectivamente, y alcanza los 13 m cerca de la desembocadura.

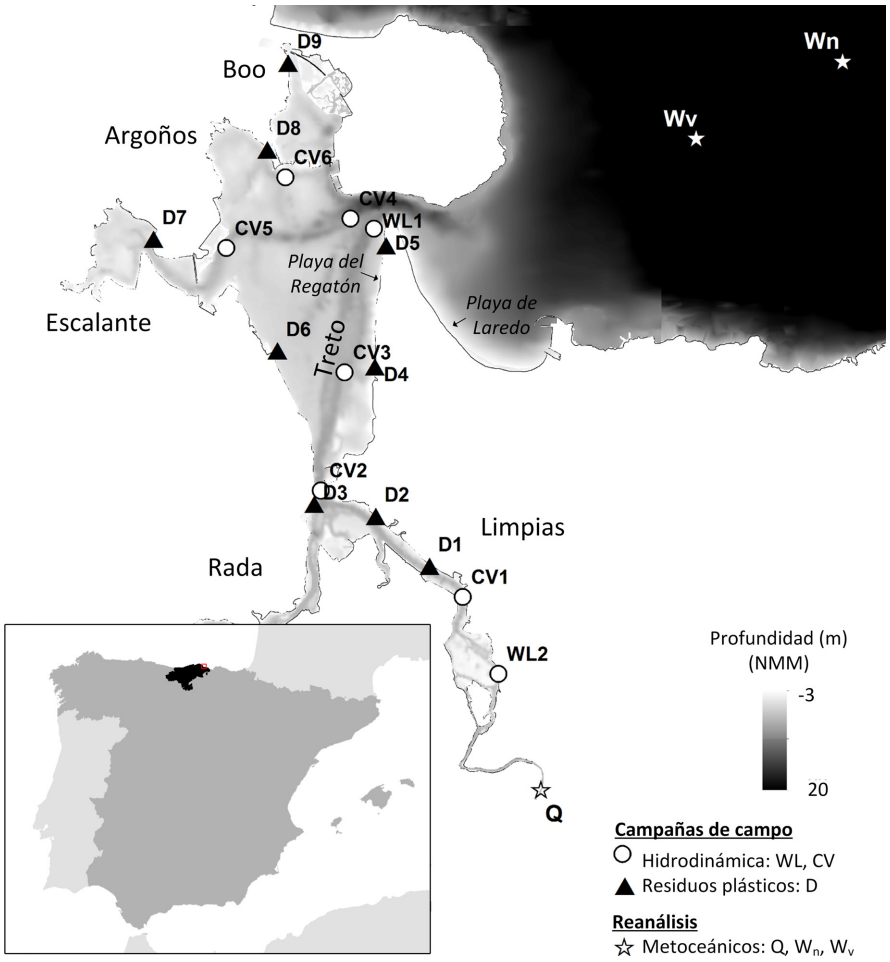

Figura 8: Localización del área de estudio y datos de partida.

La Bahía de Santoña es un estuario bien mezclado donde el factor clave de la hidrodinámica y el transporte de sustancias es la marea (Galván et al., 2010). La marea presenta un carácter semidiurno, rangos de mareas muertas y vivas de 1,5 m y 4,5 m, respectivamente, y un prisma de marea (Ω) de 45×10^6 m^3. La marea muestra un carácter simétrico en la desembocadura del estuario y se deforma al propagarse. Esta deformación genera asimetrías en el tiempo, tanto en la superficie libre como en la velocidad de la corriente. El intervalo de tiempo entre la bajamar y la pleamar se acorta, mientras que aumenta entre la pleamar y la bajamar. Dado que el prisma de marea ha de ser el mismo, las velocidades de la corriente durante las fases de llenante duran menos y son más intensas que durante las fases de vaciante. De este

modo, la marea oceánica simétrica se transforma en una marea asimétrica positiva en la parte más interna del estuario, siendo un aspecto especialmente significativo en las áreas de Limpias, Rada y Escalante y definiendo en estas áreas una tendencia a la importación de sustancias. Además de la marea astronómica, las descargas fluviales, el oleaje o el viento son elementos relevantes del transporte en zonas concretas de la bahía.

R4.4. Datos y herramientas de partida

Para aplicar la metodología propuesta en la Bahía de Santoña, se cuenta con los siguientes **datos de partida**:

- La *marea astronómica* en el exterior de la bahía se caracterizado con los datos del mareógrafo de Santander facilitados por Puertos del Estado.
- Los *aportes fluviales* medios diarios se han obtenido en la desembocadura del río Asón (punto Q en la Figura 8), entre 1970 y 2010, a partir de la base de datos de reanálisis descrita por García et al. (2008).
- El *oleaje* se ha definido en el nodo W_v de la Figura 8, en el periodo 1948-2018, a partir de la base de datos de alta resolución ($dx \simeq 0{,}005°$, $dy \simeq 0{,}004°$) DOW (Camus et al., 2013).
- Los datos de *viento* a 10 m sobre el nivel del mar se han obtenido en el nodo W_n de la Figura 8, en el periodo 1948-2018, de la base de datos SeaWind NCEP-HR, de 0.02 de resolución (Menendez et al., 2011).
- Para validar el modelo hidrodinámico se cuenta con datos instrumentales de *nivel del mar* en 2 puntos (WL en la Figura 8) y perfiles de *corrientes* en 6 estaciones (CV en la Figura 8), registrados en una campaña de campo entre los días 12 y 27 de noviembre de 1997.
- Para validar la metodología propuesta, se cuenta con *densidades medias de residuos* (*average density*, *AD*) recogidos en una campaña

de campo, en octubre de 2017. Siguiendo el método de muestreo propuesto por Rech et al. (2014), se recolectaron residuos en 9 áreas de la bahía (puntos D en la Figura 8) y, de acuerdo al protocolo OSPAR (2010), se clasificaron en diversos tipos. Los resultados mostraron que la mayoría de los residuos recogidos en la Bahía de Santoña quedaban representados por elementos de plástico seguidos por desechos sanitarios.

Con relación a las **herramientas**:

- Se aplicó el algoritmo de clusterización *K-medias* a las series temporales de las dinámicas dominantes (marea, viento, oleaje y caudal fluvial) reorganizadas para obtener patrones representativos de 15 días. Unos análisis numéricos preliminares determinaron que un horizonte temporal T de 15 días era periodo más adecuado para evaluar el transporte de residuos plásticos en la bahía.

- Para la obtención de las dinámicas de alta resolución (corrientes y oleaje) se aplicaron acopladamente los módulos hidrodinámico (FLOW) (Hydraulics, 2018a, Roelvink & Van Banning, 1995) y de oleaje (WAVE) (Booij et al., 1999, Hydraulics, 2018c) del modelo numérico *Delft3D*, previamente validado con los datos de nivel y corrientes de la campaña de 1997.

- Para describir el transporte de residuos en la Bahía de Santoña, se utilizó el módulo Lagrangiano del modelo *TESEO*. Este módulo describe el proceso de deriva de los residuos mediante un conjunto de partículas que se mueven por la acción combinada del viento, el oleaje, las corrientes y la difusión turbulenta. El módulo de transporte fue calibrado y validado con boyas de deriva lanzadas durante el accidente del Prestige (2002) y en diferentes ejercicios de lucha contra la contaminación realizados por Salvamento Marítimo en el Mar Mediterráneo y en el océano Atlántico (Abascal et al., 2007, 2017). Para una descripción más detallada se puede consultar Abascal et al.

(2009a) y Castanedo et al. (2006). Para aplicar este modelo en la Bahía de Santoña, se definieron 11 potenciales fuentes de residuos y dos tipos de capacidades de atrapamiento costero: capacidad total en áreas arenosas, fangosas o vegetadas y capacidad nula en acantilados y diques verticales. A continuación, se alimentó el modelo de transporte con las dinámicas de alta resolución generadas con Delft3D y se obtuvo una base de datos de potenciales trayectorias de residuos asociadas a una determinada probabilidad de ocurrencia.

R4.4. Resultados

El análisis probabilístico de la base de datos de trayectorias generada permite extraer diferentes tipos de resultados: (1) mapas de probabilidad de acumulación de residuos por cada fuente (P; Figura 9a); (2) mapa de probabilidad global de acumulación de residuos (P_G; Figura 9b) y (3) mapas de porcentajes de residuos procedentes de cada fuente (Pct; Figura 9c).

La comparación entre los resultados probabilísticos y las observaciones en campo permite evaluar la fiabilidad de los resultados obtenidos (Abascal et al., 2010, Barker, 2011, Liubartseva et al., 2016, Minguez et al., 2012). Esta fiabilidad no solo depende de la precisión de los modelos utilizados, sino también de la calidad de los datos de partida, así como de la robustez de la técnica de clusterización utilizada. Los resultados de P_G obtenidos en la Bahía de Santoña se compararon con las densidades medias de residuos (AD) obtenidas en campo, demostrando una adecuada concordancia entre ambas series ($\rho_s = 0.9$; Spearman, 1961). Las áreas con mayor P_G de acumular residuos se encuentran próximas a las áreas donde se registraron densidades más altas (véase la Figura 9b y d). Sin embargo, se detecta una dispersión en tres de los puntos ubicados en las zonas estuarinas más internas. Estudios posteriores con un mayor número de puntos de muestreo podrían explicar la dispersión en estas áreas.

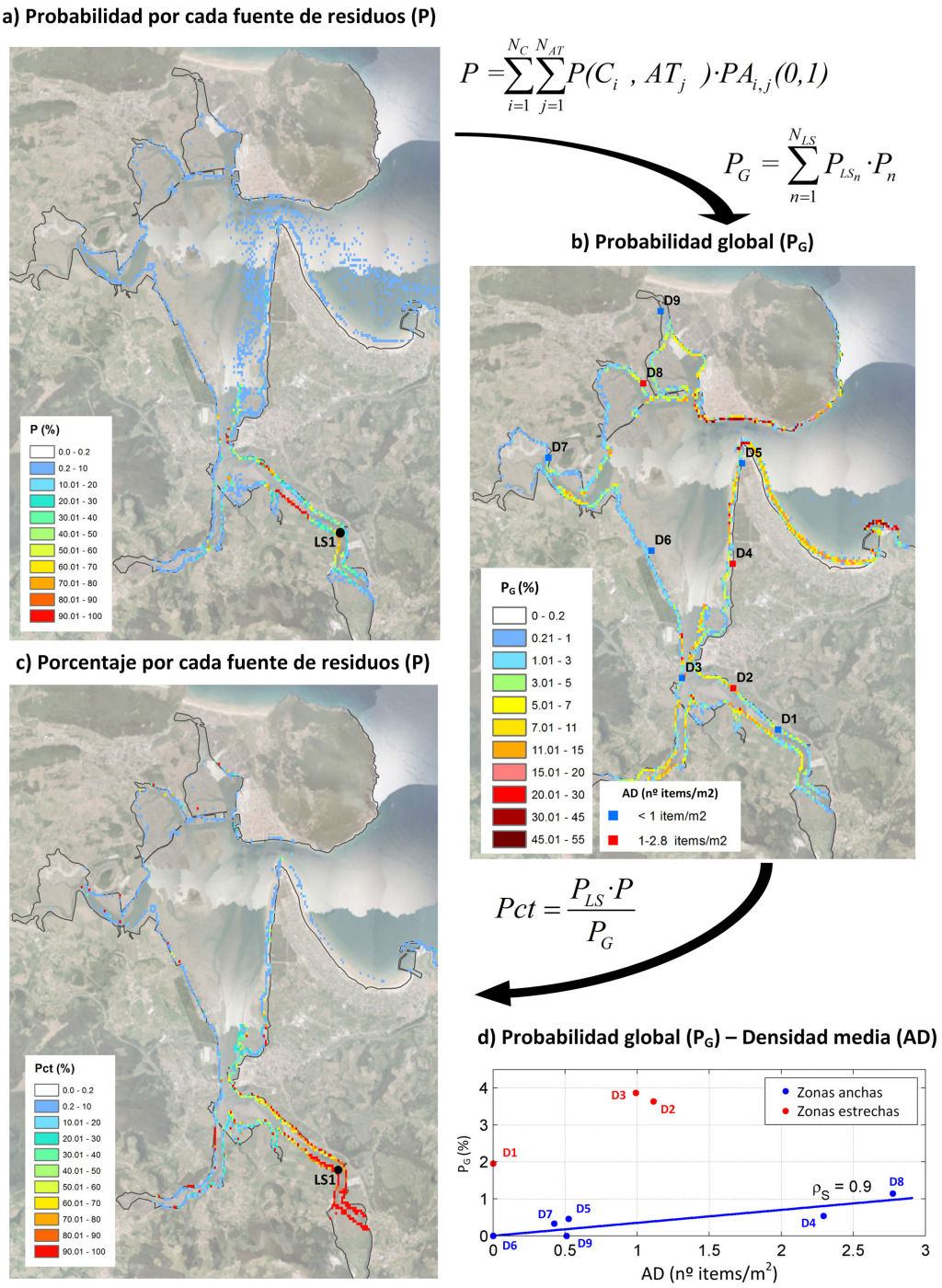

Figura 9: Análisis estadístico: a) Probabilidad de acumular residuos plásticos (P) procedentes de la fuente LS1; b) Probabilidad Global de acumulación de residuos plásticos (P_G); c) Porcentajes de residuos (Pct) procedentes de LS1 y d) comparación entre P_G y las densidades medias de residuos (AD) medidas en campo.

Los resultados de aplicar la metodología en la Bahía de Santoña indicaron que las mayores probabilidades de acumulación de residuos plásticos se producen cerca de las fuentes y disminuyen con la distancia a las mismas (véase la Figura 9a). Estos resultados concuerdan con los encontrados en estudios previos que demostraron una fuerte correlación entre las concentraciones costeras de plástico y la proximidad a los centros poblacionales (p.ej., Barnes et al., 2009, Browne et al., 2011, Yonkos et al., 2014). Por este motivo, la correcta localización de las fuentes de residuos es un aspecto clave de esta metodología, siendo necesario recopilar información a partir de fuentes documentales existentes o con campañas de observación.

Además, en el mapa de probabilidad global de la Figura 9b se observa que las playas son importantes focos de acumulación de residuos (con probabilidades que oscilan entre el 10 % y el 20 %), lo que concuerda con lo encontrado por Dekiff et al. (2014), Liebezeit & Dubaish (2012), Mathalon & Hill (2014) y Oigman-Pszczol & Creed (2007) en sus estudios y tiene importantes repercusiones turísticas y económicas.

Finalmente, de los resultados de P_G y Pct obtenidos en la Bahía de Santoña se deduce que, aunque una parte de los residuos plásticos que llegan a la playa de Laredo procede del río, éste no es la principal fuente contaminante (Figura 9b y c). El porcentaje más significativo, superior al 60 %, procede del centro urbano y puerto deportivo de Laredo y un 15 % viene del mar exterior. Por lo tanto, aunque una parte de los residuos que llegan a las playas procede de fuentes fluviales (Rech et al., 2014), se puede concluir que, en este caso, las principales aportaciones proceden de los núcleos poblacionales próximos.

R4.5. Conclusiones

Se ha propuesto una metodología para evaluar probabilísticamente la distribución de residuos plásticos en ambientes estuarinos. El uso de técnicas de clusterización para clasificar patrones temporales de múltiples variables locales dependientes (controladoras del transporte) y el modelado numérico de un conjunto de potenciales trayectorias de residuos plásticos permiten

realizar estos análisis utilizando menos recursos que las técnicas empleadas en el estado del conocimiento. Como aspecto esencial en el marco del modelado destaca la implementación de opciones para definir la influencia de la geometría del estuario y del tipo de sustrato (arena, fango, presencia de materiales artificiales o de vegetación) en la retención de los plásticos.

La metodología ha sido validada en un estuario de la costa norte de España (Bahía de Santoña) comparando los resultados obtenidos con la densidad media de residuos plásticos recogidos *in situ*. La validación concluyó que la implementación de esta metodología puede proporcionar información útil para la gestión de los residuos plásticos en los estuarios. De los resultados obtenidos en la Bahía de Santoña se puede concluir que el algoritmo K-medias es capaz de describir con éxito estados de mar quincenales constituidos por múltiples variables (que incluyen marea, descargas fluviales, velocidad y dirección del viento y componentes del oleaje) que impulsan el proceso de transporte y, por lo tanto, la distribución de residuos plásticos. Este estudio verifica, concordando con estudios previos, que los residuos plásticos tienden a acumularse cerca de sus fuentes y en las costas de las playas adyacentes.

A lo largo del desarrollo de la metodología, se han proporcionado los criterios necesarios para asegurar su aplicabilidad en cualquier otro estuario del mundo.

R5. Conclusiones y futuras líneas de investigación

R5.1. Conclusiones

El objetivo general de esta Tesis ha sido investigar la relación entre la hidrodinámica estuarina, poniendo el foco en la hidrodinámica debida a la marea astronómica y a su asimetría, y la distribución de residuos plásticos en estuarios dominados por la marea. Además, ha contribuido con el

desarrollo de una metodología general para identificar los *hotspots* de residuos plásticos en estuarios, favoreciendo la toma de decisiones para la definición de estrategias de prevención o limpieza.

Este objetivo general se logra a través de tres objetivos específicos previamente definidos en el apartado de *Introducción*. A continuación, se resumen las principales conclusiones extraídas de las investigaciones asociadas a cada objetivo.

Objetivo 1. Caracterización de la asimetría mareal a escala global para conocer su efecto como condición de contorno en los estuarios

Este objetivo específico surge de la necesidad de caracterizar la marea astronómica en la desembocadura de los estuarios. La finalidad es poder utilizar dicha información, como condición de contorno, en el estudio los procesos estuarinos en cualquier parte del mundo. Este objetivo ha sido satisfactoriamente alcanzado gracias a la aplicación de técnicas estadísticas avanzadas de clasificación y aproximaciones armónicas a la solución global de marea astronómica TPXO9-atlas. TPXO9-atlas es la solución global de mareas más completa (15 componentes mareales) hasta el momento, que cuenta una resolución espacial (1/30°) adecuada para describir las características de la marea en áreas costeras. Los resultados fueron validados con datos de 757 mareógrafos de todo el mundo, demostrando que la clasificación efectuada caracteriza bien o muy bien las zonas costeras del mundo en el 97 % de los nodos comparados y solo en el 3 % muestra una representación pobre o inaceptable.

A continuación, se presenta una serie de puntos clave que resumen las principales aportaciones científico-técnicas y los avances en el conocimiento asociados al primer objetivo específico de la Tesis:

- Se ha proporcionado una guía gráfica de asimetría y periodicidad de la marea astronómica (ambos parámetros relacionados con los procesos de transporte estuarino) a escala global. Esta guía puede ser utilizada por la comunidad científica para extraer las condiciones de contorno

para evaluar el transporte de sustancias, en general, y de plásticos, en particular, en cualquier estuario del mundo.

- Se ha demostrado que la variable "derivada temporal del nivel de marea" ($d\eta/dt$), representativa de la velocidad de subida y bajada de la marea, es capaz de describir las corrientes estuarinas de llenante y vaciante en ausencia de dinámicas adicionales y, por lo tanto, puede relacionarse con el transporte de sustancias en ambos sentidos.

- Se ha encontrado que las mareas simétricas cubren alrededor del 77.4 % de las áreas costeras del mundo y que la mayor parte de estas mareas se corresponden con el régimen mixto semidiurno (60 %), seguido del régimen semidiurno (30 %).

- Las mareas más asimétricas, tanto positivas como negativas (un 11.3 % de las áreas costeras del mundo presentan asimetrías positivas y también un 11.3 % muestran asimetrías negativas), se localizan en zonas concretas del globo relativamente adyacentes y se corresponden principalmente con los regímenes diurnos y mixtos con predominancia diurna.

- El triplete astronómico O1/K1/M2 domina en los regímenes diurnos y mixtos diurnos, mientras que la principal contribución al régimen semidiurno proviene de las componentes M2/M4.

Objetivo 2. Estudio de la evolución espacial de la asimetría mareal al propagarse en estuarios de distinta geometría y su efecto en la acumulación de residuos plásticos

El segundo objetivo específico de la Tesis se ha logrado realizando análisis numéricos hidrodinámicos y de transporte de residuos plásticos. Se han propagado diferentes mareas, definidas en las desembocaduras de los estuarios atendiendo a la propiedad de asimetría, a través de una serie de estuarios de diferente geometría. Las mareas se corresponden con algunos de los tipos representativos más diferentes entre sí en cuestión de asimetría,

que han sido identificados en la clasificación efectuada para cumplir con el objetivo anterior. De los análisis realizados, se confirman algunos resultados encontrados en estudios previos sobre la evolución de las mareas simétricas y se proporcionan algunas conclusiones novedosas sobre la evolución de las mareas asimétricas, así como los efectos de ambas sobre las acumulaciones de residuos plásticos:

- Las mareas simétricas evolucionan a asimétricas positivas con la propagación mareal a medida que aumenta la fricción con las paredes laterales y el lecho del canal. Por el contrario, la asimetría mareal puede experimentar una tendencia negativa si las fricciones son débiles o si los bajos o llanuras mareales cuentan con la extensión suficiente para contrarrestar el efecto del canal.

- De la propagación de mareas asimétricas se concluye que, en zonas estuarinas con canales de sección importante que favorecen la circulación de la mareal, el carácter asimétrico queda fuertemente condicionado por la asimetría presente en la desembocadura. Por el contrario, cuando aparece una clara oposición al flujo o un importante área de almacenamiento intermareal, el papel relevante lo adquiere la geometría del estuario.

- La influencia de la oposición al flujo mareal impuesto por la geometría de los estuarios también se ve reflejado en la acumulación de plásticos. La asimetría inicial de la desembocadura conduce la importación de residuos plásticos de los estuarios tanto más, cuanto más fácil es el flujo de la marea a través del canal. En este tipo de geometrías, las asimetrías mareales positivas muestran una capacidad de importación un 50 % superior a la que presentan las mareas simétricas y asimétricas negativas. A medida que la oposición al flujo a través del canal y el almacenamiento intermareal crecen, se define una clara dominancia de llenante, aunque se siguen apreciando pequeñas influencias de la asimetría mareal exterior. En estos casos, la probabilidad de acumulación de residuos plásticos es del 90 % para mareas asimétricas

positivas y varía entre el 70-80 % para mareas simétricas y asimétricas negativas. El hecho de que estas geometrías estén presentes en la mayor parte de los sistemas estuarinos explica el frecuente comportamiento de los estuarios como trampas de plásticos.

- Un aspecto destacable y novedoso que deriva de estos análisis es el papel regulador de la curtosis en la acumulación de los residuos plásticos dentro de los estuarios mareales. El coeficiente de curtosis aumenta con el carácter asimétrico de la marea. Para mareas asimétrico positivas/negativas, esto significa que las corrientes de llenante/vaciante más intensas van reduciendo su frecuencia y, por consiguiente, la capacidad de transporte inducida por las asimetrías.

Objetivo 3. Desarrollo de una metodología para evaluar la probabilidad de acumulación de residuos plásticos en estuarios

Finalmente, en esta Tesis se ha desarrollado una metodología de aplicación general, basada en técnicas de clusterización, modelado numérico y análisis estadístico, que permite abordar las limitaciones de las técnicas actuales del estado del conocimiento (elevada demanda de recursos económicos y temporales) para evaluar los *hotspots* de residuos plásticos e identificar, para cada una de esas áreas, su principal fuente contaminante. Además, se han proporcionado los criterios generales necesarios para poder aplicar la metodología en cualquier estuario del mundo. Esta metodología ha sido validada mediante su aplicación a un estuario de estudio, la Bahía de Santoña, localizada en Cantabria (costa norte de España). La comparación de los resultados obtenidos con medidas de campo demuestra que la implementación de la metodología puede proporcionar información valiosa para la gestión de los residuos plásticos en ambientes estuarinos. De los análisis realizados se extraen las siguientes conclusiones específicas:

- La metodología puede aplicarse con unos recursos mínimos en cualquier estuario del mundo y puede proporcionar información sobre acumulaciones medias anuales, estacionales o para un horizonte

temporal específico. Bases de datos, como CFS, que aportan predicciones sobre corrientes a un horizonte temporal de 6 meses, resaltan la potencialidad de esta metodología.

- Se ha demostrado que las técnicas de clusterización y los modelos numéricos son una buena combinación para estudiar la distribución de los residuos plásticos en la escala de estuario.

- Se ha comprobado que el algoritmo K-medias es capaz de describir con éxito estados de mar quincenales constituidos por múltiples variables que impulsan los procesos de transporte en los estuarios y, por lo tanto, la distribución de residuos plásticos.

- Se ha encontrado que las características físicas de los estuarios, asociadas a las capacidades de atrapamiento de residuos plásticos, implementadas en los modelos numéricos de transporte influyen en los resultados de las acumulaciones de plástico.

- Coincidiendo con algunos resultados recogidos en estudios previos, se ha confirmado que los residuos plásticos tienden a acumularse cerca de las fuentes de residuos y en las playas adyacentes a los estuarios.

R5.2. Futuras lineas de investigación

La investigación sobre el transporte y distribución de residuos plásticos en estuarios se encuentra aún en una fase muy preliminar y aún existen muchos frentes abiertos para abordar en futuras investigaciones. A lo largo del desarrollo de esta Tesis fueron surgiendo algunos aspectos que demandaban una mayor investigación. Además, algunos de los resultados obtenidos han sugerido ideas interesantes para ser analizadas en el futuro. A continuación, se recogen algunos de los puntos clave que pueden ser abordados en el futuro:

- Explorar en detalle la contribución individual al transporte y acumulación de residuos plásticos en estuarios de otras dinámicas

adicionales a la marea como son: el oleaje, el viento y los gradientes de temperatura y salinidad.

- Realizar estudios específicos para determinar la influencia de las características fisicoquímicas intrínsecas de los residuos plásticos que afectan a su flotabilidad (p.ej., tamaño, forma, densidad, etc.) en su transporte y acumulación final.

- Mejorar la calidad del modelado de residuos plásticos mediante el estudio de los siguientes coeficientes: el coeficiente de difusión (D), el coeficiente de arrastre del viento (C_D) y el parámetro que define el atrapamiento costero (*beaching*). Algunos estudios han analizado los coeficientes más adecuados para otro tipo de sustancias, como son los hidrocarburos, sin embargo, no hay conocimiento suficiente para definir los valores asociados a los residuos plásticos. Para lograr este objetivo, se requieren estudios específicos que analicen el transporte de diferentes tipos de residuos en mar abierto, estuarios, bahías y ríos y evalúen su interacción con los diferentes tipos de costa.

- Explorar la influencia de los fenómenos climáticos de largo plazo (p.ej., El Niño, La Niña o el Cambio Climático) en la acumulación de residuos plásticos en áreas estuarinas mediante la incorporación, además de la componente astronómica de la marea, de la variabilidad y las tendencias de largo plazo de la marea meteorológica.

- Con relación a la metodología desarrollada para identificar *hotspots* de residuos plásticos en estuarios, puede trabajarse en una validación más rigurosa mediante la adquisición de nuevos datos de campo (en un mayor número de puntos de muestreo y a lo largo de diferentes épocas estacionales), tanto en el estuario de estudio de esta Tesis, la Bahía de Santoña, como en otros nuevos estuarios con características diferentes al aquí evaluado (p.ej., con una marea asimétrica en la desembocadura, o donde los gradientes de temperatura y salinidad sean las dinámicas dominantes).

Abstract

Marine litter—mainly plastics (80%)—represents a significant threat to marine environments, causing damage at ecological, economic, and social levels. Rivers are one of the main sources of plastic debris and coastal hydrodynamics contribute to trapping the plastics within estuaries, which become significant environmental hazards.

The transport and fate of plastic debris within estuaries have been largely unexplored and most of the research has focused on open oceans or regional areas. Two different approaches have traditionally been used to assess the marine-litter distribution inside estuaries: field surveys and numerical models. Both approaches have some limitations, such as the dependence between the obtained results and the sampling method selected for field surveys and the high computational cost due to the use of numerical models at these spatial scales. Therefore, greater efforts are needed to address these limitations of plastic debris research on an estuary-scale. The first step towards this aim is to improve the understanding of the processes affecting the transport and fate of plastic debris within estuaries.

Astronomical tide plays a key role in the behaviour of tide-dominated estuaries. Tidal deformation generates sea-level and current-speed asymmetries that can lead to a net transport and cause an estuary trend to import or export substances, respectively. Tidal asymmetry arises from both the interaction among the main tidal constituents and the harmonics generated when tide propagates in shallow waters. Most previous research focuses on the deformation of the tide within estuaries; however, ocean tide may show asymmetry at the estuarine entrances, which implies that

the boundary condition is already deformed. This fact has important implications for tide propagation, estuarine transport processes, and flow exchanges between estuaries and open oceans. Therefore, a detailed characterization of tidal asymmetry at the mouth of estuaries is a key point to start the study. Regarding the transport processes, most of the published theories and studies relate tidal asymmetry with sediment transport and morphological trends in estuaries. However, no analysis on the direct effect on transport and fate of plastics debris is found.

The general objective of this Thesis is to study the effect of hydrodynamics on the transport and fate of plastic debris in tide-dominated estuaries, emphasizing hydrodynamics due to tidal asymmetry. This objective is broken down into the following specific objectives: (1) characterization of tidal asymmetry on a global scale to know its effect, as a boundary condition, in the estuarine transport processes, (2) study of the spatial evolution of tidal asymmetry when tide propagates through different estuarine geometries and its effect in the fate of plastic debris, and (3) development of a methodology to assess the probability of plastic debris accumulation in estuaries.

As the first step in this Thesis, the astronomical tide is classified on a global scale according to its asymmetry and periodicity. The purpose is to provide a guiding framework of representative astronomical tide types (*ATtypes*) on a worldwide scale to be used as a reference for further research on the transport of substances, in general, and plastic debris, in particular, in estuaries. The applied methodology is based on the use of the TPXO9-atlas global barotropic tidal solution and detailed statistical analysis. Probability density functions of the tidal elevation time derivative and the tidal form factor (parameters related to the transport of substances in estuaries) are extracted from TPXO9-atlas with a spatial resolution ranging from 1/6°, enough for open oceans, to 1/30°, more suitable for coastal areas. The K-means algorithm is applied to these parameters, and 25 representative *ATtypes* are identified. The classification is validated with 757 worldwide tide gauge records, showing that 97% of the clustered parameters

characterized well or very well the world's coastal areas and only 3% exhibit poor or unacceptable representativeness. The results show that 11.3% of coastal areas show negative asymmetries, 11.3% positive asymmetries, while symmetric tides dominate 77.4% of coastal areas. In coastal areas showing external tidal asymmetries, the propagation of the tide through estuaries may be initially conditioned by the asymmetry imposed on the mouth. Nevertheless, in symmetrical tidal areas, tidal asymmetries arise exclusively from overtides and compound tides generated during inland tidal propagation, without being externally conditioned.

Second, the effect of estuary morphology on the propagation of different (a)symmetric tidal types and on the fate of plastic debris within estuaries is analysed. The applied methodology is based on hydrodynamic-numerical modelling and Lagrangian-transport modelling. The steps consist of propagating three tidal types—positive-asymmetric, symmetric, and negative-asymmetric—through four study estuaries characterized with different morphologies, where cross-sections and tidal-flat areas change, and using the resulting hydrodynamics to move a set of representative particles of plastic debris. The skewness, representative of the difference between the flood/ebb-current intensities; kurtosis, showing the frequency of the strongest tidal currents; and average probability of plastic-debris accumulation in a neap-spring tidal cycle are the analysed parameters. The results show that the skewness of estuary mouths conditions the flood/ebb dominance and plastic debris accumulation in estuarine areas characterized by a main channel that favours tidal circulation. Positive tidal asymmetries show an import capacity 50% higher than symmetric or negative asymmetric tides. Conversely, when there are areas with significant opposing flow or intertidal storage, the estuarine geometry defines a clear flood dominance. The probability of plastic debris accumulation is 90% for positive asymmetric tides and varies from 70-80% for symmetric and negative asymmetric tides. A novel aspect derived from this study is the corrective and regulatory behaviour of kurtosis that counteracts the transport induced by skewness.

Finally, with the knowledge acquired on tidal asymmetry and transport

of plastic debris, a general methodology—that is based on numerical models and statistical analysis—is developed to identify the most probable plastic debris accumulation areas (hotspots) on an estuary scale. The purpose is to assist in the definition of cleanup and mitigation strategies in estuaries. The methodology includes four main steps: K-means clustering to identify representative metocean scenarios, dynamic downscaling to obtain high-resolution drivers with which to force a transport model, numerical transport modelling to generate a database of potential plastic debris trajectories, and statistical analysis of this database to obtain probabilities of debris accumulation. The efficacy of this methodology is demonstrated by its application to Santoña Bay, an estuary along the northern coast of Spain, by comparing the numerical results with field data. Furthermore, the necessary criteria to ensure its applicability to any other estuary are provided. As the main conclusion, the developed methodology successfully assesses the plastic debris distribution in estuaries with a minimum computational effort.

Chapter 1

Introduction

1.1. Background and motivation

Marine litter is one of the main current threats to marine environments, causing significant damages at ecological, economic, and social levels (UNEP, 2005). Currently, marine litter has become a priority issue on international environmental agendas, such as the EU Marine Strategy Framework Directive (MSFD) (Galgani et al., 2013). Regarding its composition, about 80% of marine litter is made up of plastics (Barnes et al., 2009, Derraik, 2002). In 2010, between 4.8 and 12.7 million tons of plastic debris accumulated in oceans, and an increase by an order of magnitude is estimated for 2025 (Jambeck et al., 2015). Regarding its origin, approximately 80% of the litter that reaches marine environments comes from land-based sources, mainly from rivers (Galgani et al., 2015, Rech et al., 2014). A significant part of this litter will reach the open ocean and the remaining will be retained within the estuaries, which often act as sinks of marine litter with a notable plastic fraction (Acha et al., 2003). Furthermore, the tides and waves can also collaborate to introduce litter from sea-based sources (e.g., trawling) into estuarine environments (Hinojosa & Thiel, 2009).

Estuaries are transition areas subject to marine influences —such as tides, waves, and the influx of saline water— and to riverine influences

—such as river and sediment discharges— which provide them with very particular features. These areas show high biological productivity and provide habitats for many species of flora and fauna. Countless species of fish, crustaceans, and shellfish depend on estuarine waters as safe places for their survival. In addition, estuaries serve as a refuge for a wide variety of aquatic birds, whether autochthonous or exotic. Coastal protection and carbon capture roles, as well as the socioeconomic importance of estuaries for the development of different local activities such as fishing, shellfishing, small industry, or tourism and recreational activities, among others, also stand out (Barbier et al., 2011). Therefore, the accumulation of marine litter, in general, and plastic debris, in particular, represents a significant threat to estuarine habitats and the ecosystem services they provide (Mazarrasa et al., 2019).

Consequently, there is a growing concern to address this issue by defining cleanup, prevention, and awareness-raising strategies on an estuarine scale. *Cleanup strategies* consist of the removal and management of litter already present in the marine environment. Cleanup actions involve significant direct economic costs, including litter collection, transportation, and disposal (Hall, 2000, OSPAR, 2009), and administrative costs, such as contract management (Fanshawe & Everard, 2002). The *prevention measures* aim to block and reduce the entries of litter into the marine environment by supporting direct actions on the production process (e.g., ecodesign or the promotion of new production methods) or on litter sources (e.g., installation of filters or other retention devices in stormwater spillways or sewage discharge drains) (Gallo et al., 2018). In a complementary manner, *awareness-raising initiatives* are proposed at all levels of society, for example, giving talks and workshops in educational centres or organizing volunteer campaigns with citizen participation for the collection of marine litter (Hartley et al., 2015). Fig. 1.1 shows some types of plastic debris found in coastal areas, as well as some initiatives aimed at promoting visibility and social awareness about the problem.

Figure 1.1: Plastic debris in marine environments and some initiatives promoted to increase awareness about the problem.

The study of marine litter *hotspots*, which are areas of large accumulations or hazards, allows cleanup efforts to be focused on the priority areas and, therefore, makes cleanup actions a cost-effective method for reducing marine litter in the environment (Haarr et al., 2019). The availability of this type of information at estuary levels is limited, which makes the organization and logistics of cleanup activities difficult for managers. Hence, the promotion of research aimed at increasing knowledge about the fate of plastic debris in estuaries and its application to the development of methodologies and tools to support managers in decision-making is a key aspect to face the problem.

The processes that favour the accumulation of plastic debris within estuaries are dominated by the *intrinsic properties of the plastic* items, by the *physical features of estuaries*, and, fundamentally, by the *hydrodynamic interactions* between tides, river discharges, waves, and wind (Browne et al., 2010, Carson et al., 2013, Zhang, 2017).

Specific *density, size,* and *shape* are some of the *plastic-item properties* that influence buoyancy and, therefore, affect the transport and fate of plastic debris in marine environments. Plastic debris shows a wide variability of *densities*. The most common plastics found in the marine environment are polyethylene (0.90-0.99 g/cm^3), polypropylene (0.85-0.95 g/cm^3), and polystyrene (0.95-1.1 g/cm^3) (Mazarrasa et al., 2019, Zhang, 2017). As the density of these plastics is lower than the seawater density, they float close to the surface and are mainly transported by surface currents and wind (Barnes et al., 2009, Chubarenko et al., 2016, Kowalski et al., 2016). Regarding the *size*, Isobe et al. (2014) found that the largest plastics, macroplastics (>200 mm) and mesoplastics (5-200 mm), accumulated on the shores of the Seto Inland Sea (Japan), while microplastics (<5 mm) were offshore transported by a combination of Stokes drift and the buoyancy of the fragments. In terms of *shape*, different types of plastic debris exist depending on the original product (pellets, fibres, filaments, etc.), as well as the fragmentation and degradation processes (Hidalgo-Ruz et al., 2012, Zhang, 2017). Fibres and thin films often exhibit greater buoyancy than spheres of the same volume and density (Filella, 2015).

Figure 1.2: Plastic debris in the Pas estuary (Cantabria, North of Spain). Photographs registered within the CleanLICs project (`http://cleanlics.ihcantabria.es`).

Coastal trapping ability is decisive in the fate of plastic debris inside estuaries. This parameter shows spatial variability within each estuary and is strongly correlated with the presence and type of vegetation, which frequently act as 'marine litter traps' (Viehman et al., 2011), as well as with the flood-ebb regime. Studies, such as by Mazarrasa et al. (2019), have detected high concentrations of plastic debris in the high marsh areas of estuaries that become especially significant in vegetated areas (see Fig. 1.2).

In *hydrodynamic terms*, surface currents, wind, and waves acquire relevant roles in the transport and fate of floating debris on the open-ocean beaches adjacent to estuaries (Browne et al., 2010, Isobe et al., 2014, Sadri & Thompson, 2014, Zhang, 2017, see Fig. 1.3). Plastic debris stranded on beaches returns to the sea during spring tides or storms and generate cyclical onshore/offshore transport near the coast. This transport degrades plastic items until rip currents can free them from coastal entrapment and transport them to the open ocean (Fok et al., 2017, Isobe et al., 2014). With regard to river inputs, high river discharges dominate the export of plastic debris. Thus, the highest amounts of debris have been detected in the mouths during the rainy periods (Moore et al., 2011, Yonkos et al., 2014). In the inner area of estuaries, the temperature and salinity gradients and the relevant role of tides stands out. In addition, the wind can also be important in large-area estuaries (Zhang, 2017). Stratification and mixing at the interface of fresh and saltwater influence the buoyancy of the elements with densities between 1.000-1.025 g/cm^3. This is the case of polystyrene, one of the elements most frequently detected in the marine environment. Consequently, their transport depends on the final position acquired by the elements within the water column and on the vertical current profile (Lima et al., 2015, Vermeiren et al., 2016). Finally, the astronomical tide can show flood or ebb asymmetry—due to the combined influence of some main tidal constituents or dissipation of tidal energy in shallow waters—that can lead to a net transport of plastic debris and cause a trend to accumulate or export plastic debris, respectively (Zhang, 2017). The role of tidal asymmetry is especially significant in tide-dominated estuaries.

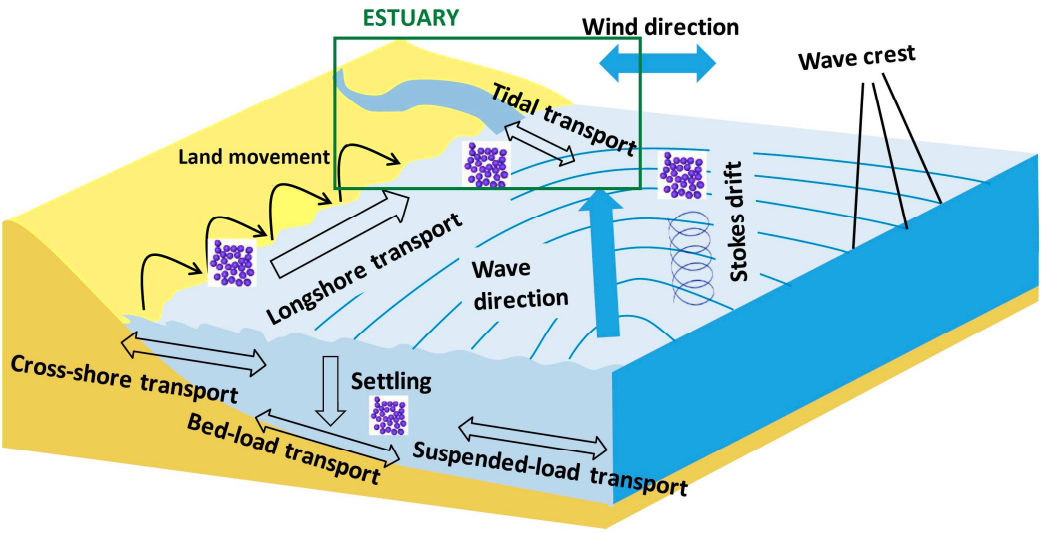

Figure 1.3: Transport of plastic debris in estuarine environments (modified from Zhang, 2017).

Summarizing, the main parameters influencing the transport and fate of plastic debris in estuaries have been listed, namely: features of plastic items; trapping ability of estuarine environments themselves; and hydrodynamics due to tides, river discharges, waves, winds, and temperature and salinity gradients. Several studies concluded that tidal asymmetry is the determining parameter of the transport and distribution of substances within tide-dominated estuaries. Most of the theories and studies published so far relate the effects of tidal asymmetry in its propagation through estuaries with the sediment transport and their morphological trend (e.g., Aubrey & Speer, 1985, Dronkers, 1986, Friedrichs & Aubrey, 1988) Similarly, some authors, such as Ballent et al. (2012), Browne et al. (2010), Costa et al. (2011), Eerkes-Medrano et al. (2015), Galgani et al. (2000), have suggested that tidal asymmetry can be related to transport and fate of plastic debris within tide-dominated estuaries. Therefore, a detailed analysis of this driver is one of the key aspects to start the study.

This Thesis aims to make a first approach to the study of fate of plastics debris within tide-dominated estuaries from a hydrodynamic perspective, focusing on the astronomical tide and its asymmetry. The purpose is to

apply the acquired knowledge in the developing of a methodology to identify the hotspots of plastic debris in estuaries and, therefore, to provide valuable information to managers and policymakers for the definition of cleanup and prevention strategies.

1.2. State-of-the-art

This section includes a state-of-the-art review of the three main topics of the Thesis: the available knowledge on tidal asymmetry; its potential effect on the transport and fate of substances in estuaries; and the existing techniques to assess the transport and fate of plastic debris in the marine environment, in general, and in estuarine environments, in particular. Moreover, a specific state-of-the-art of the statistical techniques and numerical models used to develop each one of the specific objectives of this Thesis is presented in the corresponding sections of the document.

1.2.1. Tidal asymmetry

The asymmetry of the tide plays a key role in the behaviour of tide-dominated estuaries (Aubrey & Speer, 1985, Brown & Davies, 2007, Dronkers, 1986, Friedrichs & Aubrey, 1988, Hoitink et al., 2003, Nidzieko, 2010, Zhou et al., 2018). Tidal asymmetry refers to the distortion of tidal wave caused by the flood phase occurring faster than the ebb phase, or vice versa. When the flood phase is shorter than the ebb phase, the flood currents are more intense than the ebb currents, and net transport is induced in the estuary; when the ebb phase is shorter than the flood phase, the estuary tends to export substances. This relationship has been traditionally used to explain sediment transport but can be extended to understand the transport of any other substance (e.g., plastic debris) or any other process dependent on estuarine hydrodynamics.

Tidal asymmetry arises from both the interaction between the main tidal constituents in open oceans and the harmonics generated when tide

propagates in shallow-water areas (Hoitink et al., 2003, Nidzieko, 2010). Nidzieko (2010) highlighted the importance of the asymmetry imposed by the main tides in the mouth of an estuary. Although the estuary morphology is significant in determining the dominance of the flood or ebb phase in these systems, the asymmetry imposed in the mouth must first be overcome. Hence, the fact that ocean tide shows asymmetry at the entrance of an estuary has significant implications for tide propagation and, consequently, in some of the most widely recognized estuarine processes. Some examples of estuarine issues that can be affected by the presence of an external asymmetry can be point out, namely, sediment transport and morphodynamics (Boon III & Byrne, 1981, Brown & Davies, 2007, Dronkers, 1986, Friedrichs & Aubrey, 1988, 1994, Gallo & Vinzon, 2005, Ranasinghe & Pattiaratchi, 2000), turbidity (Gallo & Vinzon, 2005), flushing times (Monsen et al., 2002), or the case at hand, plastic debris transport and fate (Hinojosa & Thiel, 2009, Mazarrasa et al., 2019).

In open oceans, the main cause of tidal asymmetry is the combined influence of the O1/K1/M2 constituents (Hoitink et al., 2003, Song et al., 2011), followed by P1/K1/S2, K1/K2, and finally Q1/K1/N2 (Song et al., 2011). In coastal areas, tide is distorted by the nonlinear effects of bottom friction and boundaries, and this distortion generates overtides (superharmonic constituents) and compound tides. Previous studies have shown that the main contribution to tidal asymmetry in shallow waters is the combined influence of the M4 overtide and the M2 constituent (Aubrey & Speer, 1985, Song et al., 2011, Speer & Aubrey, 1985). Nevertheless, this relationship between tidal constituents is not the only one that can influence tidal asymmetries in these areas and, in semidiurnal tidal regimes, the influences of the M6 (M2/M4/M6) (Blanton et al., 2002), MS4 (M2/S2/M4/MS4) (Song et al., 2011), and 2MS6 (M2/S2/M6/2MS6) constituents (Byun & Cho, 2006) can also cause asymmetry. In areas with diurnal or mixed diurnal tides, the effects of the O1/K1/M2 constituents are predominant (Hoitink et al., 2003, Ranasinghe & Pattiaratchi, 2000, Song et al., 2011).

Asymmetry has been traditionally defined by two parameters: the ratio

between the amplitudes of two tidal constituents (e.g., a_{M4}/a_{M2}), used to quantify the degree of distortion, and the difference between two phases (e.g., $2\phi_{M2} - \phi_{M4}$), used to identify the orientation (e.g., Aubrey & Friedrichs, 1988). This harmonic parametrization enables the asymmetry derived mainly from two constituents to be described. Other studies have used probability density functions (PDFs) of tidal elevations, since PDFs retain more information and hence are more suitable to characterize long-term tidal distributions (Castanedo et al., 2007, Woodworth et al., 2005). Following this research path, Nidzieko (2010) recommended the use of a parameter related to the shape of PDFs, the skewness coefficient (γ_1), and applied this coefficient to the tidal elevation time derivative, that is, a representative parameter of rising/falling tidal speed and, consequently, of flood/ebb currents in shore tidal estuaries. Nidzieko (2010) showed that for two tidal constituents, γ_1 kept the information of the traditional metric with the advantage of being applicable to any time series. Song et al. (2011) generalized this approach for any number of tidal constituents, and Nidzieko & Ralston (2012) used a variant of the skewness approach to consider asymmetry variations with changes over less than a fortnight. In summary, asymmetry can be quantified by using harmonic or statistical methods, both effective and with complementary advantages. Guo et al. (2019) found that harmonic methods are suitable for studying areas characterized by diurnal and semidiurnal regimes, while the application of statistical methods is relevant in mixed tidal regimes.

Song et al. (2011) developed a global approach for investigating asymmetry in the open ocean using the TPXO7-atlas solution with a spatial resolution of 0.25° and identified the constituents responsible for asymmetry worldwide based on the skewness parameter (see Fig. 1.4). They found a strong correlation between asymmetries due to different combinations of the main tidal constituents and tidal regimes (semidiurnal, mixed, and diurnal). However, the spatial resolution of TPXO7-atlas is insufficient to accurately simulate the tide in coastal areas. Currently, the TPXO9-atlas dataset (Egbert & Erofeeva, 2002) (`https://www.tpxo.net/`), with improved tidal

accuracy compared to its previous versions (Jeon et al., 2019), and spatial resolution (1/30°), is available. Therefore, the detailed characterization of the tidal asymmetry in the coastal areas close to the estuarine mouths constitutes a key aspect to start the study of the transport of substances, in general, and of plastics, in particular, in estuarine environments.

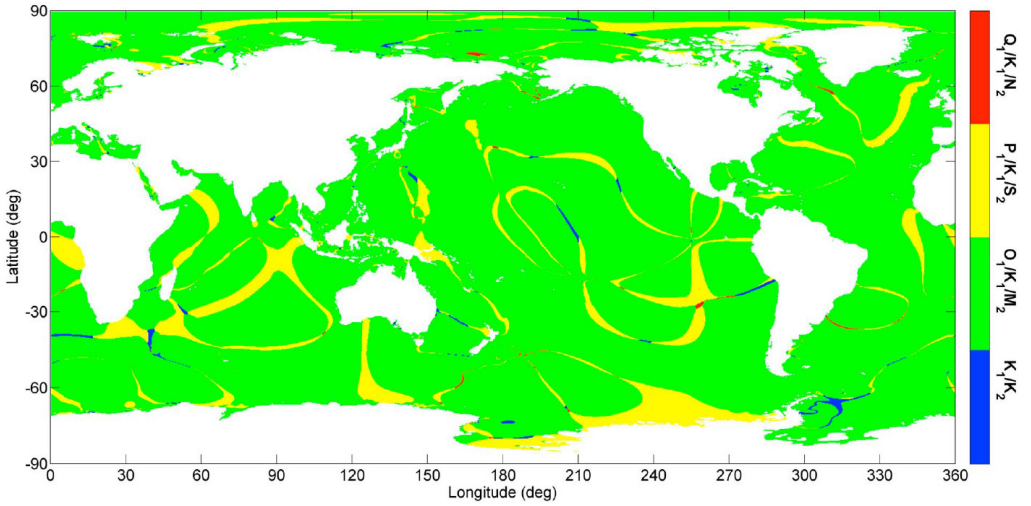

Figure 1.4: The largest contributor to tidal asymmetry in open oceans worldwide (source: Song et al., 2011).

1.2.2. Influence of tidal asymmetry on estuarine transport processes

Several studies determined that *tidal asymmetry* is the fundamental parameter that conducts the transport and fate of substances within tide-dominated estuaries. Most of the theories and studies published so far relate the *tidal asymmetry* that arises with tidal propagation through estuaries, with the sediment transport and the morphological trend of these environments. Since some research suggested that the study of the plastic debris transport within estuaries can be assimilated to the study of sediment transport (Ballent et al., 2012, Browne et al., 2010, Costa et al., 2011, Eerkes-Medrano et al., 2015, Galgani et al., 2000), a detailed review of the

state-of-the-art on the issue of asymmetries in estuaries is a good point to approach this study.

Some of the most prominent studies on the topic (Aubrey & Speer, 1985, Dronkers, 1986, Friedrichs & Aubrey, 1988, Speer & Aubrey, 1985) analysed the propagation of symmetric tides through estuaries with different geometries using analytical models or field observations to draw a series of relevant conclusions. Tidal waves deform as they propagate through shallow estuaries due to the presence of lateral boundaries and bottom friction. This deformation results in differences between flood- and ebb-phase durations and, consequently, the intensities of the flood and ebb currents. Therefore, tidal asymmetry induces net transport in the direction of the most intense currents, which determines the estuarine trends that import or export sediments. If the flood phase is shorter, the tidal asymmetry is considered positive, and the flood currents are faster than the ebb currents, and vice versa for a negative tidal asymmetry. Regarding estuarine geometries, estuaries where tidal flats occupy a small area or show high frictions tend to develop positive asymmetries and a tendency to import sediments. In contrast, if they have extensive tidal flats and weaker frictions, negative tidal asymmetries, and a tendency to export sediments arise. In short, tidal amplitudes, lateral boundaries, bottom frictions, and estuarine geometries are the factors that determine tidal asymmetries and the tendency to accumulate or export sediments or other substances, such as plastic debris. Fig. 1.5 schematically represents the effect of tidal deformation (negative asymmetries in levels and currents) when propagating through an estuary with significant tidal flats.

Up to this point, studies have linked the origin of tidal asymmetry to nonlinear tidal interactions in shallow waters. However, Hoitink et al. (2003) and Song et al. (2011) demonstrated that tidal asymmetry also arises in deep ocean waters due to interactions between some of the main tidal constituents. In addition, some research has highlighted the importance of this ocean tidal asymmetry imposed at estuarine mouths in the deformation generated after tidal propagation and, consequently, in determining estuarine morphological

trends. Moore et al. (2009) found that the positive asymmetric character of the ocean tide at the mouth of the Dee estuary (UK) induced flood dominance, which explained the large-scale accretion that occurred over the last 2 centuries. Ranasinghe & Pattiaratchi (2000) found that the sediment export observed in three estuaries located on the southwestern coast of Australia could be explained by the negative tidal asymmetry that dominates their mouths. Nidzieko (2010) investigated three Californian estuaries that also showed negative tidal asymmetries at their mouths; however, in these cases, the estuaries were characterized by very different geometric features, and the final asymmetric character depended both on the tidal asymmetries at the mouths and estuarine geometries, especially regarding tidal flat extensions. As this author concluded, tidal asymmetry develops with tidal propagation according to estuarine morphology, but tidal asymmetry at the mouths must first be overcome.

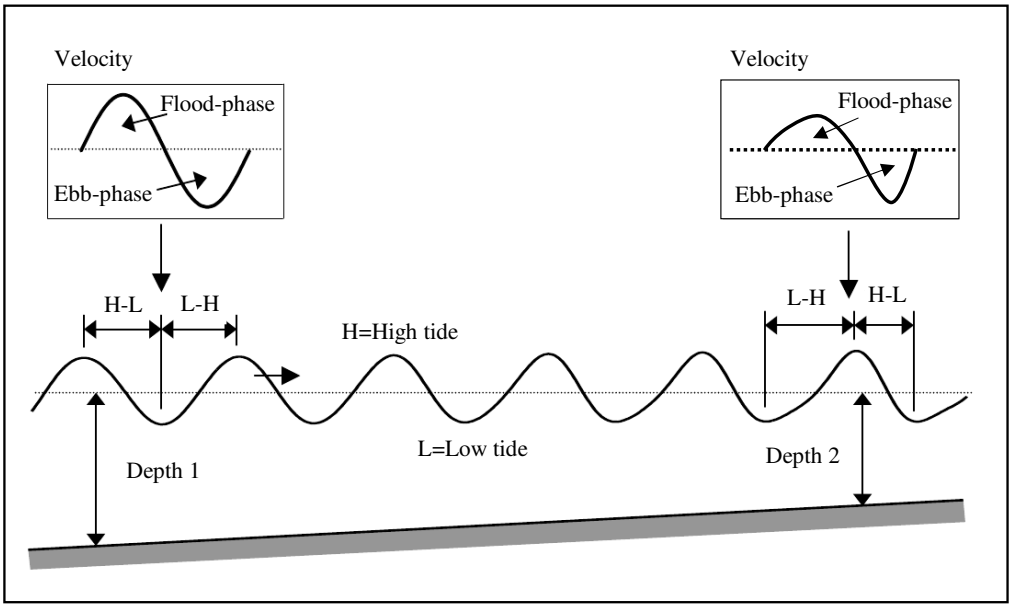

Figure 1.5: Tidal deformation in a shallow estuary (modified from: Lomónaco, 1999).

1.2.3. Techniques to assess the transport and fate of plastic debris in marine environments

Considering that 80% of marine litter is made up of plastics and that the most frequent fraction is made up of elements with densities lower than those of seawater (polyethylene, polypropylene, and polystyrene), the most widespread theories assume floating spherical particles for their studies (Zhang, 2017). Three categories of studies are distinguished according to their spatial scale of analysis: global, regional, and local.

The majority of *global studies* have been conducted using historical data of drifter trajectories, as observations of these trajectories facilitate to include in the analysis the effect of marine currents and wind drag (Carpenter et al., 1972, Law et al., 2010, Maximenko et al., 2012, Van Sebille et al., 2012). However, some authors, such as Lebreton et al. (2012), employ Lagrangian particle models to simulate trajectories from the sources to the sinks or apply numerical approaches. The results of these studies provide information about transport and worldwide concentration areas (patches) of marine litter. These 'garbage patches' primarily correspond to the convergence areas of ocean currents in subtropical and subpolar gyros (Cózar et al., 2014, Maximenko et al., 2012) (see Fig. 1.6).

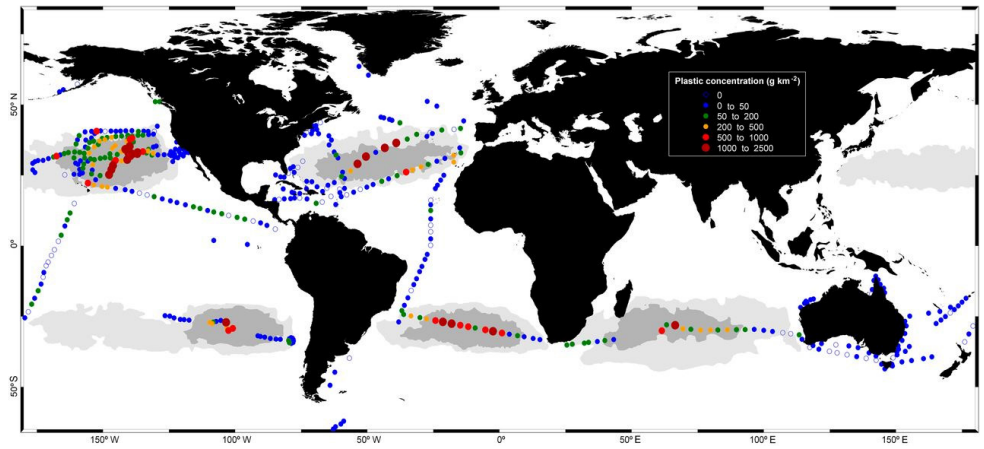

Figure 1.6: Concentrations of plastic debris in surface waters of open oceans worldwide (source: Cózar et al., 2014).

Regional studies focus on the analysis of the plastic debris distribution in basins or confined areas. At these scales, the identification of the main sources of contamination is essential (Zambianchi et al., 2014), for which authors such as Kako et al. (2011) use particle tracking models. The areas where more regional studies have been conducted are the East Asia seas (Isobe et al., 2009, Kako et al., 2014, 2011, Yoon et al., 2010), the waters near the Hawaiian Islands (Carson et al., 2013, Kubota, 1994), the Mediterranean Sea (Zambianchi et al., 2014, 2017) and the Bay of Biscay (Pereiro et al., 2018). These studies conclude that litter tend to accumulate in low circulation areas, which corresponds to sedimentary accumulation areas, such as bays, estuaries, and coral reefs (Galgani et al., 1996).

Local studies, which are considerably scarcer, analyse the distribution of marine litter inside estuaries and bays. These studies (e.g., Browne et al., 2010, Klein et al., 2015, Mazarrasa et al., 2019, Thornton & Jackson, 1998, Yonkos et al., 2014) are fundamentally based on information collected in observation campaigns that were conducted at very specific locations, and consequently, the results are not always generalizable. Fig. 1.7 shows some examples of field-survey designs carried out by Mazarrasa et al. (2019) in three estuaries of the Cantabrian coast.

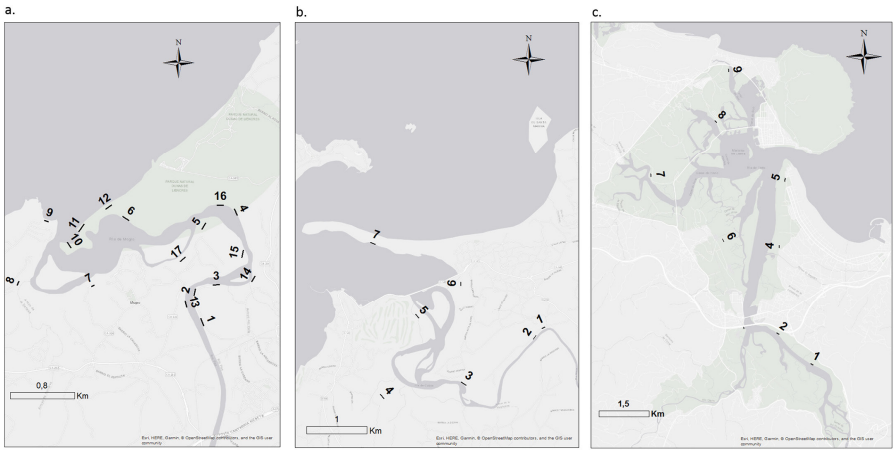

Figure 1.7: Examples of field studies and sampling areas in three estuaries of the Cantabrian coast: a) the Pas estuary, b) the Miera estuary, and c) the Ason estuary (source: Mazarrasa et al., 2019).

The main drawback of the field observation approach is the dependence of the results on the selected sampling method and the particularities of the area at the time at which the sampling was performed. For example, if the field survey has been performed after a high river discharge event or a cleanup action, the results will probably be altered and will not represent average conditions. Another approach to address these studies would be from a numerical perspective (e.g., Yoo et al., 2007). However, these kinds of studies are not widely used on an estuary scale due to the important demanded requirements. The main drawbacks of numerical modelling are the high spatial resolution required for estuarine-scale studies, the large number of drivers involved in processes (tide, river discharge, waves, temperature, salinity, and winds), and the need for long-term environmental databases (e.g., 10–30 years) to assess probabilities, that imply significant computational costs and the need for a long series of drivers to be used as boundary conditions and climatic forcings.

To sum up, different approaches can be employed to investigate the marine litter distribution in marine environments at different scales: global, regional, and local. However, each approach has its own drawbacks. Taking into account that many studies identify river inputs as the main sources of marine litter not only on beaches (Rech et al., 2014) but also in oceans (Claessens et al., 2011, Galgani et al., 2015, Klein et al., 2015), increasing efforts to develop effective methods and tools to investigate marine litter distribution at an estuarine scale is a necessary step to address the problem at the source.

1.2.4. Conclusions

The current state-of-the-art of scientific and technical knowledge on the transport and fate of plastic debris in estuaries shows, on the one hand, the scarcity of existing studies on these very small spatial scales, as well as the limitations of the techniques used for this purpose: observations in field surveys and numerical modelling. These limitations, which can be summarized in the dependence between the results and the selected sampling

method, and in the high computational effort associated with numerical modelling, make it difficult to apply these approaches to any estuary in the world.

Furthermore, the determinant factors of transport and fate of plastic debris in the marine environment, in general, and in estuaries, in particular, have been listed, namely, hydrodynamics, coastal trapping ability, and the plastic debris features themselves. All of them are aspects insufficiently explored at estuarine scales so far, requiring in-depth parallel analyses.

This Thesis aims to improve the knowledge from a hydrodynamic perspective in tide-dominated estuaries. As tidal asymmetry is one of the most relevant drivers that generally conditions the transport of substances within this type of estuaries, the present research emphasizes the study of hydrodynamics due to astronomical tide and its asymmetry. In this sense, several studies assess the tidal wave deformation that arises when tide propagates through estuaries, its relationship with sediment transport and with their morphological evolution. However, the direct influence that asymmetry originated in open oceans has, as a boundary condition, on the subsequent tidal-wave deformation generated in shallow waters, nor its effect on the distribution of substances, specifically plastic substances, has not been analysed in detail in estuaries so far.

In line with all the above, this Thesis aims to cover some of the gaps detected in the state-of-the-art techniques to identify hotspots of plastic debris on estuarine scales. Specifically, it aims to: (1) expand current knowledge about tidal asymmetry in open oceans and its effect as a boundary condition on the fate of plastic debris in estuarine environments and (2) apply the acquired knowledge in the development of a methodology, of general application, that allows to identify the most probable areas of plastic debris accumulation in estuaries, reducing the limitations of current techniques.

Regarding the type of plastic debris used as the basis of the study, generic floating spherical particles have been chosen. Generic particles because of the physicochemical features of plastic debris, although of interest, are not a research objective of this Thesis. The influence of plastic features is

too broad a topic that requires its own and independent in-depth studies. Floating because the most frequent plastic debris in the marine environment (polyethylene, polypropylene, and polystyrene) show densities lower than seawater density. Concerning the shape, following the most widespread theories, spherical particles were assumed.

1.3. Objectives

The general objective of this Thesis is to investigate the relationship between estuarine hydrodynamics and the fate of plastic debris in tide-dominated estuaries, emphasizing hydrodynamics due to the astronomical tide and its asymmetry.

This objective is specified in the following specific objectives:

1. Characterization of tidal asymmetry on a global scale to know its effect, as a boundary condition, in the estuarine transport processes.
2. Study of the spatial evolution of tidal asymmetry when tide propagates through different estuarine geometries and its effect in the fate of plastic debris.
3. Development of a methodology to assess the probability of plastic debris accumulation in estuaries.

1.4. Layout of the Thesis

The Thesis is structured in chapters covering the main developed topics, whose contents are specified below:

In *Chapter 1*, the motivation that has led to the development of this Thesis, a review of the current state-of-the-art about tidal asymmetry, its potential effect on the transport of substances in estuaries, and the techniques to assess the transport and fate of plastic debris in the marine environment, in general, and in estuaries, in particular, are presented.

In *Chapter 2*, tidal asymmetry is characterized on a global scale using global astronomical tidal solutions and advanced clustering techniques.

In *Chapter 3*, the evolution of tidal asymmetry as it propagates through estuaries characterized with different geometries and its effect on the fate of plastic debris are numerically analysed.

In *Chapter 4*, a methodology, that is based on statistical analysis and numerical modelling, to identify the most probable areas of plastic debris accumulation in estuaries is developed. The efficacy of this methodology is demonstrated by its application to an estuary located on the northern coast of Spain, by comparing the numerical results with field data. Moreover, the necessary criteria to ensure the applicability of the methodology to any other estuary in the world are provided.

Finally, in *Chapter 5* the main conclusions resulting from this Thesis are collected and the ongoing research is shown.

Chapter 2

Characterization of astronomical tide asymmetry and periodicity on a global scale [1]

2.1. Introduction

Asymmetry and periodicity of open ocean tides are relevant parameters to study estuarine transport processes. Tidal asymmetry results in a difference between the intensities of the flood and ebb currents and, consequently, in an onshore/offshore net transport of substances. Therefore, tidal asymmetry at estuarine mouths affects estuarine-ocean exchanges, tidal propagation and, consequently, internal transport processes. Tidal periodicity results from the non-linear interaction between diurnal and semidiurnal tidal constituents and, therefore, is also a parameter related to tidal asymmetry. Relevant O1/K1/M2 interactions are associated with diurnal regimes, whereas, if

[1] The findings of this chapter have been published in: Núñez, P., Castanedo, S., & Medina, R. (2020). A Global Classification of Astronomical Tide Asymmetry and Periodicity Using Statistical and Cluster Analysis. *Journal of Geophysical Research: Oceans, 125*(8), e2020JC016143.

O1/K1/M2 interactions can be neglected, semidiurnal regimes tend to predominate. In this chapter, the most recent version of the TPXO Global Tidal Solutions (TPXO9-atlas), statistical methods, and clustering and harmonic approaches were used to effectively describe the tidal asymmetry and periodicity in coastal areas before the tidal propagation through estuaries. The purpose is to obtain a graphic guide that can be applied to study the transport and fate of plastics debris in estuarine areas.

This chapter responds to the first specific objective of the Thesis, structured as follows: Section 2.2 explains the steps followed to characterize the astronomical tide; Section 2.3 describes the datasets, tools, and methods used to analyse global tide asymmetry; Section 2.4 describes the validation process; Section 2.5 discusses the results, and Section 2.6 draws the main conclusions of the developed research.

2.2. Methods

The method to characterize astronomical tide on a global scale has the following steps: (1) statistical analysis of astronomical tide; (2) clustering analysis of statistical tidal information; (3) selection of statistically representative astronomical tides types in the world; and (4) identification of the main tidal constituents that contribute to the total asymmetry in each type of tide.

The astronomical tide was parametrized according to the properties that relate tides to the transport of substances in estuaries, using the most recent version to date of the TPXO Global Tidal Solutions (TPXO9-atlas) (Egbert & Erofeeva, 2002) (`https://www.tpxo.net/`). TPXO9-atlas shows a spatial resolution (1/30°) suitable to characterize astronomical tide in coastal areas. For this purpose, *skewness* (γ_1) and *kurtosis* (g_2) parameters, which define probability density functions (PDFs), of 'tidal elevation time derivative' ($d\eta/dt$) were obtained. As the only hydrodynamic driver analysed in this study is the astronomical tide before its propagation through any estuary and without considering other phenomena, the tidal elevation time

derivative, representative of rising/falling tidal speed, can be associated to tidal currents in estuarine environments and, consequently, to the transport of substances (Hoitink et al., 2003). Despite the availability of 'barotropic tidal currents' from TPXO9-atlas, the tidal elevation time derivative was selected as the analysis variable. Indeed, sea level data are available from tide gauges, whereas tidal current records are scarce. In addition, tidal periodicity was included in the analysis through the *tidal regime* (TR) parameter, due to its influence on long-term transport in estuaries (Lesser, 2009). Then, K-means algorithm (Hastie et al., 2001) was applied to these tidal parameters (γ_1-g_2-TR) to cluster astronomical tides and obtain representative types (hereinafter, *ATtypes*) worldwide. Finally, the main tidal constituents that influences the asymmetric character of each *ATtype* were identified. This aspect allows tidal studies to be addressed, not only from a statistical approach but also using harmonic methods, which provides additional value to the graphic guide generated in this chapter. These results were validated with data from 757 worldwide tide gauges selected from the GESLA-2 (Woodworth et al., 2017) to cover the world's coastal areas.

2.3. Statistical and cluster analysis of global tide asymmetry

2.3.1. Data for classification and validation

Hourly time series of astronomical tide elevations were computed from harmonic constituents provided by the TPXO global and local tidal models developed by the Oregon State University (OSU) (Egbert & Erofeeva, 2002). These models represent an optimal least squares fit of the Laplace tidal equation to satellite altimetry data. In this study, TPXO9-atlas solution was used; this dataset combines the TPXO9.v1 global solution ($dx = 1/6°$) with local solutions in coastal areas, including the Arctic and Antarctic regions. TPXO9-atlas provides the M2, S2, N2, K2, K1, O1, P1, Q1, M4, MS4, MN4, and 2N2 harmonic constituents with a resolution of 1/30° and the

Mm, Mf, and S1 constituents with a resolution of 1/6° (for more details, see https://www.tpxo.net/global/tpxo9-atlas).

A selected set of tide-gauge records from the GESLA-2 (Global Extreme Sea Level Analysis Version 2) dataset (www.gesla.org) was used to validate the clustering results. GESLA-2 is a quasi-global dataset comprising high-frequency (hourly or more frequent) sea-level records from tide gauges distributed worldwide. Contributions to GESLA-2 come from 30 sources, 27 of which are considered public and 3 are private. The main contribution comes from the University of Hawaii Sea Level Center, which provides more than one-quarter of the total station years. A total of 39,151 station years are available from 1,355 records; i.e., an average of 29 years is available per record. However, the number of years varies between 1 year for many of the records and over 160 years in places such as Brest (France). The quality of this dataset has been controlled by each provider and has been demonstrated in its applications in previous studies (e.g., Hunter et al., 2017, Menéndez & Woodworth, 2010, Wahl et al., 2017). For a detailed description of this dataset, refer to Woodworth et al. (2017).

2.3.2. Tidal statistics

Probability density functions (PDFs) of the tidal elevation time derivative ($d\eta/dt$) were generated from tidal elevation time series, obtained from TPXO9-atlas, to characterize astronomical tide worldwide (Fig. 2.1a). A 19-year period was selected to build these $d\eta/dt$ time series and investigate the modulation of a nodal cycle. The highest spatial resolution of 1/30° offered by TPXO9-atlas models was used to represent the high variability induced by coastlines. However, a resolution of 1/6° was considered suitable for describing the tide in deep oceans, where there is no difference between 1/6° resolution TPXO9 base global solution and 1/30° TPXO9-atlas. Twenty bins were found to be adequate for representing the PDFs of astronomical tides worldwide.

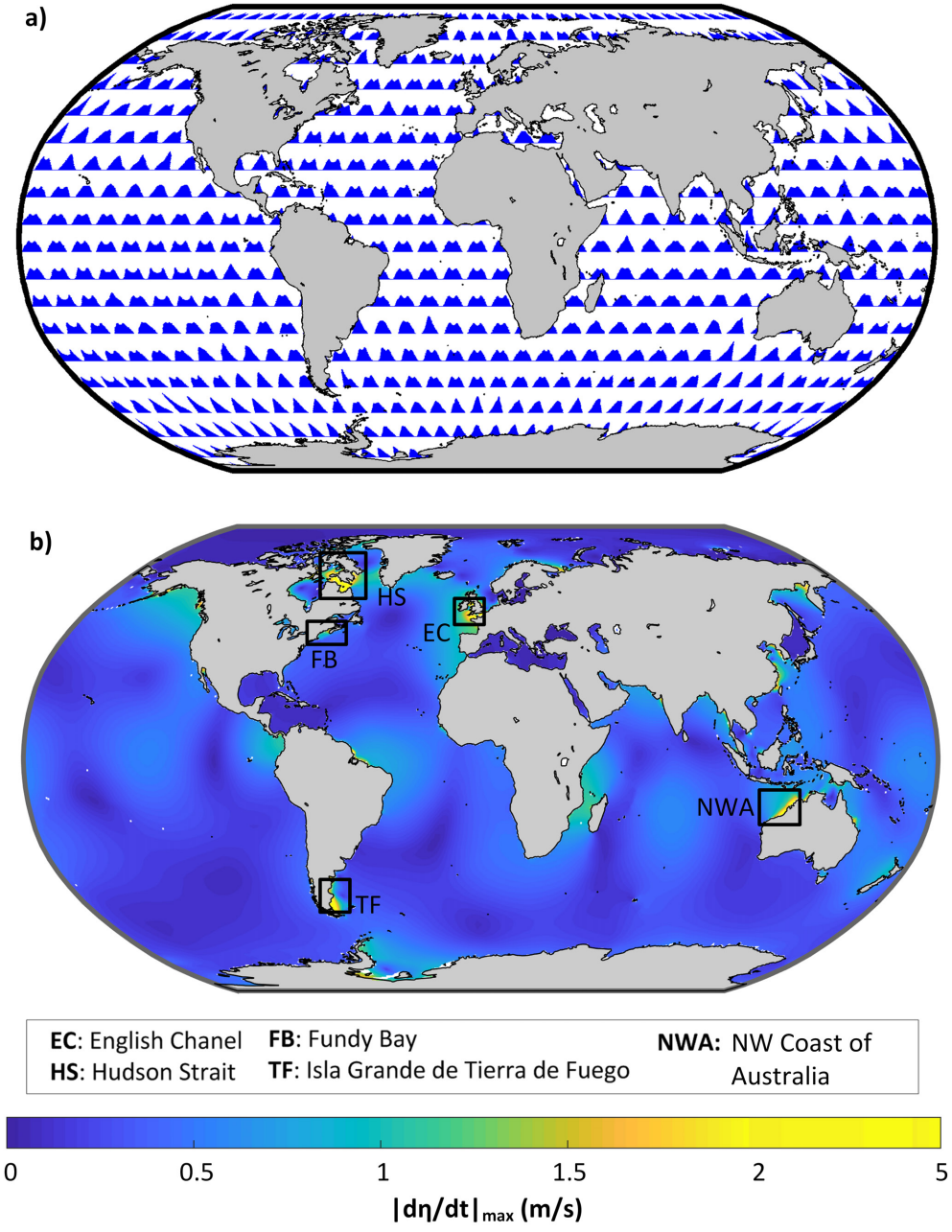

Figure 2.1: Global distribution of the tidal elevation time derivative ($d\eta/dt$): a) standardized probability density functions (PDFs) and b) maximum magnitude ($|d\eta/dt|_{max}$).

PDFs were standardized by the maximum magnitude of the tidal elevation time derivative ($|d\eta/dt|_{max}$) to find globally representative *ATtypes*. The maximum tidal elevation and, therefore, the rising/falling tidal speeds show large variations in different areas of the world. Fig. 2.1b shows the worldwide distribution of $|d\eta/dt|_{max}$ and identifies some of the areas with the highest rising/falling speeds. In general, tides in the open ocean are microtidal with small rising/falling speeds, while both the tidal range and the tidal speed can be significantly higher in coastal areas. Tidal effects can be regionally amplified, and the tidal range exceeds 8 m in specific areas of the world (Chan & Archer, 2003); the 5 regions with maximum tidal speed framed in Fig. 2.1b coincide with some of these areas. The maximum tidal speed reaches 5 m/s in the English Chanel (Dauvin, 2012), 3.5 m/s in the Hudson Strait (NGA, 2017), 3 m/s in Fundy Bay (Karsten et al., 2008), 2.4 m/s in Isla Grande de Tierra de Fuego (Bujalesky, 1997), and 1.5 m/s along the NW coast of Australia (Porter-Smith et al., 2004).

To avoid potential errors derived from the discretization in bins, the PDFs were not directly clustered; instead, two statistical parameters, namely, the skewness (γ_1) and kurtosis (g_2), defining the PDF shape were used. γ_1, calculated as the normalized sample skewness of the tidal elevation time derivative ($d\eta/dt = \eta'$) (Eq. 2.1), describes how one tail of a PDF is distributed over the other; i.e., it is a measure of the distribution asymmetry:

$$\gamma_1 \equiv \frac{\mu_3}{\sigma^3} = \frac{\frac{1}{\tau}\sum_{t=1}^{\tau}(\eta'_t - \bar{\eta'})^3}{[\frac{1}{\tau}\sum_{t=1}^{\tau}(\eta'_t - \bar{\eta'})^2]^{3/2}} \tag{2.1}$$

where μ_3 is the third sample moment about the mean, σ is the standard deviation, the square-root of the second sample moment about the mean, and τ is the number of data in the time series (hours in 19 years). This parameter was proposed by Nidzieko (2010) and then, it was used by Song et al. (2011) and adapted by Nidzieko & Ralston (2012) to characterize tides. If $\gamma_1 > 0$, the distribution is positively asymmetric, which implies that tidal falling speeds are more frequent than rising speeds; consequently, in shore tidal estuaries the flood phases are shorter than the ebb phases, and flood currents would be more intense (Fig. 2.2a). Estuaries with this

type of overall tidal asymmetry imposed on their mouths, where the tide is the key factor, can generally be associated with an accretive trend in such areas (Moore et al., 2009). If $\gamma_1 < 0$, the distribution is negatively asymmetric and is characterized by more intense speeds during the tidal fall than during the rise (Fig. 2.2c). Tidal estuaries subject to these asymmetries commonly show a tendency to export substances in their mouths (Ranasinghe & Pattiaratchi, 2000). These trends have been proven for sedimentary transport and, therefore, is expected for other substances such as plastic debris. It should be noted that γ_1 can vary (by increasing, decreasing, or even changing its sign) when tide propagates in an estuary depending on the estuarine morphology and other processes, such as river contributions. Consequently, an estuary can present, for instance, ebb dominance in its mouth and flood dominance inside (Nidzieko, 2010), or vice versa.

However, a PDF provides more information than that provided by γ_1. Three PDFs with positive asymmetries ($\gamma_1 = 0.8$), three symmetric PDFs ($\gamma_1 = 0$), and three PDFs with negative asymmetries ($\gamma_1 = -0.8$) are shown in Fig. 2.2. This figure illustrates how PDFs can take different shapes but have equal skewness. The missing information is provided with the kurtosis coefficient. The convention adopted in this study is known as excess kurtosis (g_2) corresponding to Eq. (2.2):

$$g_2 \equiv \frac{\mu_4}{\sigma^4} - 3 = \frac{\frac{1}{\tau}\sum_{t=1}^{\tau}(\eta'_t - \bar{\eta'})^4}{[\frac{1}{\tau}\sum_{t=1}^{\tau}(\eta'_t - \bar{\eta'})^2]^2} - 3 \tag{2.2}$$

where μ_4 is the fourth sample moment about the mean. Traditionally, there has been controversy in the interpretation of g_2 as a measure of *peakedness*. However, according to Balanda & MacGillivray (1988) and Westfall (2014), g_2 measures the concentration of data outside one standard deviation of the mean in either tail of the distribution; i.e., this parameter describes how the data are distributed in the areas between the peak and tails (in the areas known as *shoulders*) without saying anything about the peak. Fig. 2.2 shows how, regardless of the γ_1 value, the concentration of data in the shoulders moves towards the tails and increases its frequency with a decrease in g_2. Therefore, this parameter allows distributions with equal

γ_1 to be compared and refers to the frequencies of the higher rising/falling speeds of distributions with equal γ_1; i.e., g_2 would allow to associate tides with analogous asymmetries and similar maximum tidal currents to different transport capacities in estuarine environments.

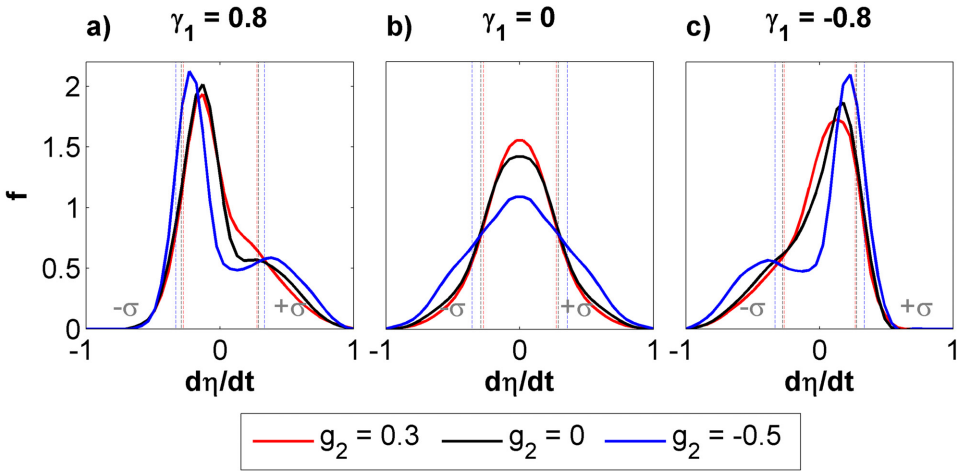

Figure 2.2: Examples of PDFs of $d\eta/dt$ with a) $\gamma_1 > 0$, b) $\gamma_1 = 0$, and c) $\gamma_1 < 0$; associated with $g_2 > 0$ (red), $g_2 = 0$ (black), and $g_2 < 0$ (blue). The σ boundaries for each PDF are shown as dotted lines.

Fig. 2.3a and b show the global distributions of γ_1 and g_2, respectively, where different tidal patterns can be identified according to PDF shapes. The largest γ_1, both positive and negative, are in very specific areas of the world that are relatively adjacent (warm-coloured areas for $\gamma_1 > 0$ and cold-coloured areas for $\gamma_1 < 0$ in Fig. 2.3a). It is worth noting that the most asymmetric tides are concentrated in the northern and southern areas of the Pacific Ocean, the area between the Gulf of Mexico and the Caribbean Sea, the coastal areas of the UK, the North Sea, the Mediterranean Sea, the Arabian Sea, the SW coastline of Australia, the China Seas and the Japan Sea. As shown in Fig. 2.3b, g_2 adopts average values of approximately -0.5 in these areas. In contrast, γ_1 close to zero dominate the central area of the Pacific Ocean, the Atlantic Ocean and the central area of the Indian Ocean, which coincide with the areas where g_2 adopts its relatively low values ($g_2 < -0.8$). The highest values of g_2 are around 0 and reaching 0.8 in some specific areas of the world, such as the Patagonian Shelf. Such g_2 values

are located in the proximity of the tidal amphidromic points where tidal amplitudes and, therefore, tidal speeds are null.

Fig. 2.3c shows a scatter plot of γ_1-g_2 and the frequencies of different types of PDFs around the world according to these parameters. Some considerations can be drawn from this figure. On the one hand, both parameters show well-defined limits, namely, -0.9 and 0.9 for γ_1 and -1.5 and 0.8 for g_2. On the other hand, symmetric distributions ($|\gamma_1| < 0.1$) can show kurtosis within the entire available range [-1.5, 0.8], indicating wide variations in the frequencies of $d\eta/dt$, i.e., from high frequencies for g_2 of approximately -1.5 to low frequencies for g_2 near 0.8. However, as the asymmetry of a distribution increases ($|\gamma_1| > 0.1$), the range of g_2 narrows around higher values [-0.2, 0.8]. Moreover, the most frequent tidal distributions in the world are symmetric ($|\gamma_1| < 0.1$) and have small kurtosis ($\gamma_1 < -0.8$), whereas this frequency decreases with increasing $|\gamma_1|$ and g_2.

To achieve a more complete description of tides worldwide, the tidal regime (TR) was included in this study. TR is calculated through the tidal form factor (F), defined as the ratio of the amplitudes of the O1 and K1 constituents to those of the M2 and S2 constituents (Defant, 1961):

$$F = \frac{K_1 + O_1}{M_2 + S_2} \tag{2.3}$$

F lower than 0.25 defines semidiurnal tidal regimes (S); F between 0.25 and 1.5 characterizes mixed semidiurnal tides (MS); F between 1.5 and 3 is representative of mixed diurnal tides (MD) and F higher than 3 reflects diurnal tidal characters (D). Fig. 2.4 shows the worldwide distributions of the tidal form factor and their associated tidal regimes (TRs). From a comparison between Figs. 2.3 and 2.4 the existence of a relationship between F and γ_1-g_2 can be detected. Previous studies, such as those conducted by Blanton et al. (2002), Byun & Cho (2006), and Hoitink et al. (2003), revealed asymmetries arising from some particular combinations of tidal constituents with specific tidal regimes, and Song et al. (2011) found a relationship between the tidal asymmetry (γ_1) generated in the open ocean and F.

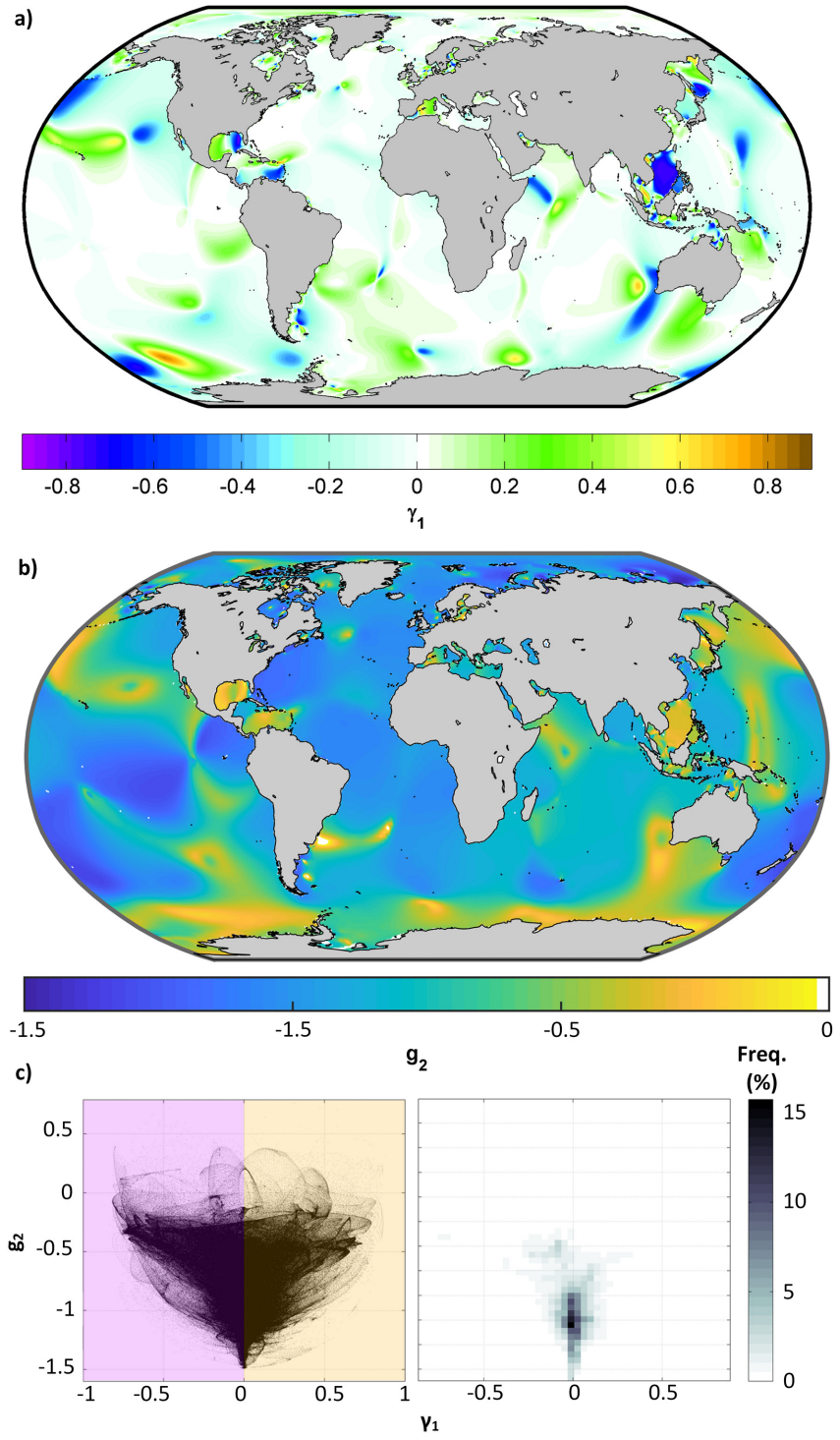

Figure 2.3: Statistical properties of the tidal elevation time derivative ($d\eta/dt$) worldwide: a) skewness (γ_1), b) excess kurtosis (g_2), and c) a scatter plot of γ_1-g_2 and the PDF frequency.

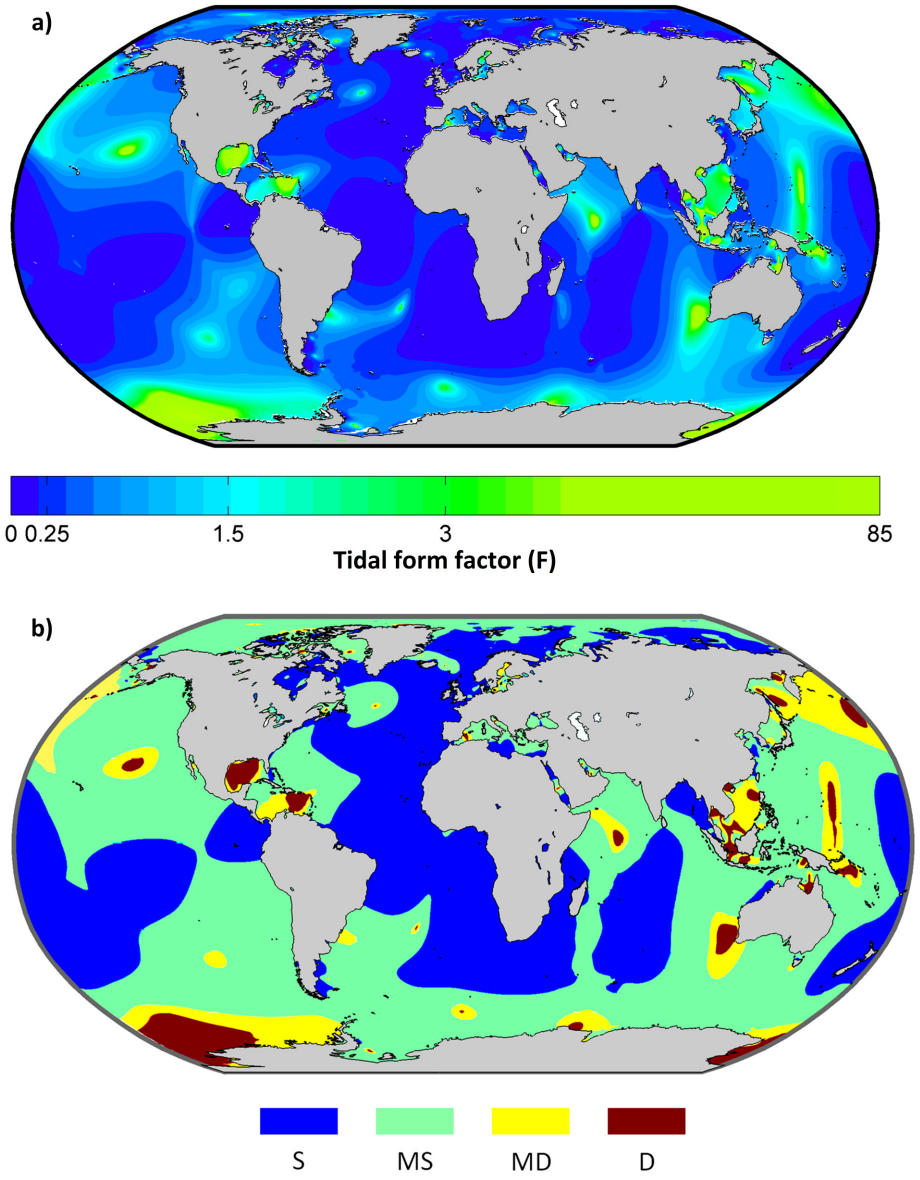

Figure 2.4: Global characterization of tidal periodicity: a) tidal form factor (F) and b) tidal regimes (TRs) (semidiurnal, S; mixed semidiurnal, MS; mixed diurnal, MD; and diurnal, D).

2.3.3. Clustering

The K-means algorithm was applied to γ_1, g_2, and TR to classify the astronomical tide into representative types worldwide. Due to the relationship among these variables, a joint clustering was performed. The K-means algorithm divides the starting dataset into a given number of subsets. Each subset is represented by a centroid or prototype and consists of the data that are best represented by this prototype (Hastie et al., 2001). In this study, K-means was initialized with the maximum dissimilarity algorithm (Camus et al., 2011c), and the parameters to be clustered were weighted according to the area that each triplet represents, $(1/30°)^2$ or $(1/6°)^2$. Once the centroids were found, the closest γ_1, g_2, and TR values of the original dataset and their associated standardized PDF were selected.

To find the optimum number of clusters (N) that best describes the *ATtypes* worldwide, K-means was preliminarily tested for different N values ranging between 2 and 98. A comparison between the original tide series and the synthetic time series reconstructed with the clusters derived from these classifications was performed using the efficiency coefficient (CE). CE was selected because it is the best objective function for reflecting the overall adjustment of a non-directional variable clustering output (Bárcena et al., 2015). CE is a normalized statistic developed by Nash & Sutcliffe (1970) that determines the relative magnitude of the residual variance (*noise*) and, therefore, reflects the accuracy with which the centroids estimate the original data (Eq. 2.4):

$$CE = \frac{\sum_1^n (O_i - C_i)^2}{\sum_1^n (O_i - \bar{O})^2} \tag{2.4}$$

where O_i is the *i-data* (γ_1, g_2 or TR) of the original series, C_i is the *i-data* (γ_1, g_2 or TR) of the representative centroid and n is the number of nodes where the tide is evaluated. CE ranges between $-\infty$ and 1.0. The level of agreement between two series is valued as excellent if CE is higher than 0.8, convenient if CE ranges between 0.6 and 0.8, poor if CE is lower than 0.5, and unacceptable if CE is lower than 0.

Fig. 2.5a shows the scatter plots of γ_1-g_2 associated with each TR from TPXO9-atlas (colour dots) and from the clustering (dots inside the black circles) for N equal to 9, 16, 25, and 36. An increasing trend is observed for the original representativeness with the number of clusters. However, in the case of 36 clusters, centroids begin to be similar for the most frequent distributions (symmetric with small kurtosis), reducing the improvement in representativeness. N equal to 25 was determined to be adequate because CE exceeds 0.8 for the three analysed parameters (γ_1, g_2, TR) and because the improvements are no longer significant for higher N values (Fig. 2.5b).

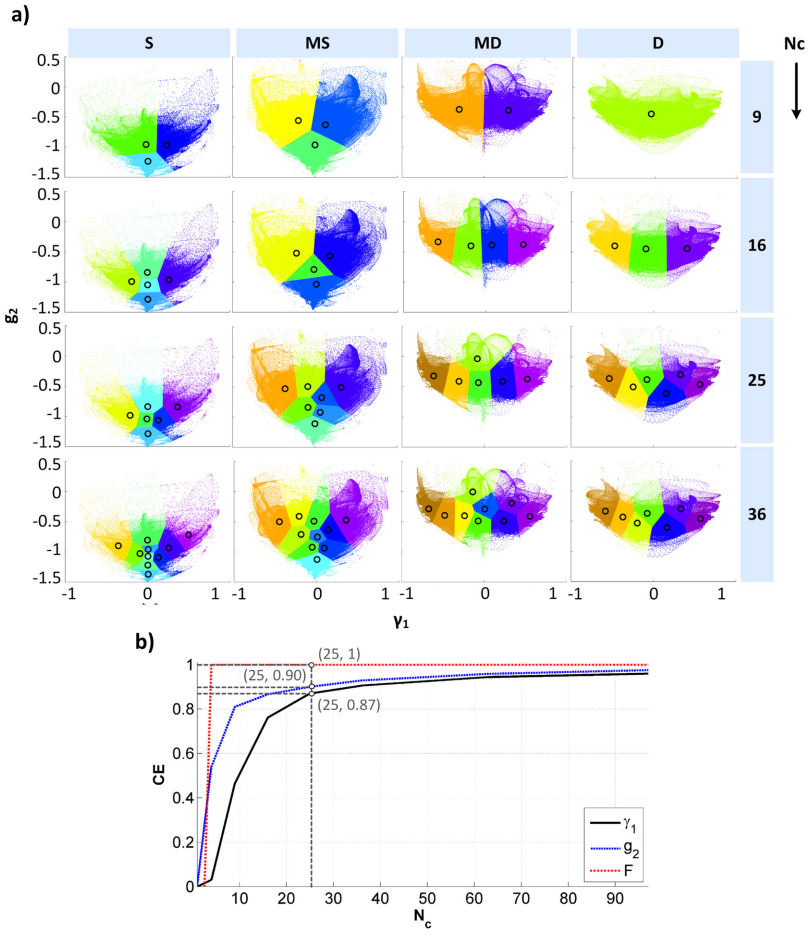

Figure 2.5: Representativity of the number of clusters (N): a) scatter plots of γ_1-g_2 associated with different TR from TPXO9-atlas (colour dots) and from the clustering (dots inside the black circles) for different N and b) efficiency coefficient (CE) of γ_1/g_2/TR.

2.3.4. *ATtypes* and contribution of combinations of tidal constituents

Fig. 2.6a shows the centroids (C_i) from clustering sorted from the highest to the lowest value of γ_1. Each C_i is defined in terms of the shape of its PDF of $d\eta/dt$ (i.e., its γ_1 and g_2 coefficients) and its tidal regime (S, MS, MD, and D) and represents an astronomical tide type (*ATtype*). Fig. 2.6b shows the geographical distribution of the 25 identified *ATtypes*.

The results indicate that symmetric tides ($|\gamma_1| < 0.1$; from C9 to C19) dominate 85.3% of the world's open ocean, as well as 77.4% of all coastal areas. Indeed, symmetric tides correspond mainly to the mixed semidiurnal regime (approximately 60% of symmetric tides for the open ocean and coastal areas) and semidiurnal regime (approximately 36% and 30% of symmetric tides for the open ocean and coastal areas, respectively). A significant part of the Atlantic Ocean, including the East Coast of the USA, the western coast of Spain, and large proportions of the Brazilian and African coasts, exhibits these *ATtypes* (light-coloured areas in Fig. 2.6b). Conversely, 14 *ATtypes* show a clear asymmetric component ($|\gamma_1| > 0.1$), where the greatest asymmetries ($|\gamma_1| > 0.5$) occur in the diurnal and mixed diurnal regimes (i.e., C1, C2, C24, and C25). On the one hand, positive asymmetries (from C1 to C8) are found in 6.5% of the open ocean, and they make up 11.3% of the coastal areas throughout the world. The western Gulf of Mexico, the northern Caribbean Sea, the Mediterranean coast of France, part of the Spanish coast, and the south coast of Australia are good examples of these *ATtypes* (warm-coloured areas in Fig. 2.6b). The estuaries located in these coastal areas display flood dominance in their mouth, but this dominance can be affected or modified as a result of the estuarine morphology as the tide propagates into them. On the other hand, negative asymmetries (from C20 to C25) cover 8.2% of the open ocean and 11.3% of all coastal areas. The southern Caribbean Sea, the north coast of Greenland, the South China Sea, and the west coast of Australia are clear examples of areas with negative tidal asymmetries, and the estuaries hosted within these areas exhibit ebb dominance in their outermost area (cold-coloured areas in Fig. 2.6b).

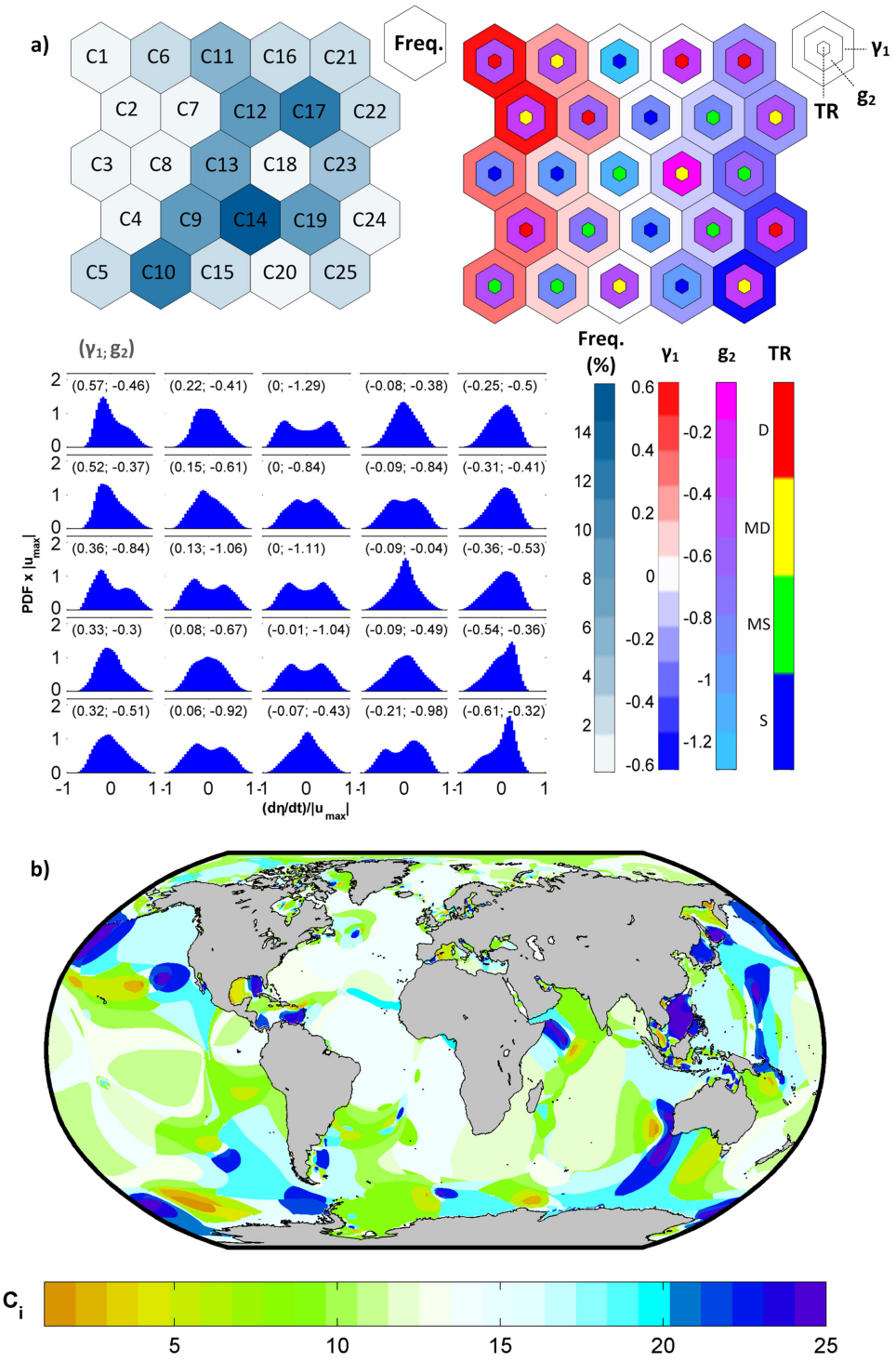

Figure 2.6: Global *ATtypes* from clustering: a) statistics of the centroids (C_i; *Freq*: frequency, γ_1: skewness, g_2: kurtosis, TR: tidal regime, PDF: probability density function) and b) worldwide distribution of C_i.

Moreover, the main tidal constituents that contribute to the total asymmetry in each *ATtype* were identified. To this end, the method proposed by Song et al. (2011) was applied to 25 clusters derived from TPXO9-atlas. At each of these clusters, the contributions (β_i) to γ_1 of the different combinations (pairs or triplets) of tidal constituents that can influence the asymmetry were calculated, i.e., the constituents for which the following frequency ratios $2\omega_1 = \omega_2$, or $\omega_1 + \omega_2 = \omega_3$ are met. Finally, the subset of tidal constituents that best explains the γ_1-g_2 pair was selected.

Fig. 2.7a shows the pairs and triplets of tidal constituents that contribute to tidal asymmetry as well as the value of each contribution (β_i), expressed as a percentage, to each *ATtype* (C_i). Each C_i on the *y-axis* is represented by a colour associated with a tidal regime, namely, blue for S, green for MS, yellow for MD, and red for D. It is worth noting that there are combinations that contribute with the same orientation as the characteristic skewness (γ_1) of each C_i (warm-coloured cells in Fig. 2.7a), while others counteract γ_1 (cold-coloured cells in Fig. 2.7a). The sum of all contributions results in the representative γ_1. As the figure shows, the symmetric tides ($|\gamma_1| < 0.1$) have a greater number of combinations that contribute a similar percentage, although with different orientations, to the resulting skewness and that all contributions are balanced between them, thereby cancelling out γ_1. Conversely, tides with a significant asymmetric component ($|\gamma_1| > 0.1$) show a clear main contribution. In general, the astronomical triplet O1/K1/M2 dominates the D, MD, and MS regimes, while the P1/K1/S2 and M2/M4 combinations play a secondary or tertiary role in the asymmetry. In the S regime, the main contribution comes from M2/M4.

Among the set of analysed combinations, the subset of constituents that best explain the γ_1-g_2 pair was selected (framed in grey). This analysis indicates that a small number of tidal constituents plays a role in the definition of γ_1; however, a greater number is necessary to characterize g_2. Fig. 2.7b shows the agreement between the total skewness and excess kurtosis resulting from the classification (γ_1-g_2) and the same statistics obtained from the main tidal constituents (γ_1'-g_2'), with R^2 exceeding 0.9 in both cases.

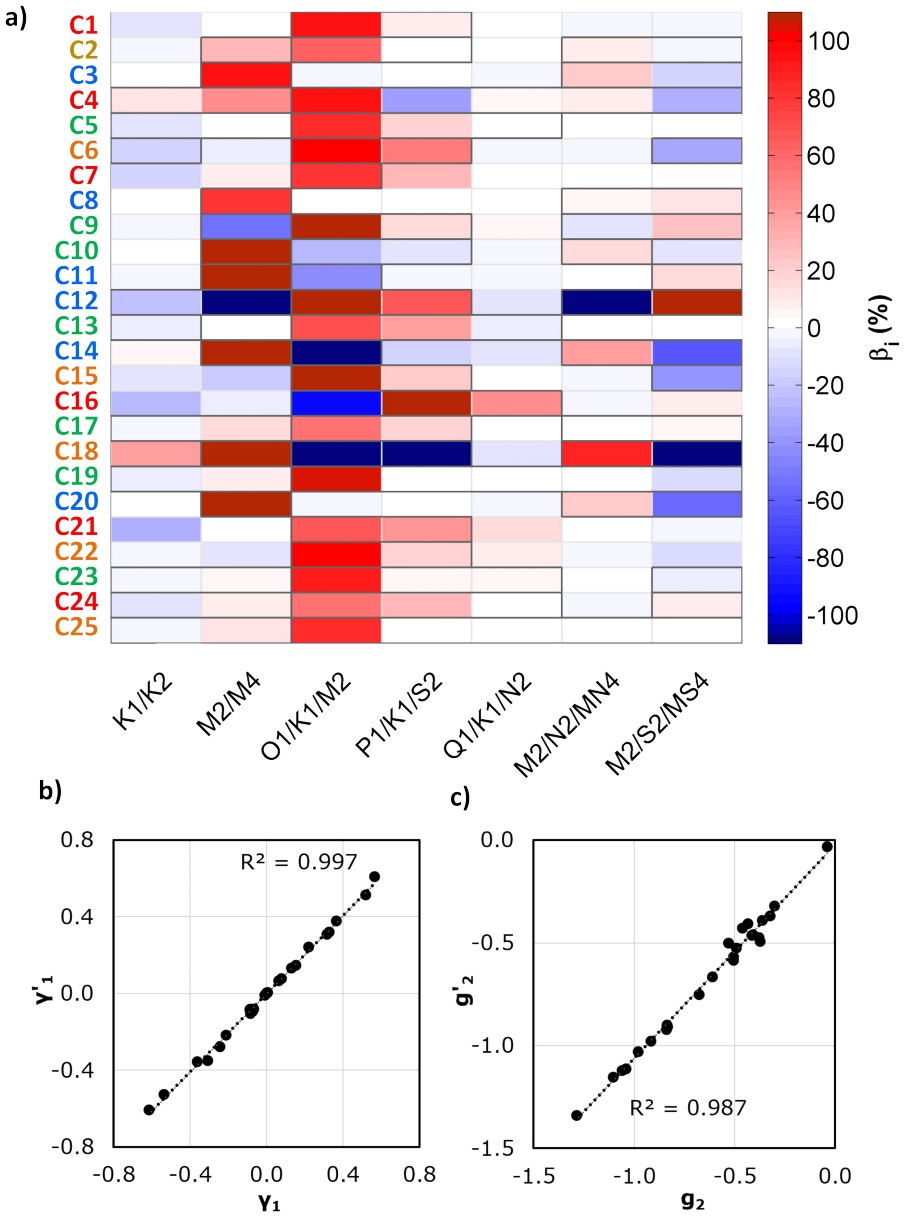

Figure 2.7: a) Contributions (β_i) of the combinations of tidal constituents to the skewness of the *ATtypes* (C_i) (the greatest contributions that explain the γ_1-g_2 pair are framed in grey); b) scatter plot of γ_1 (from clustering)-γ_1' (from the main tidal constituents that explain the PDF shape), and c) scatter plot of g_2 (from clustering)-g_2' (from the main tidal constituents that explain the PDF shape). Each C_i on the *y-axis* is represented by a colour associated with a tidal regime, namely, blue for S, green for MS, yellow for MD, and red for D.

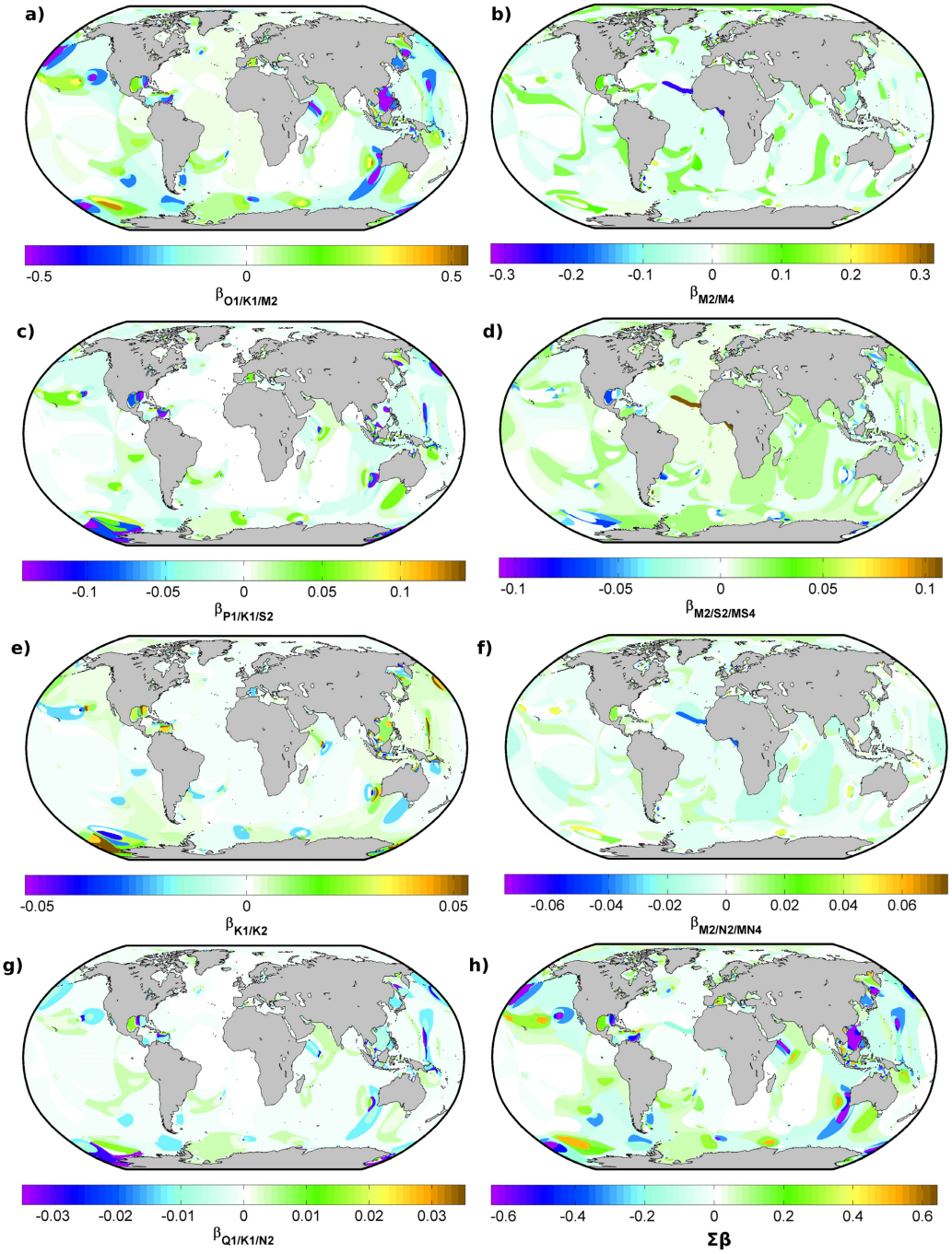

Figure 2.8: Global distributions of the contributions (β_i) of the main tidal constituents responsible for the asymmetry of the *ATtypes*: a) O1/K1/M2, b) M2/M4, c) P1/K1/S2, d) M2/S2/MS4, e) K1/K2, f) M2/N2/MN4, h) Q1/K1/N2, and h) sum of all contributions ($\sum \beta$). Note the differences in the colour scales.

Fig. 2.8 shows the global distributions of the contributions (β_i) of the main tidal constituents responsible for the asymmetry of each of the identified *ATtypes*. It is noticeable that the O1/K1/M2 and M2/M4 combinations have contributions with greater intensities. The contributions of P1/K1/S2 and M2/S2/MS4 are less significant by a factor ranging from 3 to 5, and the contributions of K1/K2, M2/N2/MN4, and Q1/K1/N2 are characterized by a lower order of magnitude. The main contributions of O1/K1/M2 and M2/M4 were estimated to account for 95% and 5%, respectively, of the tidal asymmetric areas in the open ocean. Indeed, the maps presented in Fig. 2.8a ($\beta_{O1/K1/M2}$ from clustering), Fig. 2.8h ($\sum \beta$ from clustering), and Fig. 2.3a (γ_1 from TPXO9-atlas) are very similar.

2.4. Validation

The classification results were validated with 757 selected tide-gauge records from GESLA-2. To ensure the representativeness of the external tide, one record was selected per tide gauge located at a distance of less than 10 km from the nodes where the clustering outputs are available. On the one hand, the PDFs of the $d\eta/dt$ from clustering were compared with those obtained from the tide-gauge records by applying the CE statistic (Eq. 2.4). Since PDFs depend on the analysed time window and tide gauge records cover different time periods, harmonic analysis of each record was performed to then reconstruct the $d\eta/dt$ series over the same 19-year period. On the other hand, the degree of matching between the tidal regimes from both sources was evaluated.

Regarding the comparison among the PDFs, Fig. 2.9 shows the degree to which the outputs from clustering represent the tidal conditions recorded at the tide gauges. A total of 684 tide gauges are represented in blue, which is associated with an excellent characterization (CE >0.8); 54 tide gauges are shown in green, indicative of good agreement ($0.6 < CE \leq 0.8$); 7 tide gauges are shown in yellow, which reflects poor representativeness ($0.5 < CE \leq 0.6$); 14 tide gauges show acceptable but worse than poor agreement ($0 < CE \leq$

0.5) and are represented in orange; and finally, 1 tide gauge was represented in red, indicating unacceptable representativeness (CE$\leq$ 0). Hence, 97% of the clustered PDFs characterize the PDFs of the world's coastal areas well or very well, and only 3% exhibit poor or unacceptable representativeness. As an example of the classification ability to characterize tides even in complex tidal areas, Fig. 2.9b shows the Adriatic Sea. In this region, where up to 10 different *ATtypes* with γ_1 ranging from -0.36 to 0.32 are observed, the validation verifies the classification results with an 'excellent' degree.

The main reason for the disagreement between the clustered PDFs and those obtained from the tide-gauge records is not related to the type of PDF but rather to the geometric complexity of the area surrounding the represented node. Fig. 2.9 shows that the classification represents different types of distributions with a high level of agreement, such as symmetric bimodal distributions (e.g., 'c3' - CE = 0.93, and 'e2' - CE = 0.99), asymmetric bimodal distributions (e.g., 'd4' – CE = 0.87) and asymmetric unimodal distributions (e.g., 'f2' – CE = 0.98). Fig. 2.9 shows the areas 'c', 'd', 'e', and 'f' that represent the main problem areas with regard to the representativeness. Area 'c' corresponds to the East Coast of the USA ranging from Chesapeake Bay to the vicinity of Portland (Maine, USA). This area contains the unique tide gauge that the clustering classifies with an unacceptable level ('c1' – CE = 0). The reason for this result is the location of the tide gauge in a shallow and narrow area on the NW coast of Nantucket Island (USA), where different types of tides converge (C5, C13, and C23 centroids with γ_1 values equal to 0.32, 0, and -0.36, respectively). Area 'd' corresponds to the coastlines of Ireland and the UK, where tide gauges with low levels of concordance are observed (e.g., 'd1' – CE = 0.39 and 'd2' - CE = 0.50). Due to the complex geometry of the Northern Europe coastlines (Irish Sea, the English Channel, etc.) and the effect of this geometry on the tides, almost half (45.5%) of the tide gauges located in these areas show CE values lower than 0.6. In area 'e', located along the northern Brazilian coast, two tide gauges are inadequately characterized due to their locations in very shallow-water areas that local TPXO models fail to describe (e.g., 'e1' – CE

= 0.23). In area 'f' (Japan), there are a few points with a low classification representativeness since they are embedded in narrow areas (e.g., 'f1' – CE = 0.31). Despite all of the abovementioned factors, it can be seen in Fig. 2.9 that even in these problematic areas, the number of nodes with a good or excellent level of agreement predominates over the number of nodes with poor or worse concordance.

Fig. 2.10 shows the tidal regimes (TRs: S in blue, MS in green, MD in yellow, and D in red) obtained from the selected tide gauges (outer ring) and those according to the performed classification (inner circle). In addition, the mismatched points are highlighted with a violet ring. The TRs coincide in 87% of the locations compared, while there is one regime difference in the remaining 13%. The main areas in which these mismatches are concentrated are the Gulf of Mexico and the East Coast of the USA (area 'a1' in Fig. 2.10), and the west coast of Japan (area 'a2'). Fig. 2.10b shows a scatter plot between the tidal form factors (F) obtained from the tide-gauge records and those obtained from TPXO9-atlas, where the mismatched points are highlighted with a red circle. This figure verifies that most of the points where the clustered TRs do not coincide with the recorded TRs are in the transition areas between two regimes.

As mentioned in Section 2.2, the $d\eta/dt$ variable was chosen for this study instead of the tidal current (u) because of its validation possibilities and since long tidal current records for the entire globe are scarce. To check the similarity between these two variables in coastal areas, the γ_1 and g_2 values of the 19-year time series of both the $d\eta/dt$ and u in the average direction of tidal propagation (both variables reconstructed from TPXO9-atlas) were compared at the validation points. Fig. 2.11 shows the correlations between the two statistical descriptors for both variables (R^2 is equal to 0.73 and 0.77 for γ_1 and g_2, respectively); therefore, the suitability of selecting $d\eta/dt$ to classify ocean tides according to transport capacities in the world's coastal areas is verified.

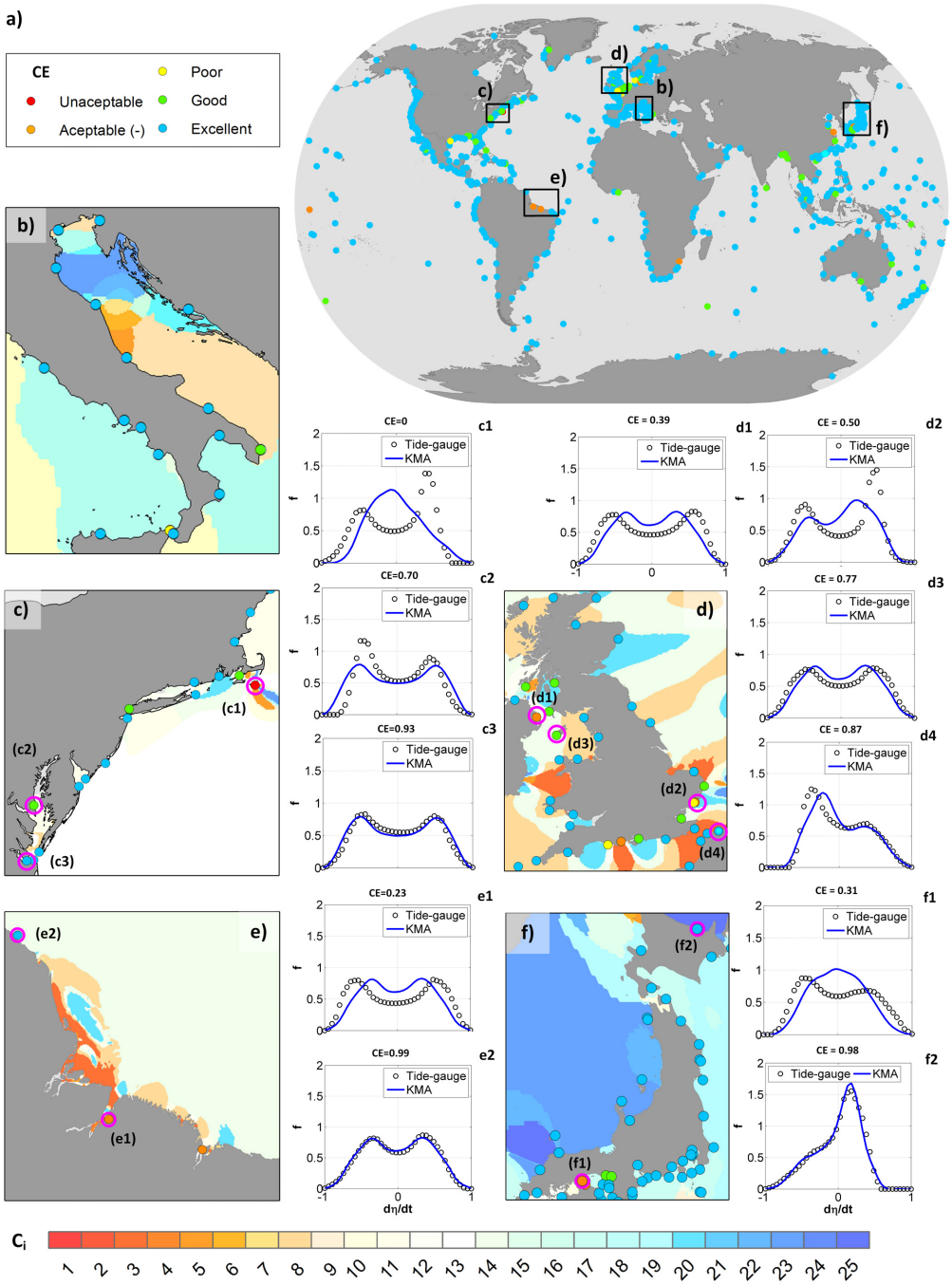

Figure 2.9: Efficiency coefficient (CE) between the PDFs from clustering and the PDFs from the tide-gauge records worldwide (a), and in the following areas: the Adriatic Sea (b), the central East Coast of the USA (c), the coastlines of Ireland and the UK (d), the northern Brazilian coast (e), and the Japan coast (f). Some examples of PDFs that show different levels of agreement in these areas are labelled c_i, d_i, e_i, and f_i.

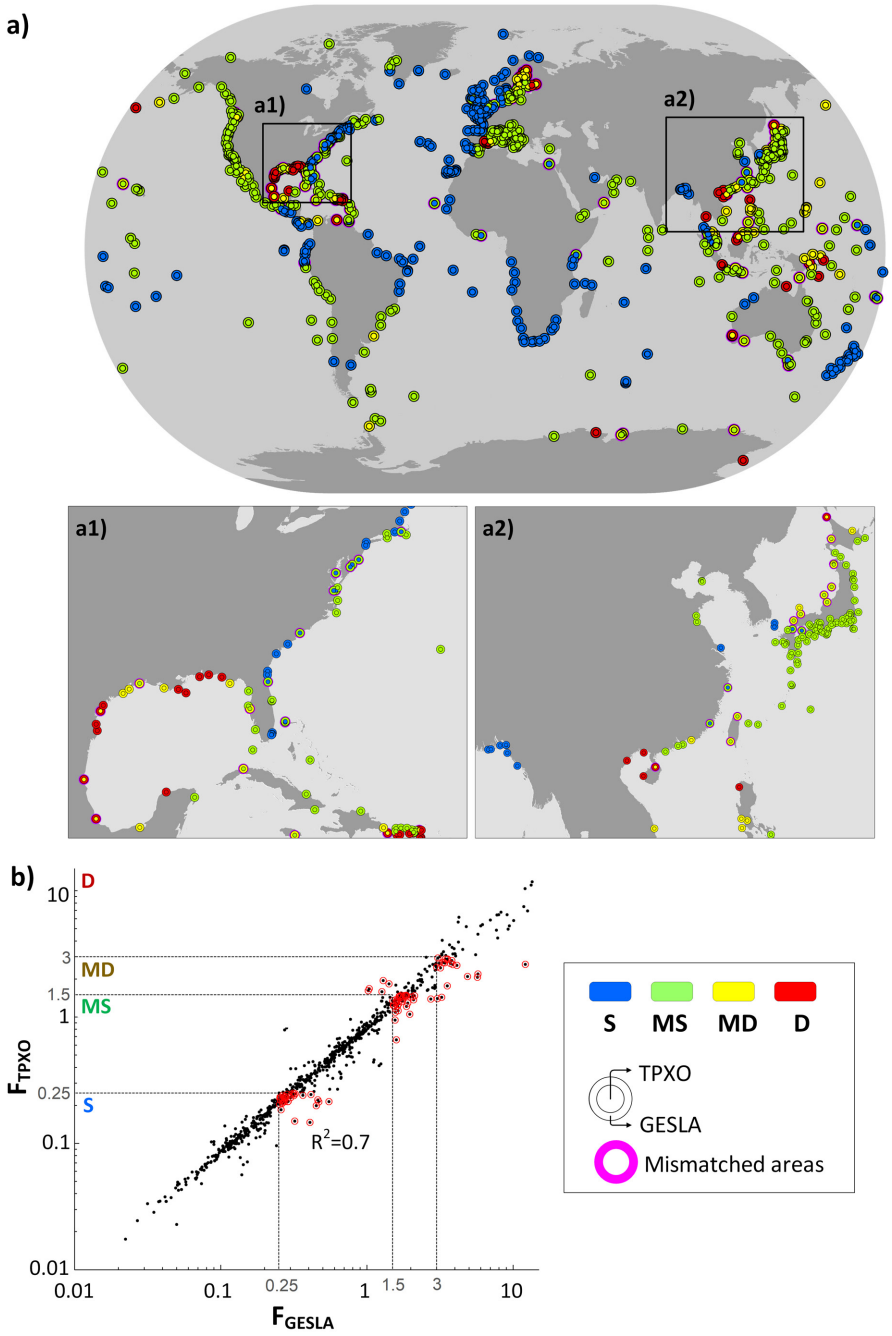

Figure 2.10: Matched/mismatched indicators between the tidal regimes (TR) from clustering and the tide-gauge records worldwide (a) and in the following areas: the Gulf of Mexico and southeast coast of the USA (a1), and the Sea of Japan and East China Sea (a2); b) scatter plot between the tidal form factor (F) from tide gauges (GESLA-2) and from TPXO9-atlas (mismatched points are highlighted in red).

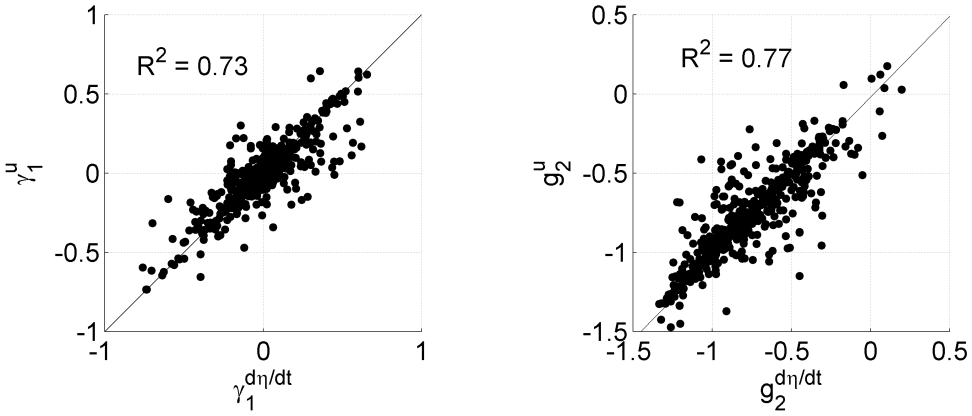

Figure 2.11: Relationships between the statistical parameters γ_1 and g_2 for $d\eta/dt$ and u (tidal currents in the average direction of tidal propagation).

The above analysis shows that a very good tidal characterization dominates the global map, even in the most problematic areas. Hence, it can be concluded that the developed tidal classification represents the astronomical tide conditions throughout the world's coastal areas with high reliability.

2.5. Discussion

It has been effectively demonstrated that tidal asymmetry evolves over relatively short distances in coastal, estuarine, and river environments and influences the behaviours of these areas (Hoitink et al., 2006). The characterization of tidal asymmetry in open oceans is a very relevant aspect for the study of estuarine processes since tidal asymmetry constitutes the boundary condition that influences the propagation of the tidal wave throughout an estuary and, consequently, the transport processes that occur within them, as well as estuarine-ocean exchanges (Ranasinghe & Pattiaratchi, 2000). In this study, the most recent version of the TPXO Global Tidal Solutions (TPXO9-atlas), statistical methods (PDFs), and clustering and harmonic approaches were used to effectively describe the tidal asymmetry in coastal areas before the propagation of tides into estuaries. Thereby, results of this study facilitate research from complementary

statistical and harmonic perspectives (Guo et al., 2019) and simplify the study of the evolution of tidal asymmetry when a tide propagates through any estuary in the world by analysing only the responsible constituents.

The high quality of the information provided by the global classification of tides was demonstrated with the excellent agreement obtained in 97% of the nodes in which the PDFs were compared (Fig. 2.9) and in 87% of the nodes in which the tidal regimes were checked (Fig. 2.10), what also confirms the accuracy of the new TPXO9-atlas solution to characterize the coastal tides. The common denominator of the few nodes in which the distributions are not well characterized is their location, i.e., areas exhibiting a complex geometry (areas too narrow or having significant depth changes, such as the interiors of estuaries) that even the local models of TPXO9-atlas do not describe with adequate precision. These features have significant local effects on tidal conditions, since they can induce overtides and compound tides which influence the resulting asymmetry and cannot be adequately reproduced by the TPXO tidal models, or generate areas where different tidal typologies converge. Therefore, to characterize the tide anywhere in the world, it is recommended to use those nodes which are far enough from these complex areas and propagate the tide from well characterized areas if necessary.

As results show, symmetric tides cover 77.4% of the world's coastal areas, and most of these tides correspond to the mixed semidiurnal regime (60%), followed by the semidiurnal regime (30%) (Fig. 2.6). The tidal asymmetries in the estuaries located in these areas depend exclusively on overtides and compound tides generated during inland propagation without being conditioned by external tidal features.

On the other hand, although asymmetric tides constitute a smaller percentage, identifying them correctly is essential for describing any estuarine process dependent on tidal hydrodynamics, since the identification of asymmetric tides can have very different consequences from the predictions derived from an assumption of tidal symmetry. The most asymmetric tides, both positive and negative, are concentrated in relatively adjacent areas of

the world and mainly correspond to diurnal and mixed diurnal regimes (Fig. 2.6). The reason for these maximum tidal asymmetries in the open ocean is fundamentally the interactions among the main tidal constituents. The astronomical triplet O1/K1/M2 dominates in the D, MD, and MS regimes, followed by the P1/K1/S2 and M2/M4 combinations, whereas the main contribution to the S regime comes from the M2/M4 constituents (Fig. 2.7a); these results are consistent with the findings of Song et al. (2011).

Positive asymmetries characterize 11.3% of the world's coastal areas and influence the behaviours of estuaries dominated by tides that exhibit flood dominance in their mouths. A good example of this type of environment is the Dee estuary (UK), which shows an overall flood dominance that is likely induced by positively asymmetric ocean tides, which explains the known historical changes in the estuarine morphology (large-scale accretion over the last 2 centuries) (Moore et al., 2009).

Negative asymmetries are also present in the same percentage as positive asymmetries (11.3%) and can influence estuaries with an external ebb dominance. Ranasinghe & Pattiaratchi (2000) studied three West Australian inlets whose mouths are dominated by ocean tides with long-term negative asymmetry. The authors showed that, despite the alternation of ebb- and flood-dominated periods, over a period of one year, the net sediment transport through the entrances of these systems was directed towards the sea. Nidzieko (2010) investigated three California estuaries with negative tidal asymmetries imposed in their mouths and demonstrated that such asymmetries increase or decrease (according to the estuarine morphology) as the tide propagates landward and, therefore, affects several internal processes. Similarly, Ferrarin et al. (2015) and Finotello et al. (2019) point out that the inlet region and the main channels of Venice lagoon were dominated by the negative tidal asymmetry of the North Adriatic Sea. Ferrarin et al. (2015) obtained the annual value of γ_1 in the period 1976-2014 with the data of a tide-gauge station located 15 km offshore from the Venice lagoon inlets and verified that γ_1 oscillated around an average value of -0.09, coinciding with the results of the classification carried out in this study. As

these authors concluded, although tidal asymmetry develops according to the estuarine morphology as the tide propagates, the asymmetry imposed at the mouth of the estuary must first be overcome.

Several authors, such as Ballent et al. (2012), Browne et al. (2010), Costa et al. (2011), Eerkes-Medrano et al. (2015), Galgani et al. (2000), have suggested that the study of the plastic debris transport and fate within estuaries can be assimilated to sediment transport. Therefore, the classification of astronomical tide carried out in this chapter constitutes a key point to initiate studies in the field of plastic debris on an estuary scale.

2.6. Conclusions

This research addresses the study of tidal asymmetry on a global scale, based on a statistical approach adequate when asymmetry results from the interaction among multiple tidal constituents. Astronomical tide has been classified by applying a clustering K-means technique to the TPXO9-atlas solution, a complete (15 tidal constituents) barotropic tidal solution with a high spatial resolution (1/30°) to describe the tidal conditions in the vicinity of coastal areas. Accordingly, this study increased the knowledge available in the current state of the art about the long-term tidal distribution on a global scale.

Twenty-five astronomical tide types were identified (through PDFs of the tidal elevation time derivatives) and the main tidal constituents associated with each tide type were estimated. The classification was validated by comparing the outputs with the data from 757 tide gauges strategically distributed to cover the world's coastal areas. The results showed that both the open ocean and coastal areas are dominated by symmetric tides (85.3% and 77.4%, respectively); negative asymmetries characterize 8.2% of the open ocean and 11.3% of coastal areas; and positive asymmetries cover 6.5% of the open ocean and 11.3% of coastal areas. In general, the astronomical triplet O1/K1/M2 controls the tidal asymmetries in the diurnal, mixed diurnal, and mixed semidiurnal regimes, whereas the M2/M4 pair of constituents is the

combination that stands out for most semidiurnal regimes.

The developed classification represents a guiding framework regarding the types of astronomical tide according to their asymmetry (orientation and degree) and periodicity on a worldwide scale. This framework can be used as a reference for further research on the transport of substances (e.g., sediments, nutrients, plastics, oil spills, and chemicals) in estuaries, as the asymmetry imposed at the mouth of an estuary may influence most internal transport processes.

Chapter 3

On the role of ocean tidal asymmetry and estuarine geometry in plastics fate within estuaries [2]

3.1. Introduction

This chapter explores the relationship between tidal deformation arising from propagation, the asymmetry shown by the ocean tide at the mouths of estuaries, and the morphological features of these environments. Furthermore, the effect of these interactions on plastic debris accumulation within tide-dominated estuaries is probabilistically assessed. To achieve these objectives, a series of analyses, which are based on the application of the hydrodynamic and particle tracking modules of the Delft3D numerical model to study estuaries that describe different morphologies, is proposed. The study estuaries were defined according to the criteria of Speer & Aubrey (1985). The high-resolution (1/30°) classification of ocean tidal asymmetry obtained in the previous chapter was used to build the boundary conditions

[2]The findings of this chapter have been submitted for publication to *Estuarine, Coastal and Shelf Science*.

of the numerical models. The probabilistic analysis of the Lagrangian model results allows us to draw some general considerations about the role of ocean tidal asymmetry and estuarine morphology on plastic debris accumulations within tide-dominated estuaries.

This chapter responds to the second specific objective of the Thesis and is organized as follows: Section 3.2 describes the study estuaries, astronomical tide dataset to define boundary conditions, Delft3D numerical model, and setup of the numerical computations used in this research; Section 3.3 describes the main obtained results; Section 3.4 discusses these results; and Section 3.5 outlines the main conclusions derived from this research.

3.2. Material and methods

The proposed methodology used to assess the effect of ocean tidal asymmetry and estuarine morphology on tidal propagation and plastic debris accumulation within tidal estuaries is based on numerical simulations of a series of hydrodynamic and particle tracking scenarios in estuaries with different geometries. Fig. 3.1 shows an overview of the applied methodology.

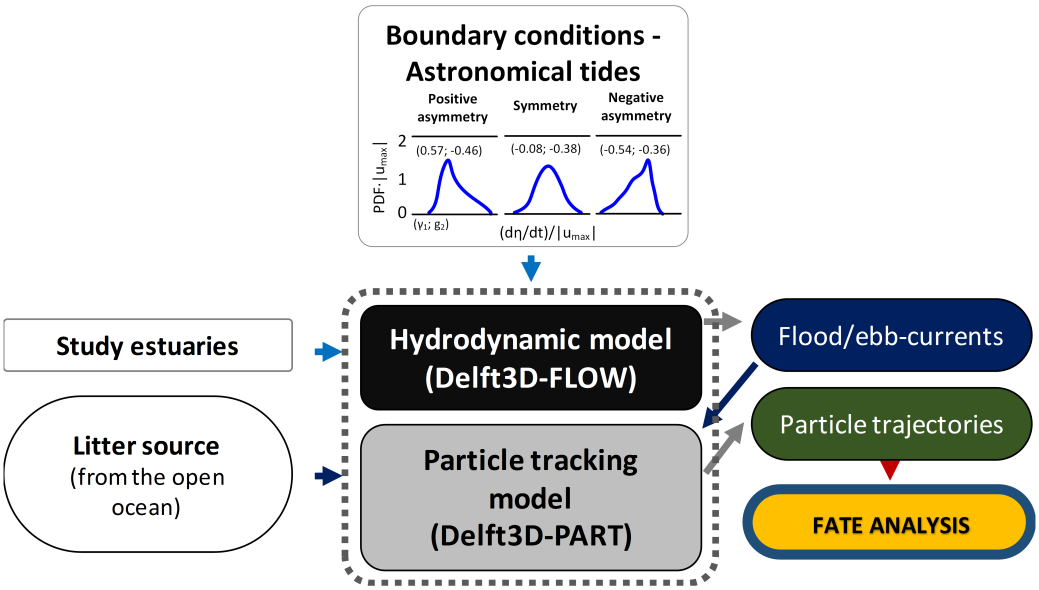

Figure 3.1: Flowchart of the model structure and data inputs and outputs.

The hydrodynamic (FLOW) and particle tracking (PART) modules of the Delft3D numerical model were applied offline to simulate plastic debris transport and fate within estuaries. Delft3D-FLOW (Hydraulics, 2018a, Roelvink & Van Banning, 1995) is an integrated flow modelling system that solves the Navier-Stokes equations for shallow water environments with the hypothesis of hydrostatic pressure and the Boussinesq approach. The model includes robust, accurate, and computationally efficient algorithms to simulate wetting-drying in intertidal flats (Lesser et al., 2004). Delft3D-PART (Hydraulics, 2018b) simulates substance transport processes using forcings from the FLOW module and a particle tracking method based on a random walk method (Rubinstein & Kroese, 1981). Substances are represented by a set of particles characterised by a certain density. Delft3D-PAR enables simulation of the transport of conservative substances by selecting the *Tracer Model* or hydrocarbons and their degradation processes using the *Oil Model*. The *Oil Model* also allows us to consider transport processes affected by wind drag additional advection or the beaching effect by defining a stickiness probability. The set of particles moves by the combined action of currents and wind (deterministic displacement) and turbulent diffusion (random displacement).

Delft3D is a widely applied state-of-the-art model used to evaluate different processes in complex estuarine systems. The Delft3D-FLOW module has been applied to several studies that have confirmed its ability to simulate hydrodynamics within estuaries (e.g., Abascal et al., 2017, Bárcena et al., 2016, García Alba et al., 2014, Iglesias & Carballo, 2010, Jiménez et al., 2014, Zhou et al., 2014). This fact and the possibilities offered by the Delft3D-PAR module to evaluate the transport of plastics (van Utenhove, 2019) have informed the selection of this model to perform this study.

3.2.1. Study estuaries

This study examines shallow well-mixed and tide-dominated estuaries where tidal flats have been discovered at low tide and channels, where most of the water flows during the ebb and flood phases, remain always flooded.

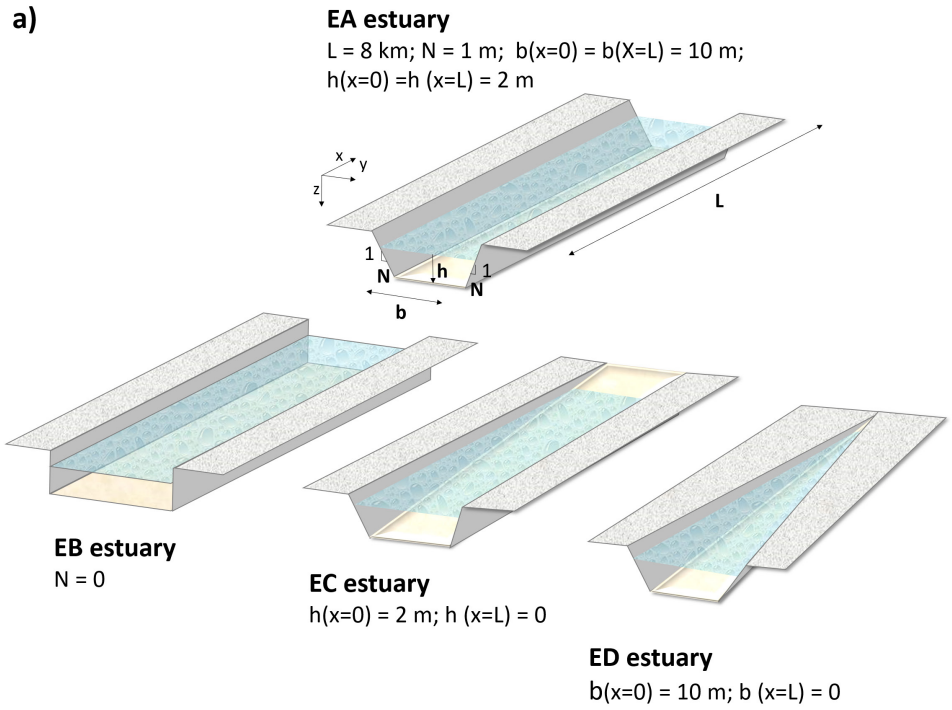

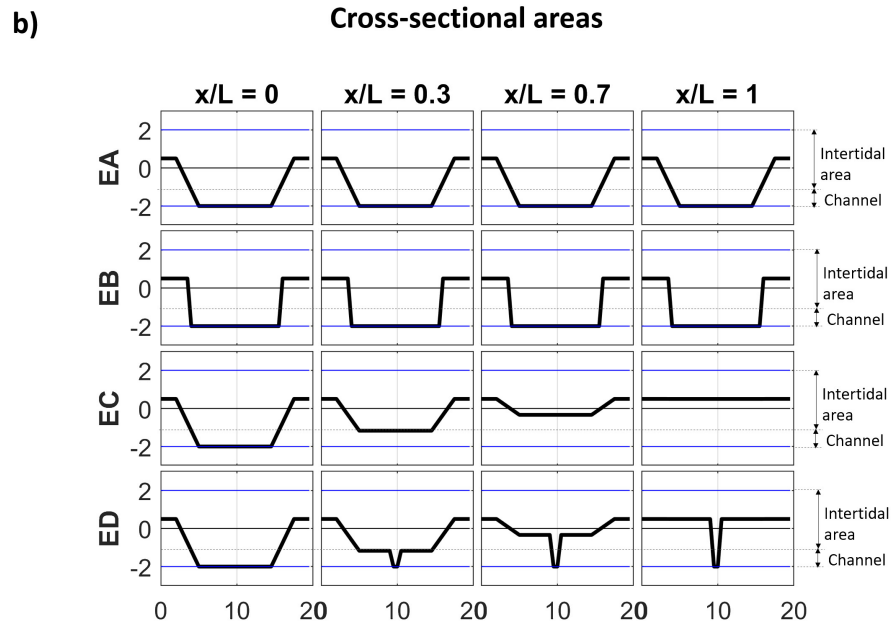

Figure 3.2: Geometry of the study estuaries: a) schemes with general dimensions and b) details of different cross sections (the mouth is located at $x/L = 0$ and the innermost area at $x/L = 1$).

To define the study estuaries, the criteria of Speer & Aubrey (1985) were followed as a reference. These authors propose the study of estuaries with constant cross-sectional areas in the longitudinal direction constituted by a main channel with a trapezoidal section and tidal flats, which are shown from a certain elevation. Four particular cases of this geometry were selected to describe different morphological features: a first estuary (EA) with a trapezoidal cross-sectional area that is constant towards land, a second estuary (EB) that also shows a landward constant but with a rectangular section, a third estuary (EC) whose trapezoidal section shows a linear reduction in depth towards its innermost areas, and finally, a fourth estuary (ED) with a trapezoidal section that linearly reduces its width towards the interior. The first EA and EB geometries show channel configurations, while EC and ED represent more widespread estuarine configurations. The dimensions, longitude (L), width (b), depth (h), and lateral slope of the channel (N), chosen for this study are within the ranges evaluated by Speer & Aubrey (1985) for shallow estuaries with long channels compared to their widths ($b/L << 1$) and small horizontal aspect ratios ($h/b << 1$). Fig. 3.2 shows the geometries and dimensions of the study estuaries. The shallow depths of the channels and tidal flats produce different tidal deformations, some of which can be detected with the naked eye.

3.2.2. Astronomical tide characterization

The classification of astronomical tide on a global scale performed in Chapter 2 (Núñez et al., 2020) was used to characterize the tidal asymmetry at the estuarine mouths. Remember that this classification is based on the TPXO9-atlas barotropic tidal solution (Egbert & Erofeeva, 2002) and identifies, with a spatial resolution of 1/30° on the coastal areas, 25 representative astronomical tide types (*ATtypes*) in the world, according to their tidal asymmetry and periodicity parameters. The tidal asymmetry is described by the probability density functions (PDFs) of the tidal elevation time derivative, $d\eta/dt$ (a variable associated with the rising/falling tidal speeds and, therefore, the flood/ebb currents in tide-dominated estuaries),

through the skewness (γ_1) and kurtosis (g_2) coefficients calculated from a 19-year hour series. The periodicity is defined through the tidal form factor and distinguishes semidiurnal, mixed-semidiurnal, mixed-diurnal, and diurnal regimes.

γ_1 of $d\eta/dt$ allows a relative comparison between flood- and ebb-current intensities, i.e., it provides a measure of tidal current asymmetry and, therefore, provides information about the ability and orientation of the transport of substances (Nidzieko, 2010, Song et al., 2011). Positive values mean that the flood-phase duration is shorter than the ebb-phase duration. As the tidal prism must be the same, flood currents have to be more intense than ebb currents, resulting in net transport towards the estuary. In contrast, if γ_1 is negative, ebb currents are the most intense and generate a trend of exporting plastic debris to the open ocean. In Chapter 2 it was proposed to use the kurtosis (g_2) parameter together with γ_1, since g_2 provides information on the frequency of occurrence of the strongest flood/ebb currents (Balanda & MacGillivray, 1988, Westfall, 2014) and, consequently, is also related to the estuary's capacity to transport substances. If the tides show a positive asymmetry, a lower kurtosis indicates a greater presence of the stronger flood currents, and this aspect can be associated with a greater trend to import plastic debris. In contrast, if the tides are negatively asymmetric, a lower kurtosis means a greater frequency of the stronger ebb currents.

3.2.3. Hydrodynamic model

As the study estuaries are shallow tide-dominated estuaries and the astronomical tide is the only analysed driver, 2D hydrodynamic modelling was suitable to represent the flow features. The hydrodynamic grids used to numerically evaluate the above-described estuaries have 160000 computational elements and an average spatial resolution of 1 m, which is suitable to describe the hydrodynamic and substance transport processes at these spatial scales.

In this study, to assess the role of different tidal asymmetric natures, the three *ATtypes* with the more different γ_1 and similar g_2 values were selected as the analysis tides. The selected types were $ATtype_1$ ($\gamma_1 = 0.57$); $ATtype_{16}$ ($\gamma_1 =$ -0.08); and $ATtype_{24}$ ($\gamma_1 =$ -0.54), where all these types show g_2 values of approximately -0.4.

$ATtype_1$ is a positive asymmetric tidal type. Positive asymmetric tides are representative of 11.3% of the world's coastal areas, such as the western Gulf of Mexico, northern Caribbean Sea, Mediterranean coast of France, and south coast of Australia, as well as part of the Spanish coast, and conditions the behaviour of the estuaries they house (Núñez et al., 2020).

$ATtype_{16}$ is associated with symmetric tides. Symmetric tides are present in 77.4% of the world's coastal areas. A significant part of the coastal areas of the Atlantic Ocean, including the East Coast of the USA, the western coast of Spain, and large proportions of the Brazilian and African coasts, exhibit symmetric tides (Núñez et al., 2020). Although within the group of symmetric tides classified in previous chapter, those with bimodal PDFs of $d\eta/dt$ show the most widespread presence (47.4% of the world's coastal areas), $ATtype_{16}$, which shows a unimodal PDF (see Fig. 3.3), was selected for this study. The reason is the interest in evaluating the behaviour of tides that differ only in their tidal skewness. $ATtype_{16}$ allows the selection of a symmetric tide type while keeping the other parameters, such as kurtosis, similar to the other two selected tidal types. Symmetric tides with unimodal PDFs are representative of 30% of the world's coastal areas.

Finally, $ATtype_{24}$ refers to negative asymmetric tides, which are found in the remaining 11.3% of coastal areas. Negative tides can be found in coastal areas located in the southern Caribbean Sea, northern Greenland, the South China Sea, and western Australia (Núñez et al., 2020).

Consequently, the importance of evaluating the influence of these tidal types is demonstrated, as they are the tidal types that can be found on the mouths of estuaries located in different areas worldwide and influence their internal processes. Fig. 3.3 shows the standardized (between -1 and 1 values) probability density functions of $d\eta/dt$ associated with the positive

asymmetric tide $ATtype_1$, the symmetric tide $ATtype_{16}$, and the negative asymmetric tide $ATtype_{24}$, as well as the 15 daily water level conditions from such tidal types.

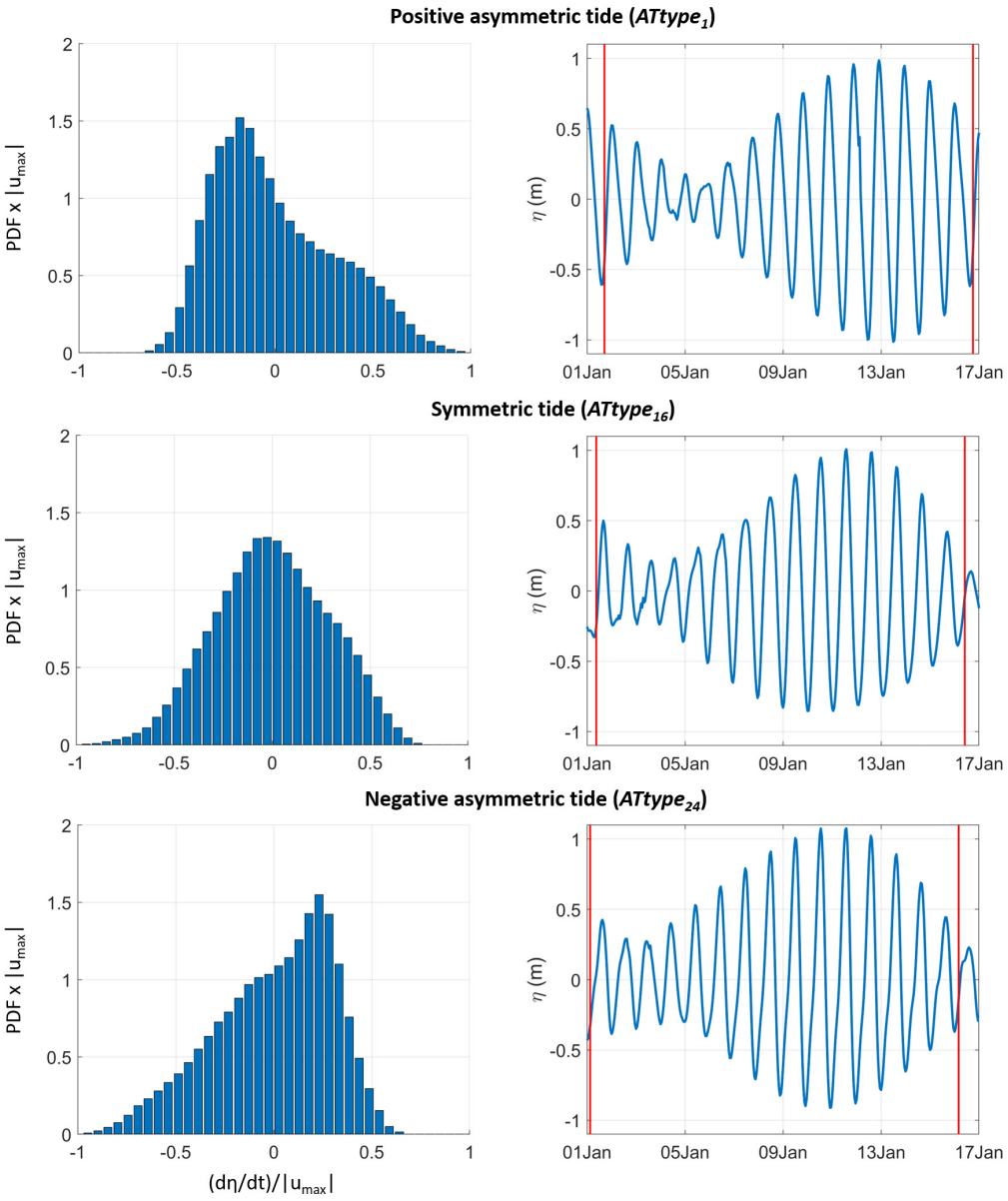

Figure 3.3: Tidal types for analysis and associated boundary and initial conditions.

Fifteen days was selected as the analysis period to contemplate the residual transport caused by complete neap-spring tidal cycles. The analysis time period is represented in Fig. 3.3 between two vertical red lines. Furthermore, to avoid the effect that different potential tidal ranges can cause on the fate of plastic debris within estuaries and to analyse only the effects of tidal asymmetry and estuarine geometry, the tidal series were standardized so that the maximum tidal amplitude took a unit value. Similarly, to obviate the effect of plastic debris inputs reaching estuaries at different tidal phases associated with different tidal ranges, it is assumed that the plastic debris reaches estuaries at low tide of a mean tidal range of 1 m in all cases. Therefore, the boundary conditions were the 15-daily time series of astronomical tides with a 10-min temporal resolution associated with the mentioned tidal types ($ATtypes_i$, where i = 1, 16, and 24). The initial conditions of analysis correspond to 10 mins after the low tide level, when the estuary begins to flood.

To evaluate 2D hydrodynamics in the study estuaries, the roughness coefficients (C) and horizontal eddy viscosities (ϵ) were defined. C was characterized as variable with depth according to the equivalent geometrical roughness of Nikuradse (k_s), and ϵ varied with cell size according to a calibration constant (k). Considering that both the geometries and the representative dimensions of the study estuaries were within the ranges evaluated by Speer & Aubrey (1985) and Bárcena et al. (2016), these parameters were consistently defined for all study estuaries by adopting a value of 0.2 for k_s and 0.1 for k.

The flood/ebb currents for the selected tidal types—positive asymmetric, symmetric, and negative asymmetric—and for the defined estuaries—EA, EB, EC, and ED—were obtained by applying the above-described models.

3.2.4. Particle tracking model

The obtained high-resolution flood/ebb currents were the inputs of the Delft3D-PAR module. The *Oil Model* was selected to include the beaching effect in the simulations of plastic debris transport. Following van Utenhove (2019), the oil degradation processes were neglected, and the only processes considered were advective transport due to tidal currents and diffusive transport. The diffusion coefficient (D) was set equal to 1 m^2/s, which is suitable for estuarine areas (Abascal et al., 2012, 2017, Viikmäe et al., 2013).

Considering that one of the most common plastics found in the marine environment is polypropylene (Mazarrasa et al., 2019, Zhang, 2017), this study represented plastic debris with floating particles of 0.89 g/cm^3 of average density. The origin of the plastic debris was assumed to be marine; the debris reached the estuarine mouths at the low tide of a mean tidal range of 1 m for all assessed scenarios. Regarding the number of particles, there is a large variability in the selection of the number of particles in the literature as a function of the extension of the study area. Studies, such as Abascal et al. (2009a), Barker & Galt (2000), Díaz et al. (2008) or van Utenhove (2019), have shown that thousands of particles per location may be sufficient on regional and local spatial scales. In this study, an order of magnitude 100 times greater was chosen to ensure the accuracy and robustness of the probability analyses derived from this study. Regarding the timestep (Δt), 5 mins was adopted to ensure the stability of the model.

As a result of the particle tracking model application with the above-described setup, particle trajectories for the four study estuaries forced with the three tidal types were obtained.

3.2.5. Probabilistic analysis

A probabilistic analysis of the particle trajectories obtained from Delft3D-PAR determined the most likely areas—defined according to their distance to the mouth—of plastic debris accumulation for the selected time horizon of 15 days. The time average over the neap-spring tidal cycle was used

to calculate the probability of plastic debris accumulation, which includes the effect of tidal hydrodynamic variability during the analysis period. Thus, the effects of the uncertainties associated with some of the assumed hypotheses, such as the origin of plastic debris or the tidal phase in which plastic debris reaches the estuary, can be mitigated.

To perform these probabilistic analyses, the study estuaries were discretized into N_{CS} estuarine units (sections) in the longitudinal direction of the estuary. Twenty (N_{CS}) sections 400 m in length were found to be suitable to characterize the plastic distribution within the study estuaries. For each of these sections (j), the average probability of the presence of particles in a neap-spring tidal cycle (P_m) was calculated (Eq. 3.1).

$$P_{mj} = n_j / N_T \times 100 \tag{3.1}$$

where n_j is the average number of particles in section j in a neap-spring tidal cycle and N_T is the total number of evaluated particles, i.e., 100000 particles.

Moreover, to check whether an estuary with a certain tidal asymmetry imposed at its mouth shows a trend to import residues, the sum of P_{mj} in all the estuarine units was calculated ($P_m = \sum_{j=1}^{N_{CS}} P_{mj}$).

3.3. Results

3.3.1. Effects of tidal asymmetry and estuarine morphology on tidal propagation

Fig 3.4 shows the evolution of the skewness (γ_1) and kurtosis (g_2) coefficients of $d\eta/dt$ when the three analysed tidal types propagate by each of the four study estuaries.

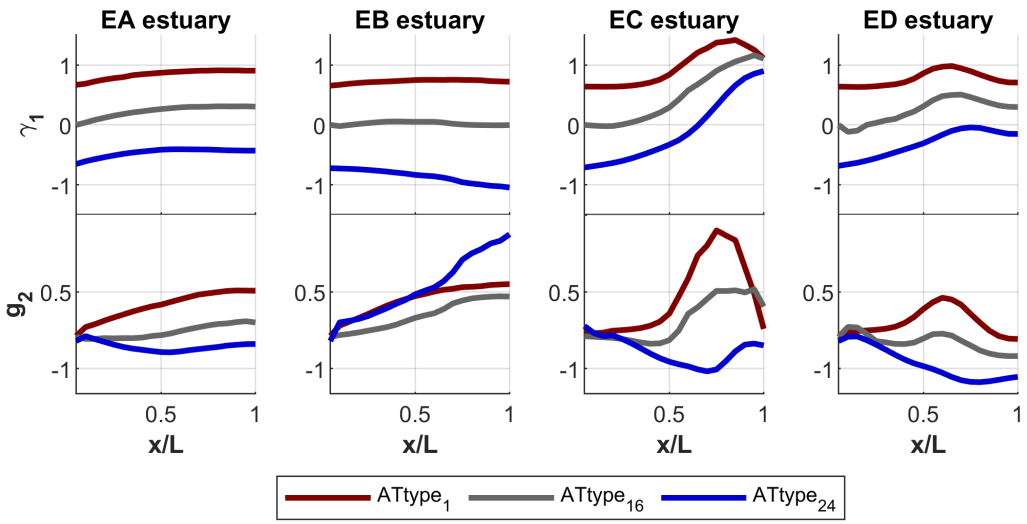

Figure 3.4: Skewness (γ_1) and kurtosis (g_2) coefficients of $ATtype_1$, $ATtype_{16}$, and $ATtype_{24}$ along the EA, EB, EC, and ED estuaries.

The **effect of the lateral boundary inclination of the channel** on tidal propagation is deduced from the comparison of hydrodynamic results in the EA and EB estuaries. The lateral boundaries of the channel oppose the tidal flow. A greater inclination translates into a greater friction, which is more noticeable at low tide than at high tide, delaying the ebb tide and generating a deformation with a flood-dominance trend (γ_1 increases). However, the flood- or ebb-dominant nature depends not only on the geometry but also on the ocean tidal asymmetry imposed at the estuarine mouths. Within the EA estuary, which shows a 45° inclination in its lateral boundaries, γ_1 gradually increases to the middle of the estuary for the three analysed tidal types, and from this point on, the change is not very significant. Thus, the positive asymmetry existing at the mouth for $ATtype_1$ increases, the symmetric tide of $ATtype_{16}$ is transformed into a positive asymmetric tide, and the initial negative asymmetry of $ATtype_{24}$ is reduced. The configuration of the EB estuary with vertical lateral boundaries generates little opposition to the tidal flow, such that the induced changes in γ_1 are not very relevant for the positive asymmetric and symmetric tides, and the (a)symmetries of the mouth are maintained. Furthermore, this geometry can generate a opposite effect (γ_1 reduces) on initially deformed tides with

negative asymmetries, favouring an even faster ebb phase and increasing the initial ebb dominance. Regarding the kurtosis spatial evolution, g_2 increases as tides become more asymmetric, either positive or negative, and vice versa. This means that the most intense flood or ebb currents decrease their frequencies in favour of average currents for positive and negative asymmetric tides, respectively, when g_2 increases and the opposite when g_2 decreases. A decrease in g_2 is observed for $ATtype_{24}$ in the outer half of the EA estuary when the negative asymmetric character is reduced. This translates to an increase in the frequency of the strongest ebb currents in this area. In the EA estuary, g_2 always reaches lower values than in the EB estuary for all analysed sections, which means that the tidal currents are more intense within the EA geometries than within the EB geometries. In summary, greater inclinations of the lateral boundaries of the channel increase the positive tidal asymmetries and counteract the negative asymmetries; however, the final asymmetric character of the tide in the innermost sections is not determined by this geometric aspect but rather by the initial tidal asymmetry shown at the mouth. Furthermore, these frictions with lateral boundaries generate an increase in the intensity of flood/ebb currents for positive/negative asymmetric tides.

The **effect of the depth reduction** in the three analysed tidal types is described from the hydrodynamics obtained for the EA and EC estuaries. EC shows a linear reduction in depth in its longitudinal direction with respect to the EA estuary. This reduction implies an increase in friction that slows down the ebb phase for all the analysed tides and stores a higher intertidal water volume in its innermost area. It is worth noting a differentiated behaviour in the EC estuary between the outer and intermediate areas, where the depth allows the full development of every tidal range, and the innermost area, where flooding-drying processes take place. Thus, in the outer half of the estuary, the positive growth of the skew for every tidal type is slow and gradual, analogous to that experienced in estuary EA. This translates into similar effects of both estuary types on tidal asymmetries. However, while this positive trend stabilizes in the second half of the EA estuary,

it grows faster in the EC estuary due to a more evident bottom effect. This growth continues until reaching a maximum—approximately 75% of the estuary length for $ATtype_1$ and near the final section for $ATtype_{16}$ and $ATtype_{24}$—from this point on, a nonsignificant decay is observed, which is probably due to intertidal storage in these areas. Indeed, all the analysed tidal asymmetries result in positive asymmetries in the interior areas of the EC estuary, and γ_1 always takes higher values than in the EA estuary. With regard to g_2 in the outer half of the EC estuary, significant changes are only observed for $ATtype_{24}$, where a decrease in g_2, i.e., an increase in the frequency of occurrence of the most intense ebb currents, takes place while reducing the negative asymmetric nature of the tide. In this outer area, the tidal currents are more intense (g_2 adopts lower values) in the EC estuary than in the EA estuary. In the interior areas of the EC estuary, tidal currents are stronger (g_2 assumes lower values) than in the same areas of the EA estuary only for $ATtype_{24}$ and weaker (g_2 adopts higher values) for $ATtype_1$ and $ATtype_{16}$. Therefore, it can be deduced that the longitudinal depth reduction leads to a positive tidal asymmetric character in the interior areas regardless of the initial asymmetry at the mouth. Nevertheless, the intertidal storage in the innermost areas slows the flood-current velocities and compensates for the positive increase in tidal asymmetries.

The **channel-width variation effect** on tidal propagation is explained by contrasting the results obtained for the EA and ED estuaries. Unlike the EA estuary, the ED estuary shows a linear reduction in the width of its channel that reaches zero in its innermost area. The behaviour of the tides is similar in both estuaries up to approximately half their lengths. The slope of the lateral boundaries of their respective channels to 45° slows down the ebb tide and induces positive asymmetries ($\gamma_1 > 0$) that add, for $ATtype_1$ and $ATtype_{16}$, or counteract, for $ATtype_{24}$, the initial asymmetries present at the mouths. As mentioned, tidal asymmetries in the EA estuary remain practically constant in its innermost area, while negative asymmetries are induced in the ED estuary ($\gamma_1 < 0$). This fact can be explained by two reasons related to the morphological configuration of the ED estuary. On

one hand, the gradual narrowing of the section reduces the inclination of the lateral boundaries of the channel—which become practically vertical slightly beyond the middle of the estuary—and reduces the friction. On the other hand, the area of the tidal flat increases in the innermost area of the estuary ED, thereby favouring intertidal storage and counteracting the deformation induced by the channel. Nevertheless, as shown in Fig. 3.4, the final γ_1 value depends both on the initial value of ocean tidal asymmetry and on the estuarine morphology. Regarding g_2, the maximum values reached in the ED estuary for the three tides are always lower than those reached in the EA estuary. Therefore, it can be deduced that a reduction in the channel section causes stronger tidal currents.

Some significant aspects can be drawn from Fig. 3.4. On one hand, a greater friction with the lateral boundaries or with the bottom of the channel produces a positive *asymmetric trend*; however, a weaker friction or certain intertidal areas can generate a negative asymmetric trend. On the other hand, the positive/negative *asymmetric character* of the tides in different sections of the EA, EB, and ED estuaries depends both on the estuarine geometry and asymmetry imposed at the mouth of these environments; however, the geometry plays a key role in the EC estuary. As for the *strongest tidal currents*, greater frictions increase their frequency, while weaker frictions or an intertidal storage favour average currents. In general, the trend of tidal current intensities in the direction of asymmetry decrease as the tide becomes more asymmetric and increase otherwise.

3.3.2. Effects of tidal asymmetry and estuarine morphology on the fate of plastic debris

Fig. 3.5 shows an example of the temporal evolution of P_m over the analysed neap-spring cycle of the symmetric tide ($ATtype_{16}$) for different sections of the EA estuary ranging from the mouth ($x/L = 0$) to its innermost area ($x/L = 1$). The evolution of the probability of plastic accumulation in each section is explained by the marine origin assumed for the plastic debris.

A high probability of plastic debris accumulation is found in the sections between the mouth and approximately the middle of the estuary during the first days of the neap-spring cycle, when the particles reach the estuary and begin to be transported. In contrast, an average probability of accumulation of plastic higher than zero begins to appear in the innermost sections of the estuary after day 10 of the tidal cycle. This implies that the plastic debris that reach the mouth of the EA estuary during the low tide of a symmetric tide do not reach the interior areas after 10 days.

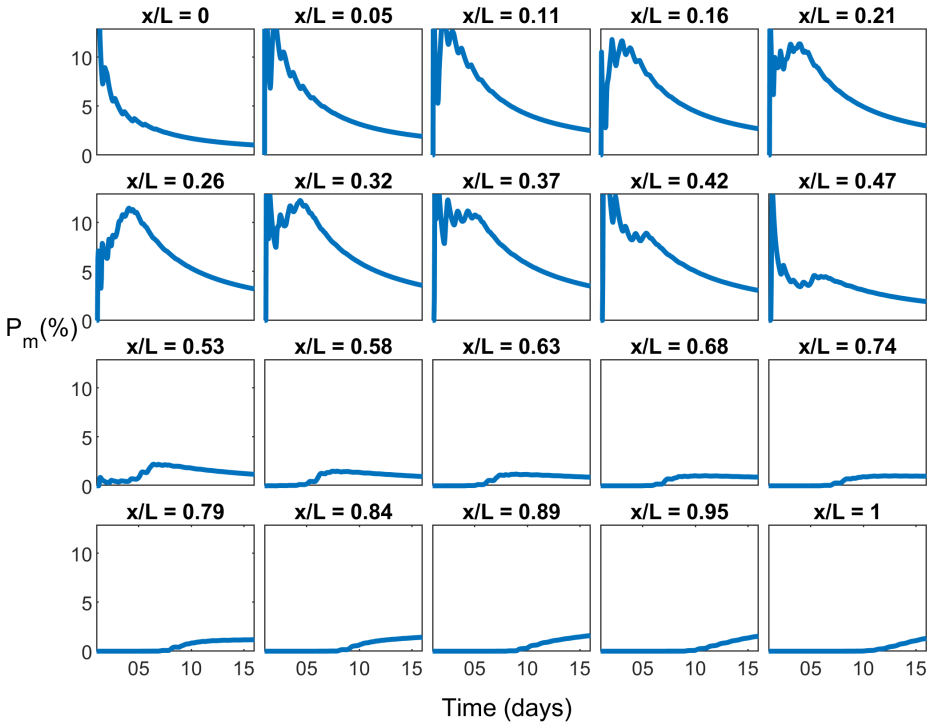

Figure 3.5: Temporal evolution of P_m from the mouth of the EA estuary ($x/L = 0$) to the innermost area ($x/L = 1$).

The P_m values of the estuarine sections on day 15 of the tidal cycle are used to reconstruct the distribution of the average probability of the presence of particles within the neap-spring cycle along the estuaries. Fig. 3.6 shows these distributions for each estuary and tide. Table 3.1 includes the sum of these probabilities within the study estuaries.

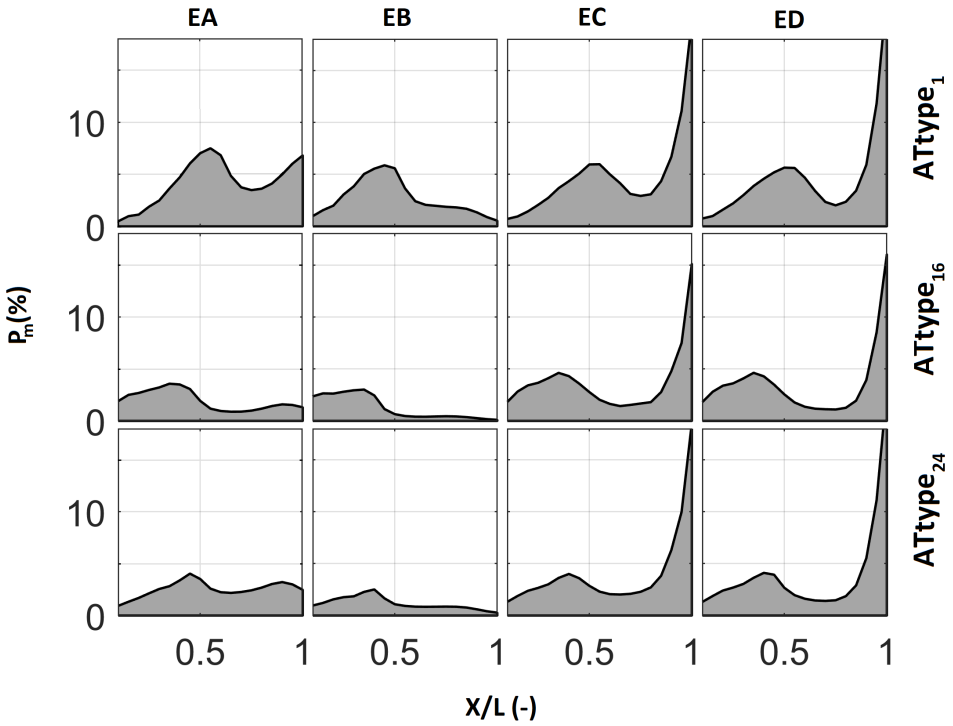

Figure 3.6: Average probability of the presence of particles P_m (%) in a neap-spring tidal cycle of $ATtype_1$, $ATtype_{16}$, and $ATtype_{24}$ for the EA, EB, EC, and ED estuaries.

	EA	EB	EC	ED
$ATtype_1$	81	52	93	92
$ATtype_{16}$	38	25	72	70
$ATtype_{24}$	49	23	78	78

Table 3.1: $\sum P_m(\%)$ within the EA, EB, EC, and ED estuaries for $ATtype_1$, $ATtype_{16}$, and $ATtype_{24}$.

The results shown in Fig. 3.6 and Table 3.1 indicate that the ocean tidal asymmetry significantly conditions the ability to import plastic debris in canal-like geometries, such as the EA estuary. With the propagation of positive asymmetric tides, the EA estuary shows a clear trend of importing floating particles ($\sum P_m^{ATtype_1} = 81\%$) and reveals a greater probability of accumulation in the vicinity of the middle and final sections of the estuary

($P_m^{ATtype_1}$ in x/L near 0.5 and 1 are close to 8%). This distribution of the peak probabilities is equivalent for symmetric and negative asymmetric tides, but in these cases, the peaks are located in slightly forward positions, and the magnitude is significantly reduced ($P_m^{ATtype_{16}}$ and $P_m^{ATtype_{24}} < 4\%$ at the peaks). In both cases, the plastic debris import ability is reduced to approximately 38% ($\sum P_m^{ATtype_{16}}$) and 49% ($\sum P_m^{ATtype_{24}}$).

As in the EA estuary, the plastic debris accumulations within the EB estuary are strongly conditioned by the asymmetry of the ocean tide. However, the EB estuary shows the lowest capacity to import floating items due to flood/ebb currents. The average probability of importation does not exceed 52% for positive asymmetric tides ($ATtype_1$), 25% for symmetric tides ($ATtype_{16}$), and 23% for negative asymmetric tides ($ATtype_{24}$). Regarding the P_m distribution along the longitudinal profile of the estuary, common patterns that differ in magnitude depending on the tidal type propagated are observed. Thus, an increasing cumulative trend between the mouth and the middle section of the estuary is observed for all analysed tidal types, and from this area, a significant reduction in the value of P_m is observed.

The geometries of EA and EB represent idealized channels where, as can be deduced from the results, the accumulation probabilities depend both on the initial tidal asymmetry at the mouths and the friction with the lateral boundaries of the channels.

The geometries of EC and ED describe estuaries with widespread morphologies. The P_m results from these geometries show that the distributions of plastic debris accumulations are very similar to each other and that these typologies of tide-dominated estuaries frequently act as traps for plastic debris, regardless of the asymmetry shown by the tide. Indeed, both EC and ED estuaries show an average probability of plastic debris accumulation greater than 90% for the positive asymmetric tide $ATtype_1$, approximately 70% for the symmetric tide $ATtype_{16}$, and close to 80% for the negative asymmetric tide $ATtype_{24}$. The longitudinal distribution of P_m in these estuaries shows a relative peak close to 5% around the middle of the estuary and an absolute peak at approximately 20% in its innermost area.

3.4. Discussion

Tidal asymmetries at the estuarine mouths, together with the frequency of occurrence of the strongest tidal currents in the asymmetry direction, as well as estuarine morphologies, are significant factors in determining flood or ebb dominance in tide-dominated estuaries and, therefore, the estuary's nature to act as traps of plastic debris.

Tidal asymmetry has traditionally been defined by mean of the ratio between the amplitudes of two tidal constituents and the difference between both phases (Aubrey & Speer, 1985). However, other approaches should be used if tidal asymmetry arises from the interaction of a number of tidal constituents greater than two. Castanedo et al. (2007), Woodworth et al. (2005) proposed the use of the PDFs of the astronomical tide level. Nidzieko (2010), Song et al. (2011) recommended the use of the γ_1 —a parameter related to the shape of the PDFs—of the tidal elevation time derivative ($d\eta/dt$) to represent the difference between the intensities of flood/ebb currents. The greater or lesser frequency of the strongest tidal currents in the asymmetry direction can be represented by the kurtosis coefficient Núñez et al. (2020). Consequently, the astronomical tide ability to transport plastic debris, or any other substance into or out of tidal estuaries can be described in a complete way through the skewness (γ_1) and kurtosis (g_2) coefficients of $d\eta/dt$. The maximum transport abilities towards the interior or exterior of the estuaries are achieved in a balance between the highest possible absolute value of γ_1 —which indicates a greater difference between the flood- and ebb-current intensities—and the lowest values of g_2 —which indicate higher frequencies of the strongest flood/ebb currents for positive/negative tidal asymmetries.

The evolution of γ_1 follows similar patterns for all the analysed tides (symmetric and asymmetric) within the same estuarine geometry. In general, the γ_1 coefficient follows an increasing trend—positive asymmetries increase, and negative asymmetries decrease—with the bottom and lateral frictions of the main channel. However, estuarine geometry is sometimes not associated

with significant friction increases. In these cases, the tidal wave may not deform in its propagation, and consequently, γ_1 may remain unchanged or even experience a negative trend if it was initially so. Furthermore, in estuaries that present sufficiently large tidal flat areas to counteract the deformation induced by the channel, any γ_1 may also be reduced. These conclusions on tidal deformation during propagation are in agreement with the findings of Dronkers (1986), Friedrichs & Aubrey (1988) or Speer & Aubrey (1985), which only analysed the propagation of symmetric tides. For the evolutionary trend of g_2, it has been found that g_2 increases with the absolute value of γ_1, that is, when positive and negative asymmetries increase and decrease in the opposite case. That is, g_2 increases with the asymmetric nature of the tide, which means that the frequency of the more intense flood/ebb currents decreases when tidal asymmetry becomes more positive/negative.

The γ_1 and g_2 evolutions arising from tidal propagations have some implications for the transport and accumulation of plastic debris within tidal estuaries. On one hand, the tides whose asymmetries (positive or negative) increase as they propagate show increasing differences between the flood- and ebb-current intensities and, in principle, should show an increase in the transport capacity towards the estuary for positive asymmetries or towards the open ocean for negative asymmetries. However, since g_2 also increases with $|\gamma_1|$, the frequency of the most intense flood/ebb currents with positive/negative asymmetries decreases and partially offsets the increased transport intensity due to γ_1. On the other hand, the tides whose asymmetries are reduced with propagation also show a reduction in g_2. Consequently, as long as some residual asymmetry remains, there will be a transport trend in the direction of tidal dominance due to the stronger currents. From the obtained results, it was proven that the EC and ED geometries—which ideally represent estuaries with widespread configurations—always act as traps for plastic debris, confirming the findings of Acha et al. (2003) and Mazarrasa et al. (2019). Furthermore, the accumulation of plastic debris that has reached the mouth within estuaries

is more likely if a positive asymmetry characterizes the outer area.

To date, few previous studies have linked ocean tidal asymmetry and substance transport, and all of them have focused on sediment transport (Moore et al., 2009, Nidzieko, 2010, Ranasinghe & Pattiaratchi, 2000). This study has focused in a novel way to study the transport of floating plastics representative of polypropylene—a plastic material with a great presence in the marine environment (Mazarrasa et al., 2019, Zhang, 2017)—and has also incorporated the effect of strongest tidal currents through the kurtosis of $d\eta/dt$. The results note that the estuarine geometry conditions the distribution pattern of plastic debris, i.e., the location of the areas of high or low accumulations; however, the tidal type quantifies the magnitude of such accumulation probability—which is higher for positive asymmetric tides and lower for both symmetric and negative asymmetric tides. Symmetric and negative asymmetric tides show similar probabilities of plastic debris accumulation in a neap-spring tidal cycle, with values much lower than that of the positive asymmetric tide. This aspect can be explained by the marine origin of plastic debris and tidal asymmetry imposed at estuarine mouths. If tidal asymmetry in this area is positive, the greater intensity of the flood currents would favour a greater importation of plastics that have reached the mouth. Estuaries as important as the Dee estuary (on the west coast of the United Kingdom), Seine estuary (northern France), and Murray estuary (southern Australia), as well as the estuary where the Paraná and La Plata rivers flow (between Argentina and Uruguay), show positive asymmetric tides in the vicinity of their mouths, which condition their import capabilities (Núñez et al., 2020). Conversely, if a tide is symmetric, its flood and ebb currents would be in equilibrium, and if it is negatively asymmetric, the ebb currents would be more intense. Consequently, the percentage of plastics with marine origin that accumulates in estuaries subjected to symmetric or negative asymmetric tides at their mouths results from the evolution of ocean tidal asymmetry due to estuarine geometry and coastal trapping ability. Almost 89% of the world's coastal areas show symmetric (77.4%) and negative asymmetric tides (11.3%). The estuaries within these areas

show a lower ability to import plastic debris. Estuaries such as Chesapeake Bay (on the east coast of the United States), San Francisco Bay (on the west coast of the United States), and Thames Estuary (southeast coast of the UK) show symmetric tides at their mouths. While the Severn Estuary (south west coast of the UK), Swan River Estuary, Peel-Harvey Estuary, Wilson Inlet (on the south west coast of Australia), Tomales Bay, Elkhorn Slough, and Tijuana River Estuary (in California) or Venice Lagoon (in the North Adriatic Sea) show external negative tidal asymmetry (Núñez et al., 2020).

It would be interesting for further research to include the study of new representative estuarine geometries (e.g., larger bays), new possible litter sources (e.g., river sources), or effects of plastic debris that reach estuaries in different tidal phases. On the other hand, in addition to tide, river discharges, temperatures and salinity gradients, wind patterns, and waves (Browne et al., 2010, Carson et al., 2013, Zhang, 2017), the intrinsic properties of plastic debris that affect its buoyancy, such as specific density, size, and shape (Barnes et al., 2009, Chubarenko et al., 2016, Kowalski et al., 2016), or the estuarine trapping ability (Mazarrasa et al., 2019, Viehman et al., 2011), can play relevant roles. Coastal trapping ability is decisive in the fate of plastic debris inside estuaries. This parameter shows spatial variability within each estuary and is strongly correlated with the presence and type of vegetation, as well as with the flood-ebb regime. Studies, such as those by Mazarrasa et al. (2019), Viehman et al. (2011), have detected high concentrations of plastic debris in the high marsh areas of estuaries that become especially significant in vegetated areas. Hence, research on the transport and fate of plastic debris within estuaries is still in a very early stage, and there are many open fronts that are worth addressing in future research.

3.5. Conclusions

This research studies the effect of ocean tidal asymmetries and estuary morphologies on tidal propagation and the fate of ocean plastic debris

within tide-dominated estuaries. Numerical experiments were performed by applying the hydrodynamic and Lagrangian transport models of Delft3D to four study estuaries (defined with different cross-sectional areas that cause different tidal flat extensions) using three tidal types (selected according to their asymmetry) as boundary conditions. The analysis parameters were selected to describe the tidal nature (skewness—which represents tidal asymmetry—and kurtosis—which refers to the frequency of the strongest tidal currents—of the tidal elevation time derivative) and estuarine morphology (lateral boundary inclination, depth, and width of the main channel). The results confirm previous findings about the evolution of symmetric tides and provide new considerations about the evolution of asymmetric tides and the effects of both on plastic debris accumulation.

Symmetric tides evolve to positive asymmetric with tidal propagation as the boundary and bottom friction of the channel increase; conversely, tidal asymmetry may experience a negative trend if frictions with lateral boundaries are weak or if the tidal flat area is large enough to counteract the effect of the channel. Symmetric tides explain the behaviour of estuaries located in 77.4% of the world's coastal areas; however, in the remaining 22.6%, the tides show positive or negative asymmetries. As with symmetric tides, evolutionary trends of asymmetric tides are modulated by estuarine geometry, and the coefficient of skewness follows the same pattern; nevertheless, the value adopted by tidal skewness within estuaries is also conditioned by its external value. From the analysis of the propagation of asymmetric tides, it is concluded that the initial skewness present at the mouths strongly conditions flood or ebb dominance and, therefore, the import degree of ocean plastic debris in estuarine areas where the main channel shows low flow opposition and favours tidal circulation. In this type of geometries, positive tidal asymmetries show an import capacity 50% higher than those of symmetric and negative asymmetric tides. In contrast, if there is a clear opposition to the flow or an important intertidal storage area, the relevant role in defining flood or ebb dominance is played by the geometry of the estuary, although small influences of the external tidal asymmetry are

also appreciated. Thus, the probabilities of plastic debris accumulation are approximately 90% for positive asymmetric tides and range between 70-80% for symmetric or negative asymmetric tides.

However, the import and distribution of plastic debris within estuaries is not exclusively determined by the positive or negative value of the skewness but also by the kurtosis coefficient. The regulatory role of kurtosis, which corrects the tendency induced by skewness in the fate of plastics within tidal estuaries, is a remarkable and novel aspect that is derived from this study. The kurtosis increases while the asymmetric character of the tide also increases. This means that the frequency of the strongest flood currents is reduced for positive asymmetric tides and vice versa for negative asymmetric tides. Consequently, the astronomical tide's ability to transport plastic debris into or out of the estuary can be described in a complete way through the skewness and kurtosis coefficients.

Chapter 4

Methodology to assess the probability of plastic debris accumulation in estuaries [3]

4.1. Introduction

In previous chapters, tidal asymmetry has been characterized at the mouth of estuaries worldwide and its effect on estuarine transport of plastic debris has been analysed. However, as indicated in Chapter 1, the astronomical tide is not the only driver involved in the process, but temperature and salinity gradients, river discharges, wind, or waves are also relevant. Furthermore, the roles of trapping ability of the different areas that make up estuaries, and the physical properties of plastic debris stand out.

In this chapter, a general methodology, that is based on numerical modelling and statistical analysis, is developed to address the limitations of the state-of-the-art approaches to assess the plastic debris hotspots on an estuary scale, that is, to reduce the necessary economic and temporary

[3]The findings of this chapter have been published in: Núñez, P., García, A., Mazarrasa, I., Juanes, J. A., Abascal, A. J., Méndez, F., Castanedo, S. & Medina, R. (2019). A methodology to assess the probability of marine litterF accumulation in estuaries. *Marine Pollution Bulletin, 144*, 309-324.

resources. This methodology provides the most likely areas where plastic debris tends to accumulate and, for each of these areas, the largest contributing litter source. These results can be valuable information for assisting in the management and optimization of the cleanup logistics in estuaries, bays, and beaches, and in the definition e implementation of mitigation strategies (e.g., installing filters and other devices to catch plastic items near the most polluting sources).

Furthermore, the criteria for applying the proposed methodology in any estuary of the world are provided. On the one hand, the steps to include the study of all the drivers involved in the estuarine transport of plastic debris, and not only astronomical tide, are described. On the other hand, a first approach to consider the trapping ability of estuaries is shown. However, the influence of physicochemical characteristics of plastic debris is too broad a topic that requires numerous additional studies beyond the scope of this Thesis. For this reason, generic floating particles representing the most common types of plastics in the marine environment (polyethylene, polystyrene, and polypropylene) continue to be used as the basis for the study developed in this chapter.

To illustrate how this methodology works, its application in a real estuary is described. Santoña Bay, an estuary along the North coast of Spain, dominated by tides and characterized by symmetric ocean tide at its mouth is selected. As a selection criterion, the possibility of collecting field data for validation purposes is considered a priority over the symmetric or asymmetric character of the ocean tide. Finally, the methodology is validated with field data.

This chapter responds to the third and last specific objective raised in this Thesis following this structure: Section 4.2 presents the proposed methodological framework; Section 4.3 describes the estuary selected as the study area and the available data to assess how this methodology works; Section 4.4 develops each of the methodological steps via its application to the study area; Section 4.5 includes the discussion of the specific results obtained here; and Section 4.6 provides the main conclusions.

4.2. Methodological framework

The methodology is based on the combined application of statistical techniques and numerical modelling to probabilistically assess the distribution of plastic debris inside estuaries and bays. Fig. 4.1 shows a scheme of the proposed methodology, which is structured in the following steps: a) identification of statistically representative metocean scenarios; b) dynamic downscaling to obtain high-resolution drivers; c) modelling of potential plastic debris trajectories; and d) statistical analysis to calculate probabilities of plastic debris accumulation.

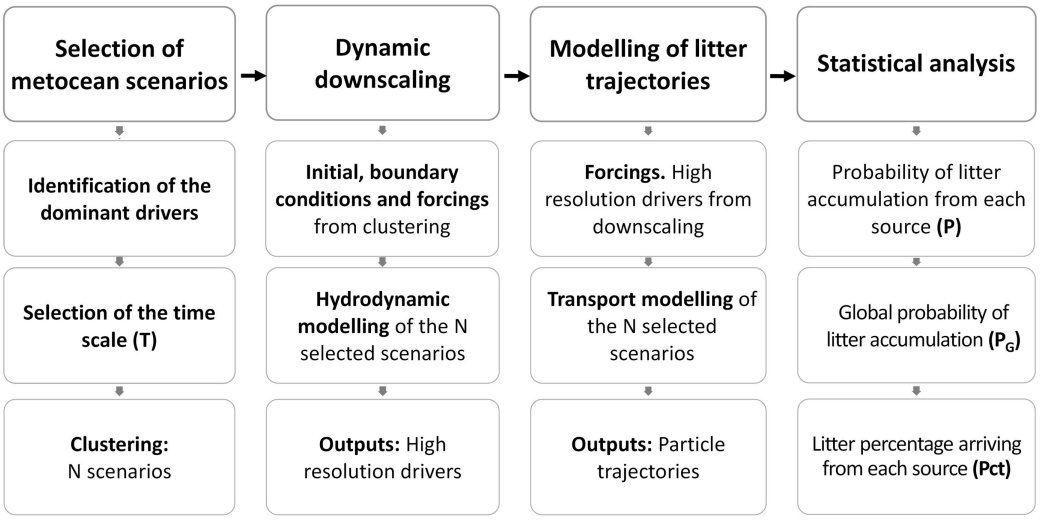

Figure 4.1: Methodology to identify plastic debris accumulation on an estuarine scale.

As depicted in the diagram of Fig. 4.1, the first step of the methodology is to select the representative metocean scenarios of the study area. To complete this step, identifying the dominant drivers (tide, river discharge, waves, temperature, salinity, and wind) and gathering a sufficiently long (years) time series to statistically analyse the drivers are necessary. These data can be obtained from observations or numerical simulations (reanalysis).

As one of the key points, the most suitable time horizon (T) for the analysis should be selected. An adequate T value enables the most stable plastic debris distribution. On the estuarine scale, this distribution occurs

when a significant portion of plastic debris reaches coastal areas, where it can be retained for years or decades (e.g., Lebreton et al., 2012), or when the plastic debris reaches open oceans to be transported to the global convergence areas (Barnes et al., 2009, Cózar et al., 2014, Law et al., 2010). The hydrodynamic timescales should be considered for the selection of the T value, since current velocities determine transport (Hoitink et al., 2003) and, therefore, influence the time for plastic debris to reach the coast or be lost into the ocean. However, current velocity is not the only influential parameter, the distance travelled by plastic debris from its source and the ability of the coast to retain it are also important. For instance, in small linear estuaries with a high vegetation density, plastic debris will reach coastal areas, where it will likely be restrained and accumulate for a long time, faster than in unvegetated large bays. Consequently, the parameters that influence the selection of T are the hydrodynamic timescales and those related to the physical configuration of the study area, such as width, length, coastal sinuosity, sediment typology and presence/absence of vegetation (Zhang, 2017).

From the gathered environmental data and for the chosen T time scale, N scenarios with the probability of occurrence P_i, where $i = 1, 2 \dots N$, are selected by applying clustering techniques. With the identified metocean cases, atmospheric forcings and initial and boundary conditions of the hydrodynamic numerical model are defined. Every scenario is run to generate high-resolution dynamics, which are employed as forcings of the transport model to obtain the potential plastic debris trajectories from a set of litter sources (LS) for every scenario. The last step is to statistically analyse the trajectory database to obtain different types of outputs to assist in the management of plastic debris.

Considering the probability of occurrence of each metocean scenario and identifying presences/absences of particles at different locations of the study area, a probability (P) map of plastic debris per LS is obtained. These results will allow stakeholders and policymakers to choose priority areas to act if the source of an important plastic debris input is known. A global probability (P_G) map of plastic debris distribution is calculated according

to the probabilities of every single source to generate plastic debris, which provides information about the most likely areas where plastic debris will be retained, considering all potential sources in the estuary. Maps of plastic debris percentages (Pct) that arrive from each source to every location can facilitate decision-making to treat the problem at the source. Thus, if an area presents a special interest as it is a tourist area, serves as a refuge for birds, or is the habitat of threatened species, knowledge of the locations of the most significant polluting sources for this type of area would aid in prioritising locations in which measures to reduce litter inputs should be implemented.

Defining a cleanup plan for a specific period can also be interesting (prior to a sporting event and a holiday period). In addition to the average values of the mentioned outputs, one of the main advantages of these techniques is that they enable a response to the accumulation of plastic debris at different time intervals with a minimal computational effort, by calculating the probability of occurrence of each transport scenario for this specific period (e.g., monthly, seasonal, and for a specific month or season of a year).

4.3. Study site and data

4.3.1. Study area

Santoña Bay, hereinafter referred to as SB, (43.3563/−3.4296 lat/lon ED50) is the second largest estuary in Cantabria (northern Spain) (Fig. 4.2). The configuration of SB is complex and distinguishes the following estuarine areas: Boó, Argoños, Escalante, Rada, Limpias and Treto. The maximum length of SB, which is approximately 13.3 km with a N-S orientation, extends along the main channel between the estuary mouth and Limpias, where the Asón River flows. SB has extensive intertidal flats (approximately 65% of its total area) located in its western area and two adjacent beaches: Regatón (inside) and Laredo (outside). The average depth ranges between 0.5 m and 4 m in the tidal flats and in the main channel, respectively, and attains 13 m near the mouth.

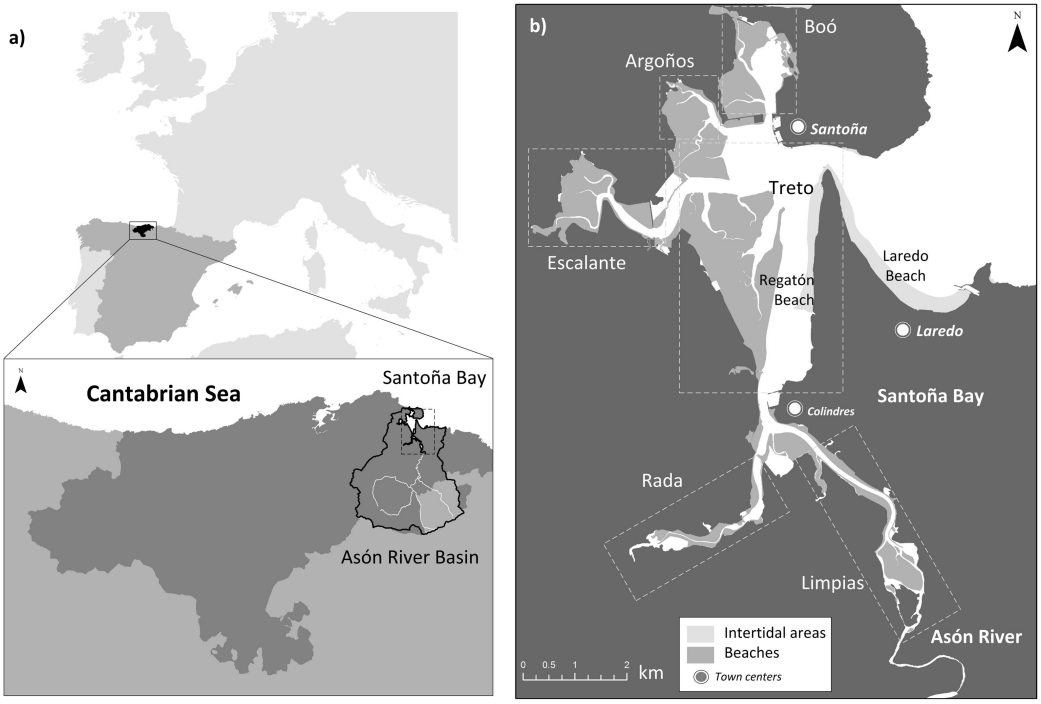

Figure 4.2: Map of: a) Asón River Basin and b) Santoña Bay.

SB is a well-mixed estuary (Galván et al., 2010) where the key driver of hydrodynamics and transport is the tide. The tide is semidiurnal with neap, mean, and spring tidal ranges of approximately 1.5 m, 2.8 m, and 4.5 m, respectively, and a tidal prism (Ω) of 45×10^6 m^3. Astronomical tide shows a symmetric character at the estuary mouth (corresponds to *ATtype* number 14 identified in Chapter 2) and is deformed when propagates through the SB. This deformation lead to asymmetries in time, both the free surface and the current velocity. The time interval between low tide and high tide is shortened, while it increases between high tide and low tide. Since the water volume exported by astronomical tide must be the same as that previously entered, the current velocities during flood phases last less but are more intense than during ebb phases due to continuity. Hence, symmetric ocean tide is transformed into positive asymmetric tides in the innermost part of the SB estuary, which becomes especially significant in the areas of Limpias, Rada, and Escalante and defines a trend to accumulate substances.

The river discharge, waves or winds are also critical depending on the area. The main river input is obtained from the Asón River with an average annual discharge of 16 m^3/s (García et al., 2008). According to the ratio between the average volume of river discharged over a half tidal cycle (Q_6) and the tidal prism, tidal drivers dominate river drivers ($Q_6/\Omega < 0.2$) (Galván et al., 2010). Regarding the wave climate, the orientations of the most frequent sea states are NW (50%) and NNW (25%). Due to the E orientation of the estuary mouth, it is protected from the dominant waves. The 50th and 80th percentiles of the significant wave heights are reduced by 50% in the mouth, where they have values of 0.8 m and 1.25 m, respectively. Predominant winds in the outer area are primarily derived from the W direction and are modified by the effect of the coast in the inner area.

SB is a wetland of international importance for the conservation of waterbird populations and a strategically located area within the North-Atlantic migratory route. SB is located 800 km from the next main suitable stopover area (Navedo et al., 2010), which serves as a refuge for both the wintering season (Navedo et al., 2007) and the migration season (Navedo et al., 2010). For this reason, SB has been included in some European protected areas (e.g., Special Protection Area for Birds) and consequently, has become a priority interest area for addressing the plastic debris issue.

4.3.2. Bathymetric data

In SB, the areas above mean sea level (MSL) have been defined with topographic data LIDAR (2012), from the Spanish National Geographic Institute (`http://centrodedescargas.cnig.es/CentroDescargas/`), with a density of 0.5 points/m and an altitude accuracy of 20 cm. Depths located below MSL are derived from several sources: Nautical Chart 24b, 940, and 941 from the Spanish Navy Hydrography Office (IHM) and detailed bathymetry (1997) from the Spanish Natural Resources Management Plan (Fig. 4.3a).

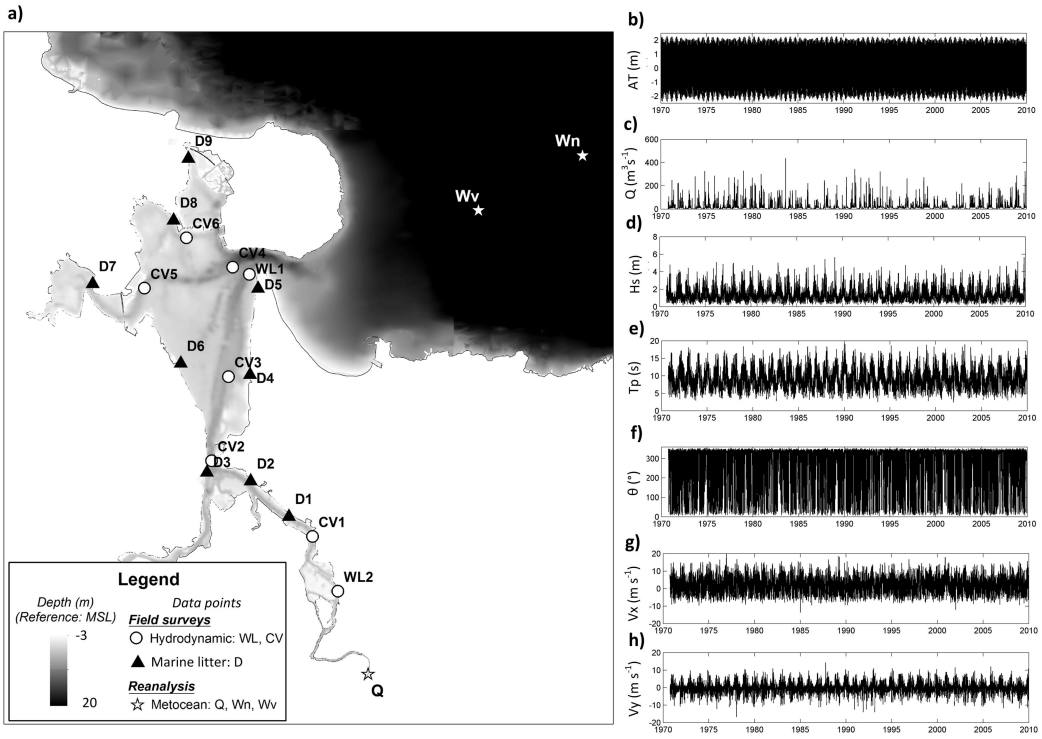

Figure 4.3: Available data in SB: a) bathymetry and points with data of water level (WL), current velocity (CV), litter mean density (D), river discharge (Q), wind (W_n), and waves (W_v); 40-year (1970–2010) time series of b) astronomical tide water level (AT), c) Asón River discharge (Q), d) significant wave height (H_s), e) peak wave period (T_p), f) mean wave direction (θ), g) W-E wind component (W_x), and h) S-N wind component (W_y).

4.3.3. Instrumental data

To characterise the astronomical tide, data from the Santander tide gauge supplied by the Spanish National Port Administration have been employed. Although this tide gauge is located in Santander Bay (43.46 N/3.79 W lat/lon), 30 km from the study area to the west, it can adequately represent the tide at the mouth of the Cantabrian estuaries (Bárcena et al., 2015). This tide gauge provides sea level data from 07/01/1992 to the present, with a temporary resolution of 1 h. In this study, a harmonic analysis (Pawlowicz et al., 2002) of this series was performed to characterise the tidal wave outside SB (Fig. 4.3b). The harmonic analysis reveals that M2 is the main harmonic,

followed by S2, N2, and K2, which confirms the semidiurnal character of the tide in this area.

In addition, water level (WL) data are recorded in a field survey conducted between November 12, 1997 and November 27, 1997, in two areas inside SB. Current velocity (CV) profiles at 6 stations are measured during four tidal phases (high tide, mid-ebb tide, ebb tide and mid-high tide) for two tidal cycles (spring tide and neap tide). These data are used to validate the hydrodynamic model. Fig. 4.3a shows the locations of these sampling points.

4.3.4. Reanalysis data

River discharge data are obtained from a database that covers the period 1970–2003 (García et al., 2008); the data are subsequently updated until 2010. The data include average daily discharges obtained from numerical simulations of the Asón River at one point close to its mouth (point Q in Fig. 4.3a). Fig. 4.3c shows the simulated freshwater inputs of Asón River into SB.

Waves at the Spanish coast can be defined from the high-resolution ($dx \simeq 0.005$, $dy \simeq 0.004$) downscaled ocean waves (DOW) database (Camus et al., 2013). The time series of propagated sea states can be extracted with an hourly temporal resolution from 1948 onwards at each point of the grid using a nonlinear interpolation technique (Camus et al., 2011a). Fig. 4.3d–f show the significant wave height (H_s), peak wave period (T_p), and mean wave direction (θ) series that were reconstructed between 1970 and 2010 at an outer point of SB (point W_v in Fig. 4.3a).

Wind data at 10 m above sea level have been obtained from the *SeaWind*NCEP-HR database (Menendez et al., 2011). Data can be extracted with a spatial resolution of approximately 0.02° and a temporal resolution of 1 h from 1948 to the present. Fig. 4.3g–h show the W_x and W_y wind components, from 1970 to 2010, at an outer point of SB, which is not influenced by the coast (point W_n in Fig. 4.3a).

4.3.5. Plastic debris density data

In October 2017, a marine litter field survey was performed in 9 sampling areas selected according to the representative hydromorphological conditions of SB (Fig. 4.3a). The aim was to obtain the field data necessary to assess, as a first approach, the goodness of the proposed methodology. In each area, litter items larger than 0.5 mm were quantified within 3–5 circular sampling units (diameter of 3 m), that were equidistantly distributed along transects (lengths from 50 to 100 m) parallel to the coastline (following Rech et al., 2014), and covering a total area between 21 and 35 m^2. Litter items gathered were classified into types following the protocol by OSPAR (2010). Mostly litter items were represented by plastic debris and followed by sanitary waste. From these data, the average density (AD) of plastic debris (number of items per square metre) was estimated. Mazarrasa et al. (2019) describe in more detail the sampling methods used for the field survey.

4.4. Methodological development and application to Santoña Bay

4.4.1. Selection of metocean scenarios

The specific objective of this step is to select statistically representative scenarios of plastic debris transport in the study area.

The time horizon (T) was selected according to the estuary extent and the timescales that govern hydrodynamics and transport. The main hydrodynamic drivers in SB are tide, river discharge, waves, and winds. The tide, with its 15-day spring-neap cycles, is the key factor. According to previous runs of the trajectory model, when T is equal to 15 days and in some of the most unfavourable transport conditions (discharge rates of 8 m^3/s, which are lower than the typical average discharge of 16 m^3/s), most of the particles that are representative of plastic items reached the coast or the open sea, which enables a relatively stable plastic debris distribution.

Following Castanedo et al. (2016), clustering techniques were applied to identify representative environmental scenarios from 40-year hindcast data-bases (1970–2010). Due to the deterministic nature of the tide, the selection of tidal cases was independent from the remaining variables. Therefore, the total number of scenarios (N) were obtained from combining a determined number of astronomical tide scenarios (N_{AT}) with the representative states of local dependent variables: river discharge, waves, and wind (N_C).

The algorithm chosen for the selections was K-means, the same one used to classify astronomical tide in Chapter 2, also initialized with the maximum-dissimilarity algorithm (Camus et al., 2011b). Subsection 2.3.3 briefly describes the iterative process followed by K-means algorithm to obtain representative clusters of the analysed variables. A more detailed description about K-means algorithm is found in Hastie et al. (2001).

The clustering of multiple time-varying parameters that include directional information (15-daily series of wind, river discharge, and waves selected from 40-year series) is more complex than the classification made in Chapter 2. For this reason, a statistical descriptor as demanding as the CE used in Chapter 2 would not provide relevant information about the resulting clustering. A suitable statistic to compare the original series and the synthetic time series—reconstructed with clusters from these classifications—when directional variables are involved is the mean *skill index* (s) (Willmott, 1981):

$$s = 1 - \frac{\sum_{i=1}^{r}(|x_s - x_o|^2)^2}{\sum_{i=1}^{r}(|x_s - \bar{x_o}| + |x_o - \bar{x_o}|)^2} \tag{4.1}$$

where x_o is the original time series, x_s is the synthetic time series reconstructed with centroids from classifications, and r is the length of both time series. The skill coefficient reflects the accuracy with which classified variables estimate the original variables: an s value equal to 1 is indicative of a perfect agreement between the two series, while a value of 0 is associated with a complete disagreement. The selection process is explained below for

both the astronomical tide and the local dependent variables.

To select biweekly astronomical tides, following Bárcena et al. (2015), a rearrangement of the hourly water level series was performed before applying K-means. To consider all possible chronological evolutions of the tide, an array to be clustered was built by applying a one-day moving-window over a 15-day interval of the daily tidal range time series (Fig. 4.4a). To obtain the optimum number of representative tidal scenarios (N_{AT}), K-means was applied to this array to test different numbers of clusters. According to the skill index, a suitable number of representative tidal scenarios (N_{AT}) obtained for T equal to 15 days was 6. As shown in Fig. 4.5a, the mean skill index exceeds 0.9 for this value. The K-means algorithm was applied with N_{AT} equal to 6 to select statistically representative tidal range cases (centroids). For each centroid, its associated real water level series of astronomical tide ($AT_j; j = 1, 2 \dots N_{AT}$) with its probabilities of occurrence (P_{AT}) were obtained.

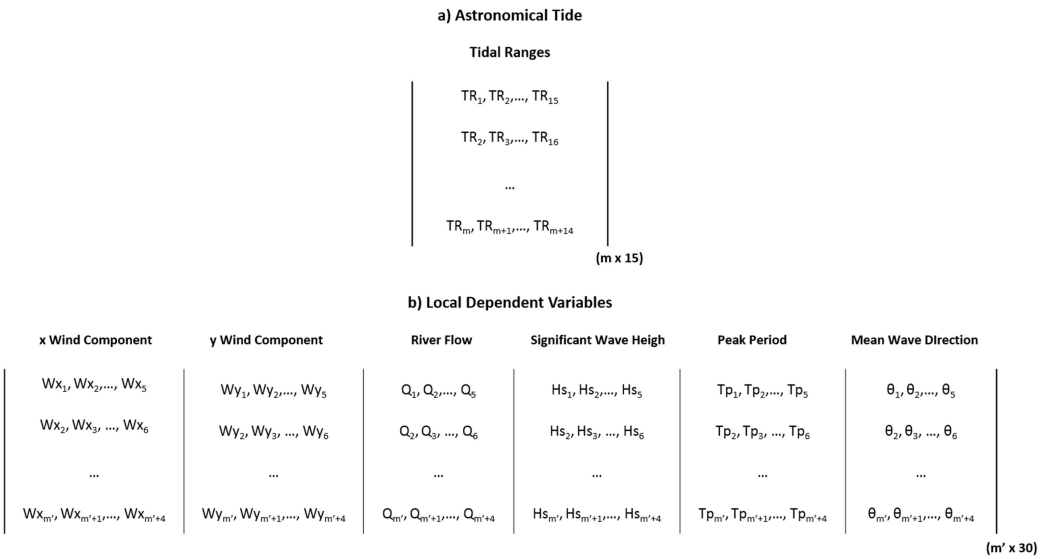

Figure 4.4: Arrays to be clustered of: a) astronomical tide and b) local dependent variables.

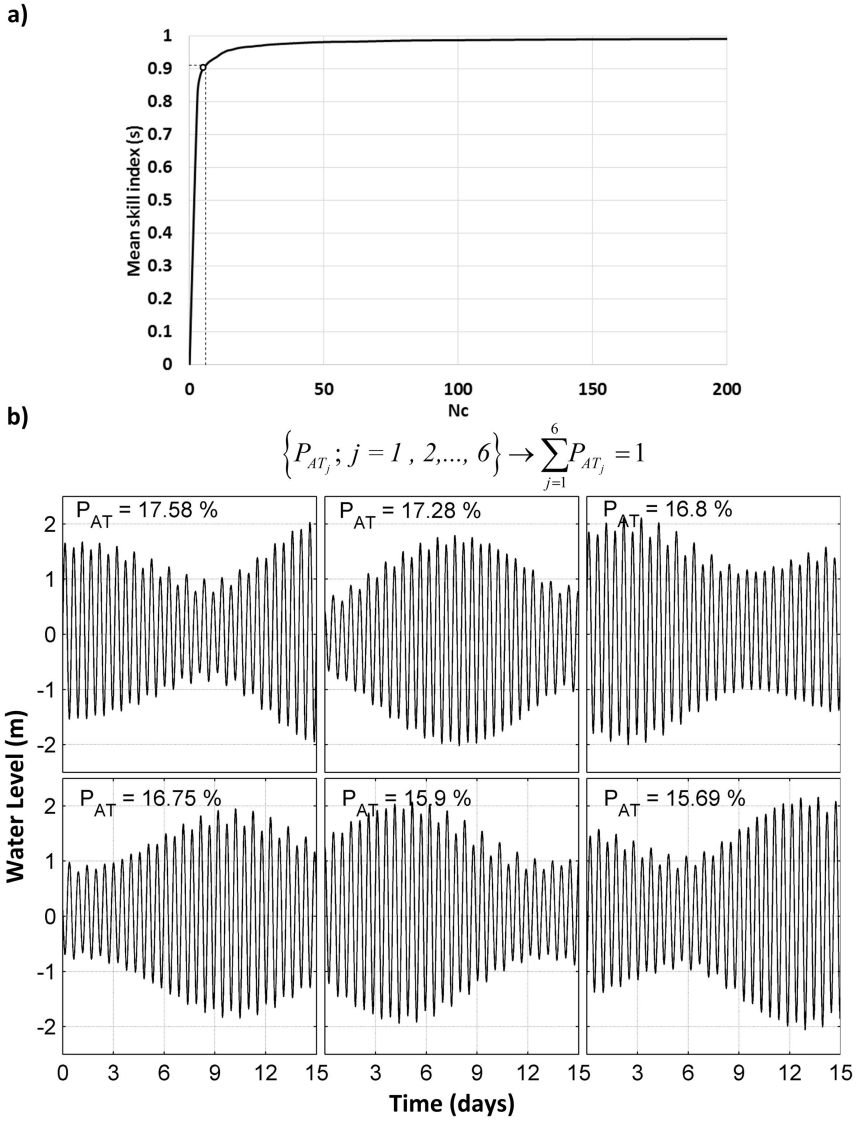

Figure 4.5: Representative biweekly cases of astronomical tide (AT_j) at SB: a) mean skill index (s) and b) hourly water level series with probability of occurrence P_{AT}.

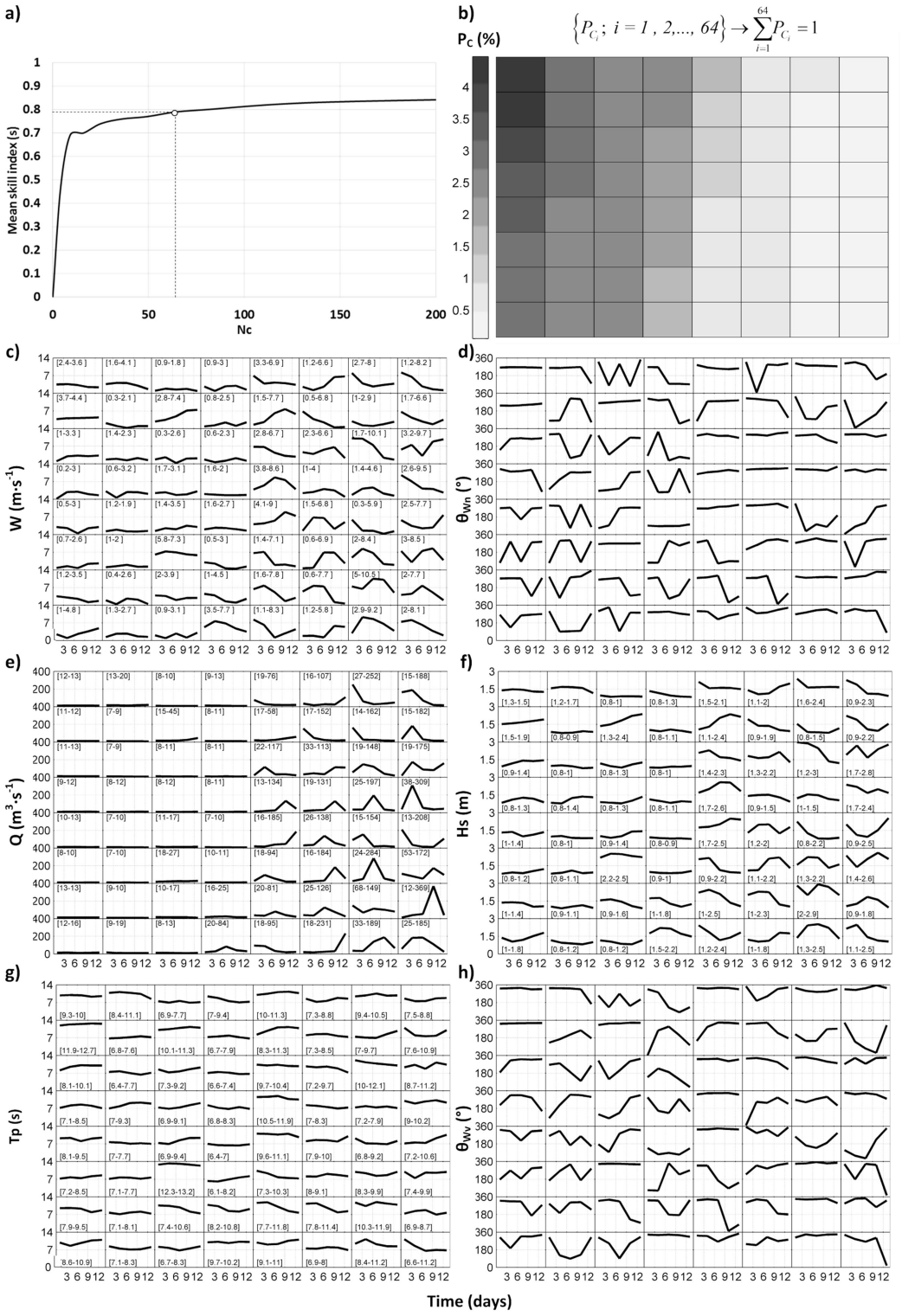

Figure 4.6: Representative biweekly cases of local dependent variables (C_i) at SB: a) mean skill index (s); b) joint probability (P_c); c) wind module series (W); d) wind direction series (θ_{W_n}); e) river discharge (Q); f) significant wave height (H_s); g) peak wave period (T_p), and h) mean wave direction (θ_{W_v}).

The selection of 15-day patterns of local dependent variables (wind, river discharge, and waves) required a resizing of the available hourly series of each variable to configure the algorithm's inputs. An array was built by applying a three-day moving-window over a 15-day interval of the 3-day time series of river discharge (Q), significant wave height (H_s), peak wave period (T_p), mean wave direction (θ), and x-y wind components (W_x, W_y) (Fig. 4.4b). The chosen time span was 3 days based on the average storm persistence in the Cantabrian Sea, that is representative of the metocean conditions (Méndez et al., 2006). The optimal number of representative scenarios (N_C) obtained for 15 days was 64. Fig. 4.6a shows that the mean skill index has a value near 0.8 and the improvement is not significant from this point. K-means was applied to the input array with N_C equal to 64 and statistically representative wind, wave, and river discharge conditions ($C_i; i = 1, 2 \dots N_C$) were selected; each C_i shows a probability of occurrence (P_C). Unlike the tide selection process and given the complexity of working with multiple local dependent variables, the value of each centroid was directly applied instead of selecting the real data closest to the centroid. In this way, the statistical representativeness of the set of all drivers is retained.

The results of applying the K-means algorithm to the astronomical tide with N_{AT} equal to 6 and local dependent variables with N_c equal to 64 are shown in Fig. 4.5 and Fig. 4.6, respectively. The set of these cases comprises a total number of 6×64 representative metocean scenarios (N).

4.4.2. Dynamic downscaling

The goal of the second step of the methodology is to obtain high-resolution drivers to be used as forcings of the transport model for each of the previous 6×64 selected scenarios.

As SB is a well-mixed estuary, a 2D hydrodynamic modelling was suitable to represent the flow features. To take into account the current-wave interaction, hydrodynamics and waves were propagated in an online coupled way with the hydrodynamic (FLOW) and wave (WAVE) modules of the

numerical model Delft3D. Delft3D-FLOW (Hydraulics, 2018a, Roelvink & Van Banning, 1995) has been described in Chapter 3. Delft3D-WAVE (Hydraulics, 2018c) implements the SWAN wave propagation model (Booij et al., 1999), which is a third-generation wave model that is based on the spectral action balance equation that represents the effects of spatial propagation, refraction, shoaling, generation, dissipation, and nonlinear wave-wave interaction.

To define the hydrodynamic and wave model domains, two two-dimensional curvilinear grids, which allow the resolution to be adapted to the needs of the study, were built (Fig. 4.7). Both grids show a similar extension that covers the SB area with hydrodynamic continuity. The main difference between both grids is the resolution attained inside the bay, conditioned by the type of drivers to be evaluated. In this area, the hydrodynamic grid needs to have a high discretisation to differentiate channels from intertidal flats and adequately characterise flow features. The highest discretisation of the wave grid is required near the outer beach, as it is coarser in the inner area sheltered from waves. Therefore, the hydrodynamic grid has 614×186 elements and a variable resolution from 150 m at the outermost area of the bay to 9 m at the innermost area. The wave grid has 242×113 elements and a variable resolution within 150 m outside, and attains its highest resolution near Laredo beach, where it has values of approximately 30–40 m.

To evaluate 2D hydrodynamics in SB, the most suitable roughness coefficient (C) and horizontal eddy viscosity (ϵ) were defined. C was characterized as a variable with depth according to the equivalent geometrical roughness of Nikuradse (k_s), and ϵ is a variable with cell size according to a calibration constant (k). A calibration process was conducted to test different values of k_s and k parameters, and the numerical results were compared with available instrumental data (water level and current velocity gathered during field surveys on November 12, 1997 and November 27, 1997). The results indicated that the optimal parameters were 0.1 m for k_s and 0.1 for k. The time step adopted for hydrodynamic simulations is 0.1 min. Fig. 4.8 shows

the numerical results (solid line) versus the recorded data (dotted line) at points WL1 and WL2 (water levels) and points CV1, CV2, CV4, and CV5 (current velocities) when these parameters are adopted.

Figure 4.7: Hydrodynamic and wave grids at SB.

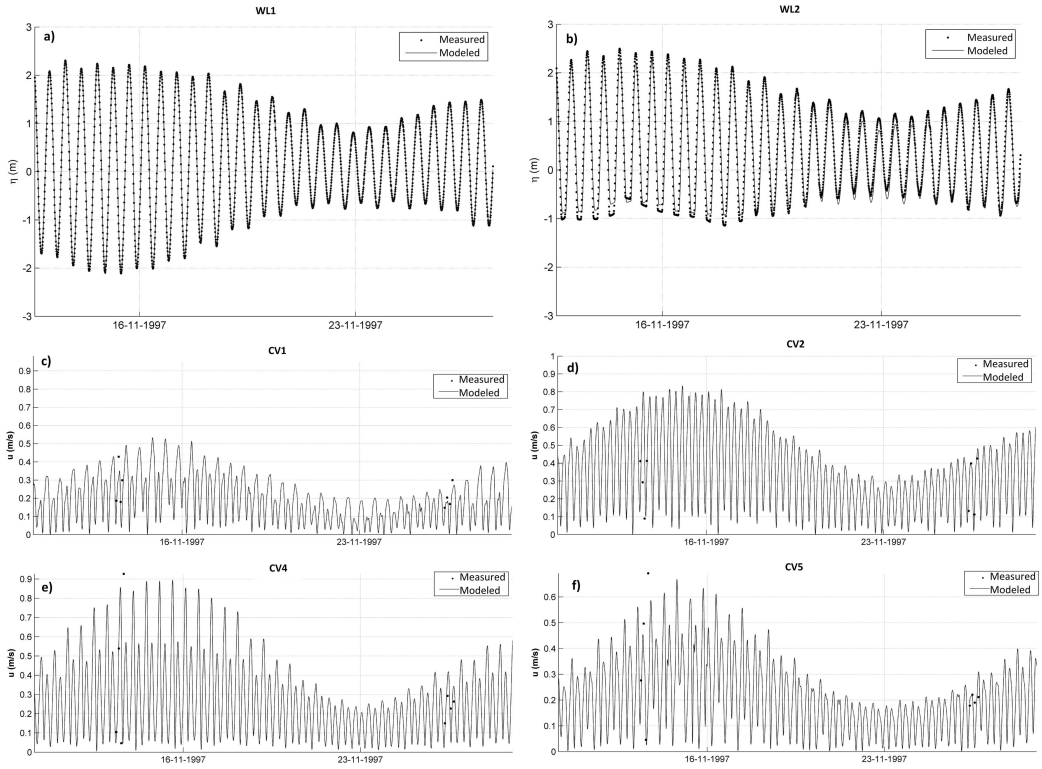

Figure 4.8: Comparison between modelled and observed: water levels at WL1 (a) and WL2, (b) and current velocities at CV1 (c), CV2 (d), CV4 (e), and CV5 (f).

To include the waves influence in the hydrodynamics and transport outside the bay, the JONSWAP friction model with $C_b = 0.067$ m^2/s—which is suitable for wind sea conditions in shallow water areas—was adopted (Booij et al., 1999). The time step adopted to simulate waves is 15 min and a coupling between the hydrodynamic module and the wave module was established every 15 min to assess the current-wave interaction.

The hydrodynamic model with the previously described setup for spatial discretisation (hydrodynamic and wave grids) and parameters (C, ϵ and C_b) was fed with forcings (wind), initial conditions (water level) and boundary conditions (water level, river discharge, and waves) from the N metocean scenarios. Every scenario was modelled to obtain high resolution currents and waves.

4.4.3. Modelling of plastic debris trajectories

The aim of this step is to generate a database of potential plastic items trajectories to identify the presence/absence of particles at different locations of the study area for each scenario.

Due to the need to include the analysis of plastic debris transport by waves, in addition to those due to currents, simulations were performed with the Lagrangian transport module of the TESEO model (Abascal et al., 2007). This module describes the drift process by a set of particles that move by the combined action of wind, waves, currents, and turbulent diffusion. The numerical model solves the following equation:

$$\frac{d\vec{x}_i}{dt} = \vec{u_a}(\vec{x_i}, t) + \vec{u_d}(\vec{x_i}, t) \tag{4.2}$$

where $\vec{u_a}$ and $\vec{u_d}$ are the advective velocity and diffusive velocity, respectively, for the $\vec{x_i}$ point and t time. The advective velocity is calculated as the lineal combination of the wind, waves (Stokes drift), and currents according to:

$$\vec{u_a} = \vec{u_c} + C_d\vec{u_w} + C_H\vec{u_H} \tag{4.3}$$

where $\vec{u_c}$ is the surface current velocity, $\vec{u_w}$ is the wind velocity at 10 m over the sea surface, $\vec{u_H}$ is the wave-induced Stokes drift, C_d is the wind drag, and C_H is the wave coefficient. The turbulent diffusive velocity is obtained using Monte Carlo sampling in the range of velocities $[-\vec{u_d}, \vec{u_d}]$, which are assumed to be proportional to the diffusion coefficients (Hunter et al., 1993, Maier-Reimer & Sündermann, 1982). For each timestep Δt, the velocity fluctuation is defined as:

$$|\vec{u_d}| = \sqrt{\frac{6D}{\Delta t}} \tag{4.4}$$

where D is the diffusion coefficient, whose values range between 1 and 100 m^2/s depending on the spatial scale (ASCE, 1996). The model has been previously calibrated and validated with drifting buoys on both the regional

scale and local scale (Abascal et al., 2012, 2007, 2009a,b, 2017). For a detailed description refer to Abascal et al. (2009a,b) and Castanedo et al. (2006).

In this study, the model has been adapted for the analysis of plastic debris. The stranding (or beaching) algorithm was modified to take into account the effect of environmental features on the accumulations. To achieve this objective, the retention capacity of the shoreline was defined based on two indexes: 0, for areas with high trapping ability (sand, mud, and vegetation) and 1, for areas with low trapping ability (cliffs and vertical dikes). When a particle reaches the coast, if the shoreline is defined with an index equal to 1, the particle can continue moving according to the forcings. Conversely, if a particle reaches a coastal area defined with an index of 0, it will be retained. Particles can be re-incorporated into the sea to properly model wet and dry areas that frequently appear in estuarine environments.

To apply this model to SB, a grid was built to distinguish water areas, where particles move due to forcings, from land areas, where particles remain fixed. This grid has 547×574 regular elements with a spatial resolution (Δx) of 20 m (Fig. 4.9). Based on the features of the bay, shorelines with a high trapping ability and a low trapping ability, were identified for modelling; Fig. 4.9 shows these areas in white and black colours, respectively. Regarding litter sources, most items were assumed to derive from land-based sources (urban centres, beaches, rivers, industries, ports, and wastewater treatment plants) or fishing activities in the sea (Li et al., 2016). Taking into account the existing sewage discharges, 11 litter sources (LS) were selected at SB (Fig. 4.9): a) 10 litter sources from land-based points at the Asón River mouth (LS1); the area of Rada (LS2); industrial areas, urban centre and harbour of Colindres (LS3); Regatón beach (LS4); area of Escalante (LS5); urban centre and harbour of Santoña (LS6 and LS7); urban centre of Laredo (LS8 and LS9); marina of Laredo (LS10) and b) one source that corresponds to a marine origin (LS11).

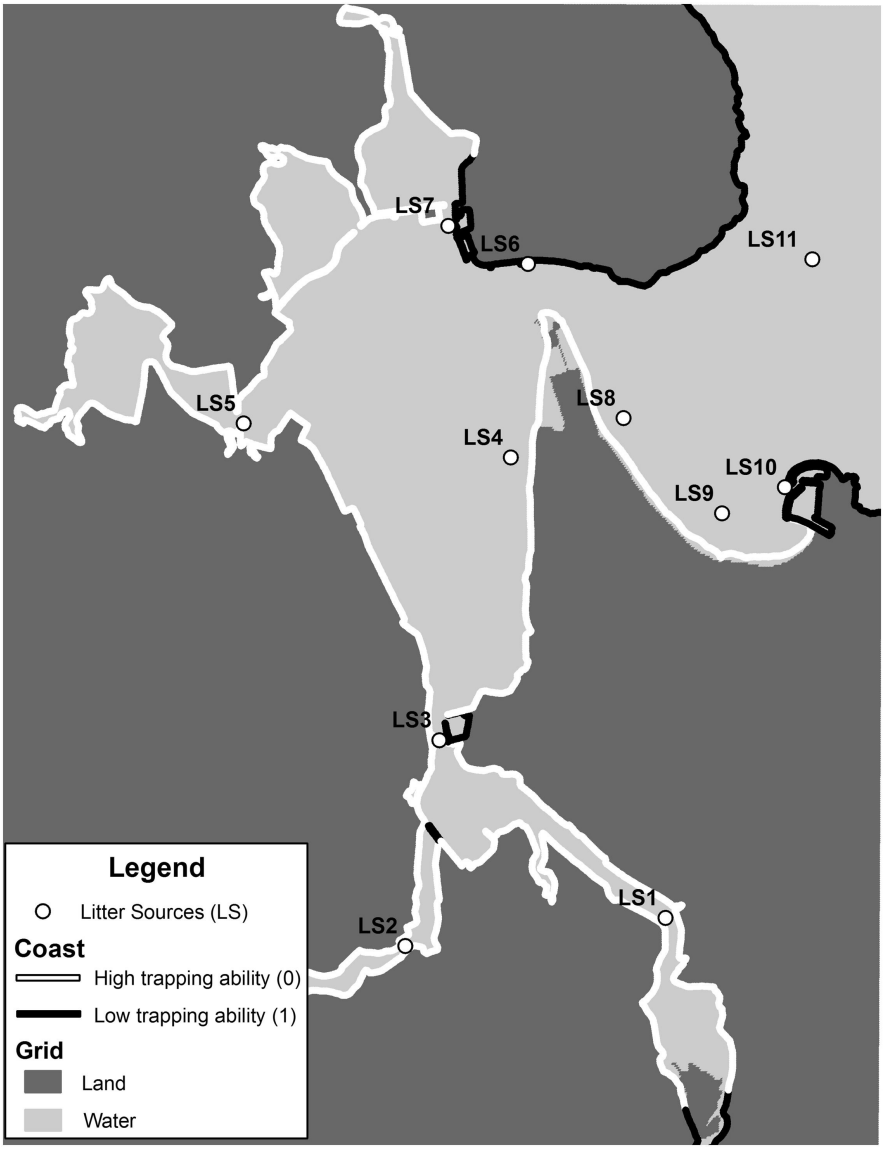

Figure 4.9: Transport grid with water and land cells ($\Delta x = 20m$), coastal areas with high trapping ability (white) and low trapping ability (black), and main potential litter sources (LS) at SB.

According to the location of litter sources and taking into account the relevance of the drivers, the setup of the numerical simulations was defined. The parameters and model options to represent the transport conditions are wave (C_H), diffusion (D), and wind drag (C_D) coefficients, number of particles, and timestep (Δt). Currents comprise the most important element

that influences the transport of plastic debris inside SB. In the outer area, especially near the beach, the waves also have relevance. Therefore, C_H and D were set in each area according to the literature. These values are 0.01 for C_H (Abascal et al., 2009b, Castanedo et al., 2006), 0.5 m^2/s for D in river areas, 2 m^2/s for D in the estuarine area, and 15 m^2/s for D in the open sea (Abascal et al., 2012, 2017, Viikmäe et al., 2013).

Concerning wind drag coefficient (C_D), studies such as Yoon et al. (2010) describe the relation between the shape and buoyancy ratio of floating plastic items and the wind effect on the transport at a regional scale. However, enough information is not available to define C_D at an estuarine scale. In absence of more specific information, previous numeric transport tests including generic particles and wind drag were carried out. With C_D values higher than 0, results showed unreal transports inside the narrowest areas of the bay where, following wind direction, particles were retained on shorelines near the sources from the initial instants of the simulations. Consequently, wind drag was not included to assess transport in this work ($C_D = 0$).

Regarding the number of particles, based on previous studies such as Abascal et al. (2009a), Barker & Galt (2000) and Díaz et al. (2008), 1000 particles were considered to be suitable to represent plastic inputs at each LS. With regard to the timestep (Δt), 5 s was adopted to ensure the stability of the model. As the study area has an important intertidal surface, the wetting-drying option was activated. When a cell is dry, the particles remain fixed at the same position until the cell is flooded.

High-resolution currents and waves generated with dynamic downscaling were employed as forcings of the TESEO model with the above defined setup. Each trajectory was simulated for a 15-day period, and the results were recorded with a 5-min temporal resolution. As a result, a dataset of N (number of scenarios) $\times M$ (number of particles) trajectories was obtained for each litter source (LS).

4.4.4. Statistical analysis

A statistical analysis of the trajectory database generated in the previous step determined the most likely areas of plastic debris accumulation from each LS, for the selected time horizon of 15 days, and with a spatial resolution of 20 m. The probability of occurrence of each scenario ($P_{\{C,AT\}}$) was calculated according to the probabilities of the selected cases of river, wind, waves (P_C), and astronomical tide (P_{AT}):

$$P_{\{C_i,AT_j\}} = P_{C_i} \cdot P_{AT_j} \rightarrow \sum_{i=1}^{N_c} \sum_{j=1}^{N_{AT}} P(C_i, AT_j) = 1 \tag{4.5}$$

From the trajectories generated with the transport model, the presence/absence (PA) of particles at different domain points were identified per scenario and per LS:

$$PA = \begin{cases} 0 & \text{if there is no particle (absence)} \\ 1 & \text{if there is one particle at least (presence)} \end{cases} \tag{4.6}$$

Knowing the LS where a plastic debris input occurs, the probability ($P_{\{C,AT\}}$), and presences/absences (PA) of every scenario, the accumulation probability (P) was calculated as follows (Fig. 4.11a):

$$P = \sum_{i=1}^{N_C} \sum_{j=1}^{N_{AT}} P(C_i, AT_j) \cdot PA_{i,j}(0,1) \tag{4.7}$$

Fig. 4.10 shows these results for some of the most representative LSs of SB. Although the probabilities were extracted with a spatial resolution of 20 m, figures show their aggregate values in cells of 50 m to facilitate their graphic visualisation. Plastic debris inputs from the Asón River (LS1) are more likely to accumulate inside the area of Limpias, primarily on its left shoreline where P attains values higher than 90%. Furthermore, a portion of plastic debris from this source is distributed through the rest of SB, but with a probability less than 10% (Fig. 4.10a). Similarly, plastic debris derived from

sources located upstream of Rada (LS2) and Escalante (LS5) are more likely to accumulate in both margins inside these areas. The highest probabilities —greater than 90%— are close to the sources and decrease with distance (Fig. 4.10b and d). Regarding plastic items from Regatón beach (LS4), they are distributed throughout SB concentrating on its right shoreline—where the mean P ranges from 40% to 50%—, especially near the source, where P exceeds 90% (Fig. 4.10c). Plastic debris from the town and harbour of Santoña (LS7) are more likely to accumulate in the urban shorefront, where P exceeds 90% due to hydrodynamics conditions despite its low trapping ability, and in the area of Boó, where P ranges between 40% and 70% (Fig. 4.10e). Concerning inputs from the urban centre of Laredo (LS8), they show a tendency to accumulate on the Laredo's beach—with a mean P of approximately 70–80%—, Colindres harbour—with a mean P from 60% to 70%—, and the Santoña urban shorefront—where P oscillates between 40% and 50%—(Fig. 4.10f). Plastic debris from the marina of Laredo (LS10) accumulates within the harbour—P exceeds 90%—and around the adjacent area of the beach—P about 70%—(Fig. 4.10g). Plastic debris arriving from the outer sea (LS11) tends to be retained on both sides of the estuary mouth. Areas with low trapping ability, such as the Santoña shorefront and the rubble mound breakwater of marina of Laredo, show probabilities higher than 90%. This fact can be explained by the high intensities of drivers (currents and waves) in these areas. The probability that this plastic debris accumulates on the Laredo and Regatón beaches ranges between 10% and 20% (Fig. 4.10h).

An average global probability (P_G) was estimated for the set of all sources according to Eq. 4.8:

$$P_G = \sum_{n=1}^{N_{LS}} P_{LS_n} \cdot P_n \tag{4.8}$$

where P_{LS} is the probability of the source LS to generate plastic debris, P is the probability of litter accumulation from LS, and N_{LS} is the total number of litter sources. As a sufficient amount of information about P_{LS} is not available, a hypothesis extensively applied in the literature was adopted. 80%

of plastic debris was assumed to derive from land-based sources (considering the same probability in the sources from LS1 to LS10) and the origin of the remaining 20% is marine (LS11) (Faris & Hart, 1994). According to this premise, the average global probability of plastic debris accumulation was calculated at SB for the selected time horizon (Fig. 4.11b).

Regarding the numerical results, the highest probabilities —approximately 40%— are primarily concentrated on both sides of the estuary mouth and in the surroundings of the marina of Laredo. With mean probabilities that range between 10% and 20%, the areas of the Laredo and Regatón beaches, the south margin of Escalante, both margins of Limpias and Rada, especially in the narrowest sections, and the shorelines of Treto near Colindres town show the next highest probabilities.

As an example, Fig. 4.12 shows P_G for the months of January and June. Similar distributions are observed in both maps, which also coincides with the average global map distribution, with greater accumulations near sources and beaches. These results, which extend to the remaining months of the year, maybe attributed to the tide, since its six (6) representative scenarios present similar probabilities independent of the time of year, whereas the remaining drivers (river discharge, waves, and wind) show greater stational dependence. Therefore, in the specific case of SB, the role of astronomical tide and the asymmetry arose during its propagation determine the plastic debris distribution, compared to river discharge, waves, and wind drivers.

Maps of the plastic debris percentages (Pct) from each LS were obtained by applying Eq. 4.9, which depends on the probability of each LS to generate plastic debris (P_{LS}), the probability of each area to accumulate plastic from each LS (P), and the global probability (P_G) of the set of all LSs (Fig. 4.11c):

$$Pct = \frac{P_{LS} \cdot P}{P_G} \tag{4.9}$$

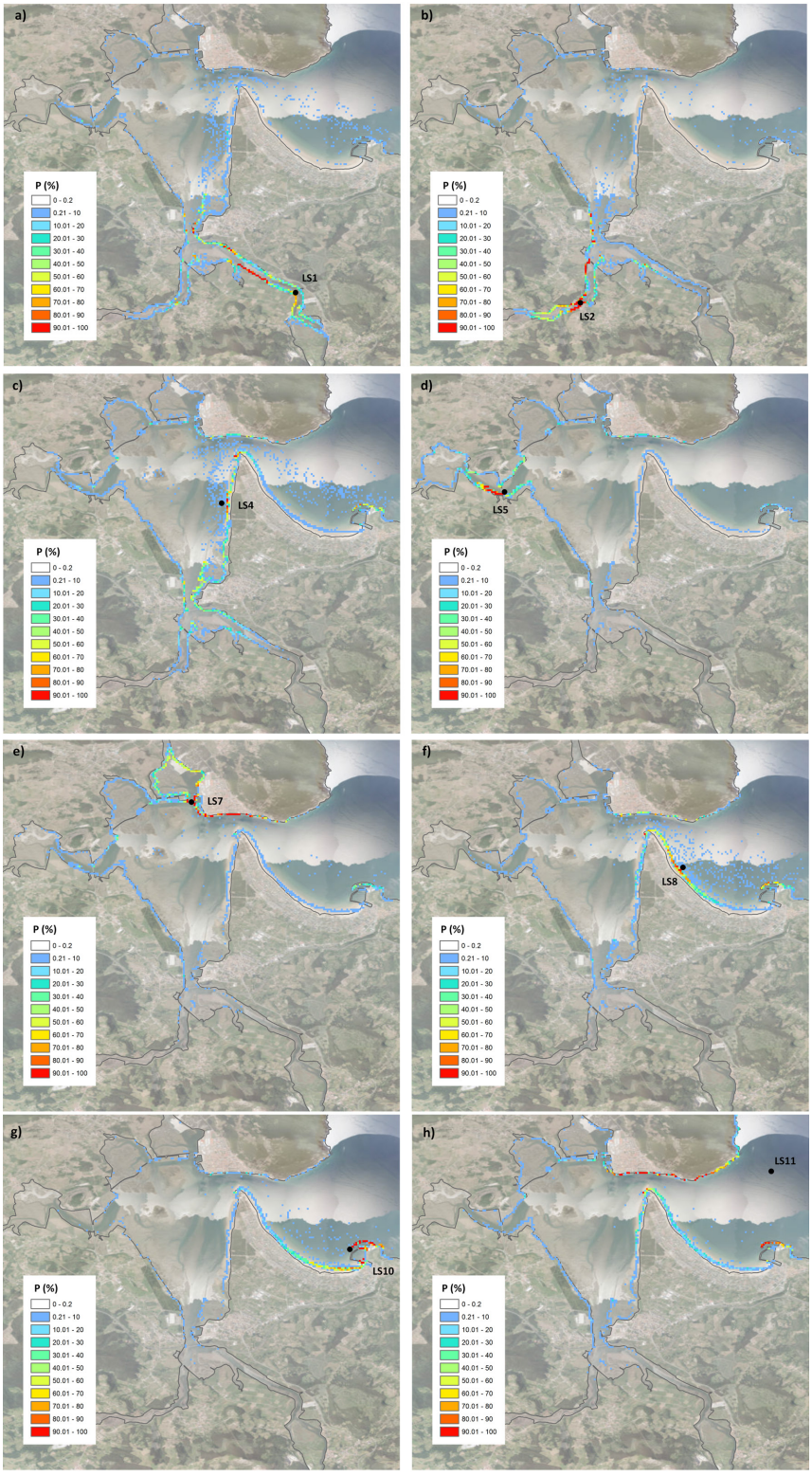

Figure 4.10: Probability to accumulate plastic debris (P) from: a) LS1, b) LS2, c) LS4, d) LS5, e) LS7, f) LS8, g) LS10, and h) LS11.

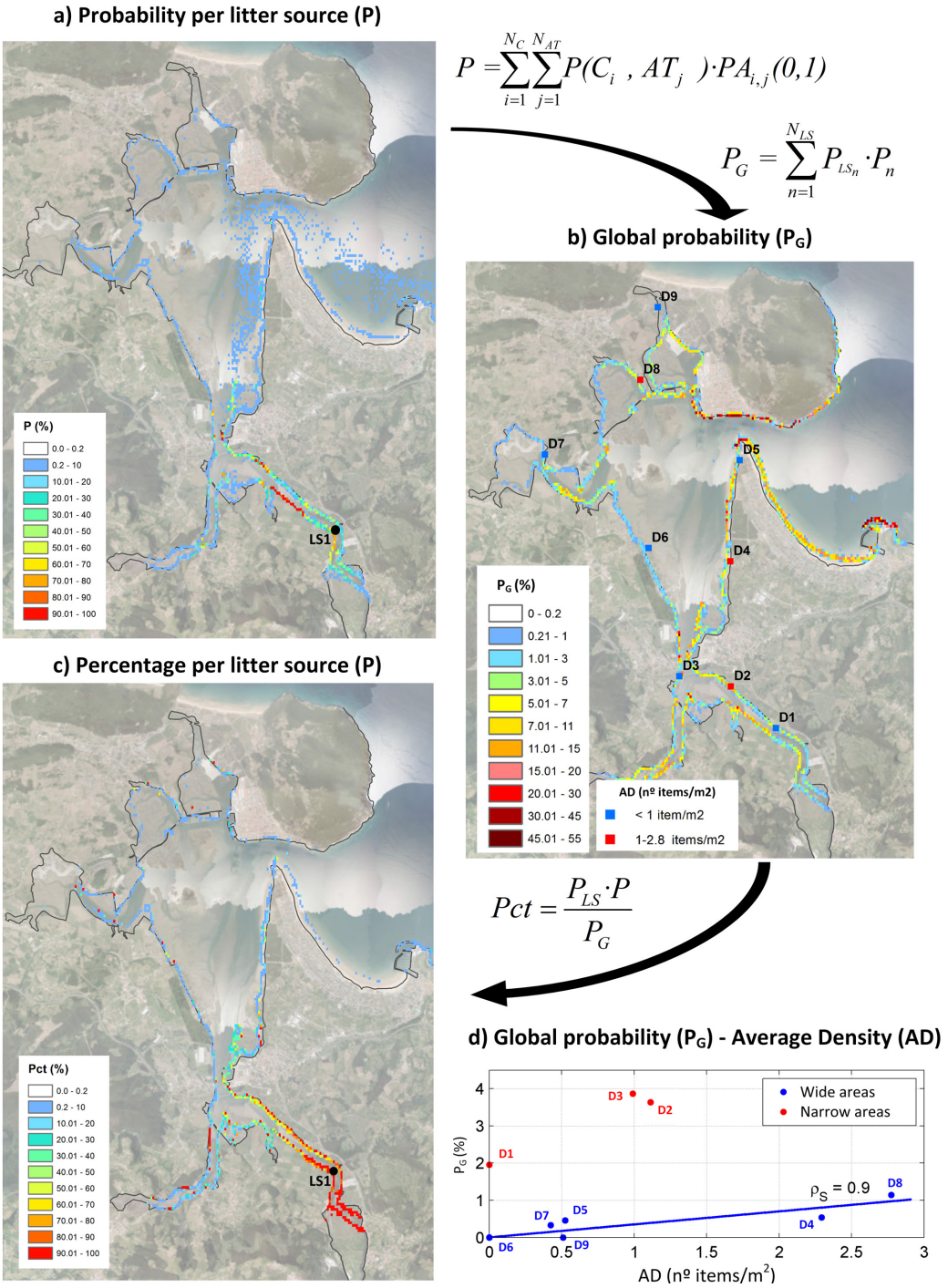

Figure 4.11: Statistical analysis: a) Probability (P) to accumulate plastic debris from LS1; b) Global probability (P_G) of plastic debris accumulation; c) Litter percentages (Pct) from LS1, and d) comparison between P_G and average densities (AD).

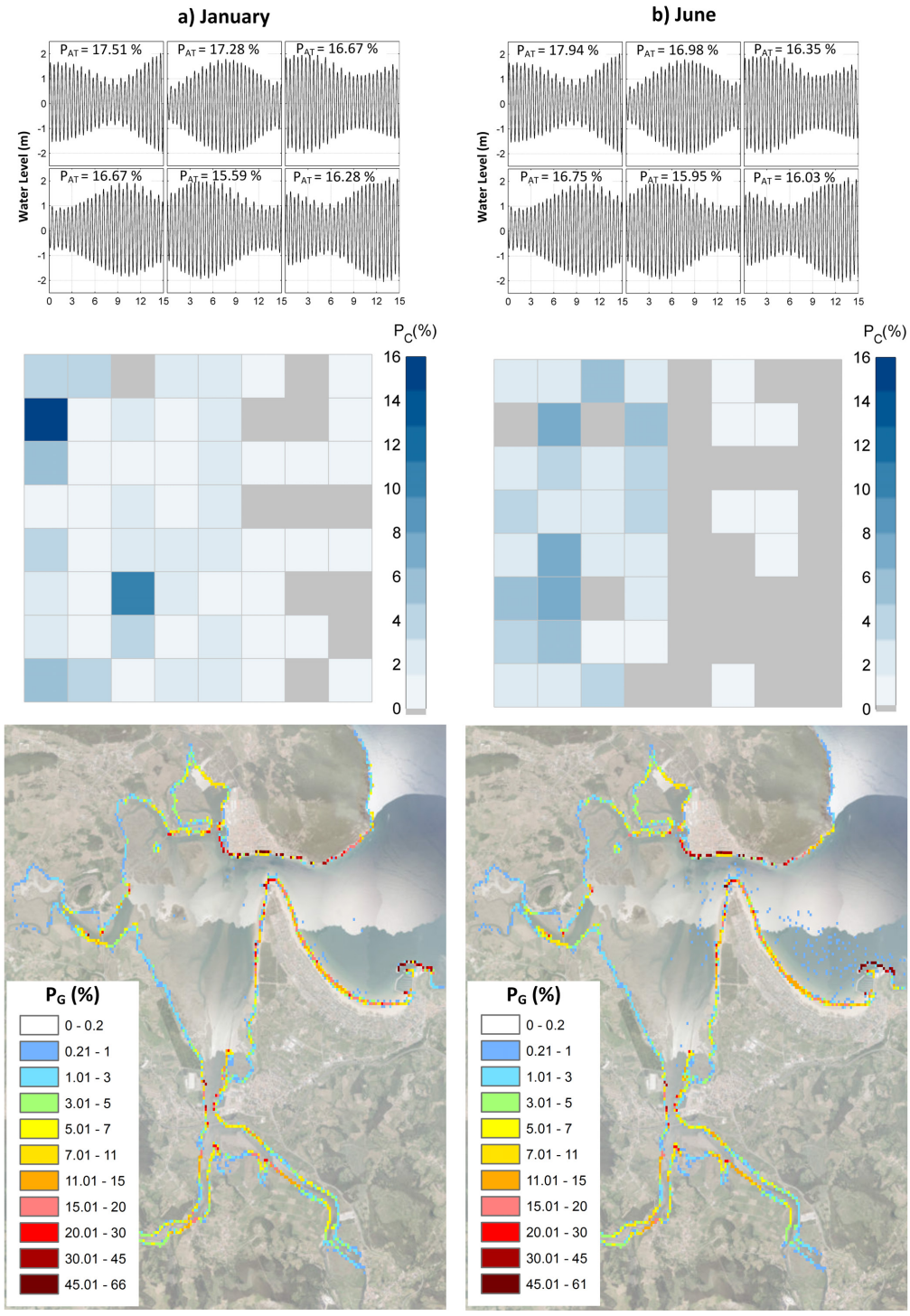

Figure 4.12: Global probability (P_G) of plastic debris accumulation for the months of: a) January and b) June.

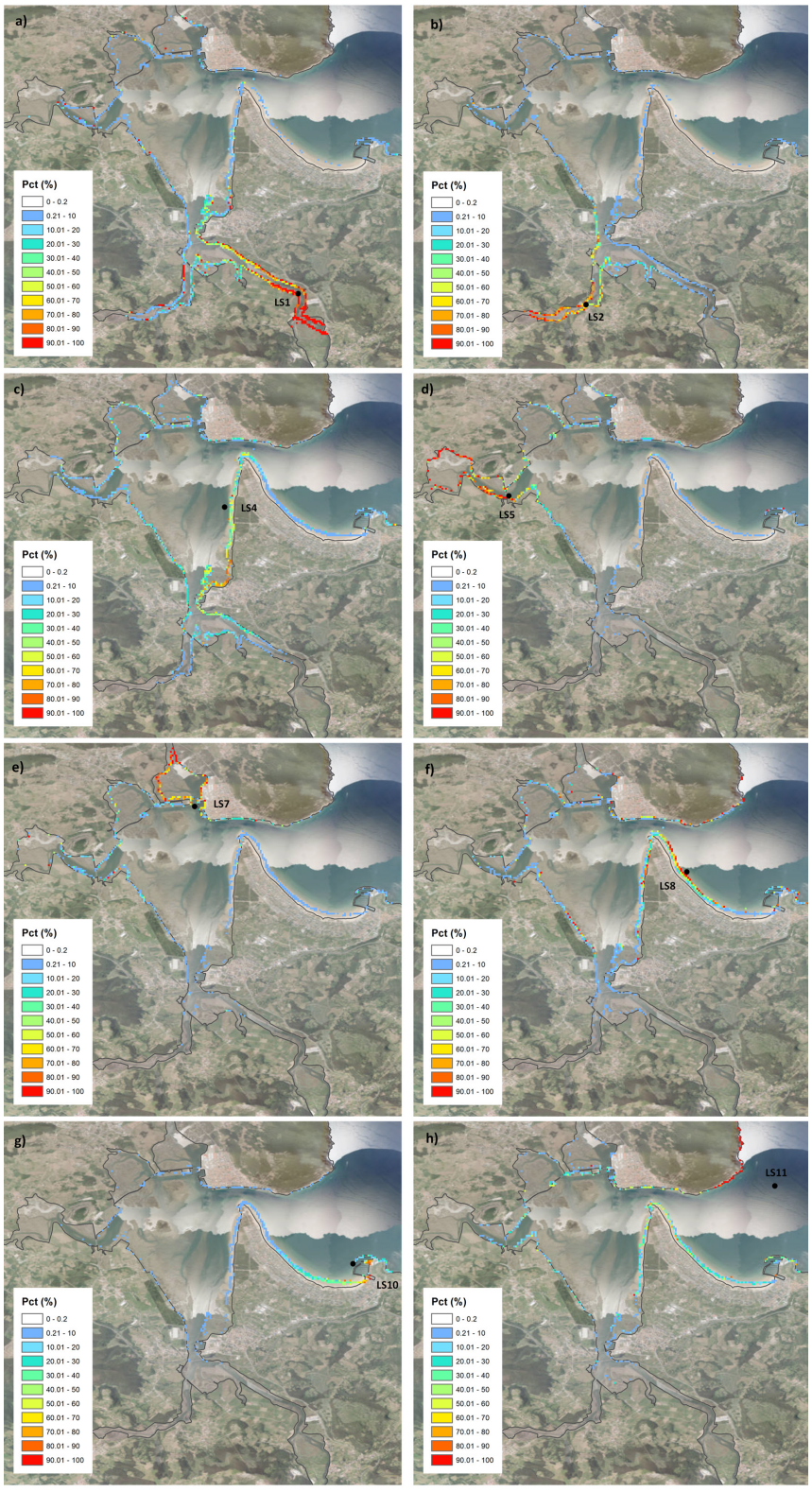

Figure 4.13: Plastic debris percentages (*Pct*) from: a) LS1, b) LS2, c) LS4, d) LS5, e) LS7, f) LS8, g) LS10, and h) LS11.

Fig. 4.13 shows the maps of the plastic percentages from LS1, LS2, LS3, LS4, LS7, LS8, LS10, and LS11. In general, the same behaviour pattern is observed in all maps. In each area, the higher proportion of plastic debris is derived from its nearest source and gradually decreases with distance. The greatest percentages —higher than 90%— are obtained for the innermost estuarine areas (Figs. 4.13a, b, d, and e). They are narrow areas with a high trapping ability and, consequently, most of the plastic debris derived from upstream sources quickly reaches the coast where remains retained. Conversely, LS4, which is outside these areas, affects with a mean intensity—average Pct of approximately 50%—to a larger area and with percentages close to 80% on the coasts of Regatón beach and Colindres (Fig. 4.13c). In Laredo beach, the highest percentage of plastic debris is primarily derived from the representative sources of the Laredo urban centre, LS8, which contributes 60% of plastic debris in the westernmost area of the beach (Fig. 4.13f) and LS10, with an average value that ranges between 40% and 70% in the easternmost area (Fig. 4.13g). Likewise, a non-negligible percentage of approximately 10–20% is obtained from the outer sea (LS11) (Fig. 4.13h).

Fig. 4.11b shows the numerical outputs of P_G and the average density (AD) data gathered in the field survey, and Fig. 4.11d illustrates the scatter plot of AD and the average P_G within a radius of 100 m. Highlighting the preliminary character of the comparison and taking into account that a description of the sample behaviour is sought, the non-parametric coefficient of Spearman (1961) was applied to estimate the correlation between both series (refer to Eq. 4.10):

$$\rho(P_G, AD) = \frac{\sum_{i=1}^{r} (P_{G_i} - \overline{P_G}) \cdot (AD_i - \overline{AD})}{\sqrt{\sum_{i=1}^{r} (P_{G_i} - \overline{P_G})^2 \cdot \sum_{i=1}^{r} (AD_i - \overline{AD})^2}} \tag{4.10}$$

where r is the length of each series.

Sampling areas where higher plastic debris densities were obtained are near areas where models show higher accumulation probabilities, and vice

versa (Fig. 4.11b). A general behaviour is observed, and P_G numerical values increase with AD observations (Fig. 4.11d). In the widest area of SB (sampling points D4 to D9), the ρ coefficient between both series has the value 0.9. In the narrowest areas (points D1, D2, and D3), an increase between P_G data and AD data is observed, with a different rate of growth. As only three points were assessed in these narrow areas, rigorous conclusions cannot be drawn and more research should be performed.

4.5. Discussion

The available state-of-the-art techniques to study the problem of plastic debris on an estuarine scale demand important investments in experiments, samplings or computational efforts. To address this problem, a methodology that is based on the use of long hindcast meteorological databases, clustering techniques, and numerical modelling was proposed. The methodology was validated in Santoña Bay (SB), an estuary of the northern coast of Spain, by comparing the probabilistic results with field data. The necessary criteria for its application to any estuary in the world were provided.

4.5.1. Inputs of transport modelling

Estuarine and near-shore transport are influenced by tide, river discharges, waves, winds, and thermohaline gradients (Zhang, 2017). Depending on the study area, some of these drivers predominate and the application of the proposed methodology in any estuary requires their proper selection. Gathering and analysing all available information about driver databases is a fundamental preliminary step to identify those that dominate hydrodynamics and plastic debris transport. In the case study of SB, where the two-dimensional character of the flow is distinguished (well-mixed), transport is dominated by tide, river, waves, and wind; and the effect of temperature and salinity can be disregarded.

A probabilistic analysis of the transport and distribution of plastic debris

requires long enough time series (years) of these key drivers to reduce the uncertainty associated with the stochastic nature of some processes. The first step of the methodology aims to explain the variability of these long series and reduce the computational cost by selecting N representative scenarios of T days. The proposed criterion to select the most suitable T value consists of performing some test cases with typical hydrodynamic conditions of the study area. An appropriate T value is the value for which the majority of the particles have been retained along the coast or have left the study area towards the sea. To select the N scenarios, clustering techniques, specifically K-means, were employed. Bárcena et al. (2015, 2016) proposed an approach to select scenarios of only river and tide. Castanedo et al. (2014) and Castanedo et al. (2016) proposed a methodology to classify multiple variables on a local scale for a 24 h period. This work innovates in the classification of multiple variables for mid-term periods (15 days) and verifies that K-means efficaciously describes biweekly multivariable ocean states. The methodology achieves efficiency when the number of scenarios is the minimum from which the improvement in the representation of drivers is not significant. *Skill index* (s) around 0.8 is proposed to select the optimal value of the scenarios.

In addition to the temporary representativeness, numerical models must be input with drivers with an appropriate spatial resolution to simulate plastic debris transport on local scales Ballent et al. (2013). Dynamic downscaling proposed in the second step of the methodology allows the resolution of the available drivers to be adjusted to the needs of estuarine features, characterising currents in channels and in wet-dry areas, and waves on the outer beaches. Due to the two-dimensional character of the flow in SB, a 2D hydrodynamic model was successfully employed to obtain high-resolution currents and waves to feed the Lagrangian transport model and simulate the trajectories of floating debris. In the case that the analysed estuary was characterized by important 3D currents (for instance, as a consequence of thermohaline gradients), the hydrodynamic model needs to be configured with a suitable vertical discretization to capture the peculiarities of the flow at different depths.

4.5.2. Modelling of plastic debris transport

The third step of the methodology proposes numerically assessing plastic debris transport using high-resolution and statistically representative hydrodynamic inputs. Hardesty et al. (2017) highlights the need to incorporate some additional and specific aspects of plastic debris transport into the modelling framework.

One of the key aspects in the modelling of any substance is the *beaching* parametrization. These type of parametrizations have been defined in the field of numerical modelling of oil spills based on the knowledge acquired over many years of experience. Some oil spill models, such as Delft3D-PART, TESEO, and GNOME, take into account the oil retention capacity according to the type of shoreline. However, there is not the same level of knowledge for plastic debris. Field or laboratory studies are necessary to know how each type of plastic behaves in each type of shoreline (e.g., the hours in which a plastic bag, a crystal bottle, an ear stick, etc. are retained by a vegetated, sandy, muddy, etc. shoreline). As this knowledge is currently not available, it was decided to implement a simple approach that enables defining coastal areas with total capacity to retain plastic debris and areas without any ability. This aspect may introduce some uncertainty in the results, and it is necessary to improve it to advance in the modelling of plastic debris.

Taking into account that the diffusion coefficient (D) usually has higher values in open oceans than in closed or semi-closed areas (estuaries and bays) (Abascal et al., 2017), we defined different values of D depending on the location of each litter source. Another potential development for the transport model is to define the diffusion coefficient (D) in a spatially variable way. Thus, particle transport would be driven by forcings affected by a D coefficient, whose value depends on the position of each particle at each instant.

4.5.3. Statistical analysis of the outputs

By the statistical analysis of the model outputs, the fourth and last step of the methodology seeks to provide information about plastic debris distribution inside estuaries. In addition to annual average outputs, the developed methodology allows responding to plastic debris accumulations at different times of the year; considering only the probabilities of each transport scenario within this time period. Applying the same principle, these techniques allow making probabilistic forecasts on the accumulations with a minimum computational effort and knowing the prediction of the dynamics for a specific time horizon. Databases, such as CFS (Saha et al., 2011), which provides current predictions over a 6-month time horizon highlight the power of this methodology. In addition, the methodology allows to analyse the contribution of the estuary to the global problem considering the particles that escape outside the domain for the different metocean scenarios.

A direct comparison between probabilistic outputs and observation data allows to assess the consistency of the developed methodology (Abascal et al., 2010, Barker, 2011, Liubartseva et al., 2016, Minguez et al., 2012). This reliability depends not only on the accuracy of models, but also on the robustness for clustering a multivariable dataset and the quality of the inputs that define both the transport drivers and the physical configuration of the estuary.

The outputs obtained for SB were compared with data from the field survey performed in October 2017. The results exhibit a suitable concordance between both series. Areas with a higher probability to accumulate plastic debris are close to areas where higher densities were recorded and, therefore, a coherent behaviour is observed. However, dispersion is detected in three of the points located in the innermost estuarine areas. Further studies with a greater number of sampling points would explain the scatter in these areas.

The results of applying the methodology to SB indicated that the highest probabilities of plastic debris accumulation are close to the sources and decrease with distance (see Fig. 4.10). These results match the findings of previous studies (e.g., Barnes et al., 2009, Browne et al., 2011, Yonkos et al., 2014), which demonstrated a strong correlation between the plastic concentrations on the coast and the proximity to the population centres, that is, some of the most important litter sources (Li et al., 2016). For this reason, the correct location of the litter sources is a key aspect of this methodology and collecting information about them by combining existing documentary sources with observation surveys is necessary. As shown on the global probability map (Fig. 4.11b) and corroborated by the findings of Dekiff et al. (2014), Liebezeit & Dubaish (2012), Mathalon & Hill (2014), and Oigman-Pszczol & Creed (2007), beaches are important areas for plastic debris accumulation with the consequent tourist and economic repercussions. For the adjacent beaches to 4 rivers that flow into the SE Pacific Ocean, Rech et al. (2014) discovered that most litter is obtained from these rivers. According to the results obtained for SB, although a part of the plastic debris that reaches the Laredo beach comes from the river sources, it is not the greater amount (refer to Fig. 4.13). The most significant percentage is primarily obtained from the representative sources of the urban centre and marina of Laredo—with average percentages higher than 60%—and 15% from the outer sea. This aspect does not contradict the findings of Rech et al. (2014). Instead, it is explained by the greater proximity to the beach of other polluting sources, such as urban centres and ports, other than river ones.

4.6. Conclusions

In this chapter, a methodology to probabilistically assess the distribution of plastic debris in estuarine environments was proposed. The use of clustering approaches to classify temporal patterns of multiple local dependent variables (transport drivers) and numerical modelling of a set of potential plastic debris trajectories allows these analyses to be performed

with fewer resources than the state-of-the-art techniques. Regarding numerical modelling, due to the importance of estuarine geometry and the type of substrate (sand, mud, man-made materials, and presence of vegetation) for the retention of plastic, the implementation of options to define these abilities are essential aspects in the framework of modelling.

The methodology has been validated with a case study in an estuary of the northern coast of Spain (Santoña Bay, SB) by comparing the obtained results with the average density of plastic debris gathered *in situ*. The validation concluded that the implementation of this methodology could be a helpful tool for plastic debris management in estuaries. From the results of SB application, the K-means algorithm successfully describes the biweekly multivariable (including tide, river discharge, wind velocity, and direction and wave components) ocean states that drive transport process, and therefore, plastic debris distribution. This study verifies, in accordance with previous studies, that plastic debris tend to accumulate near its sources and on the shorelines of adjacent beaches.

During the development of the methodology, the necessary criteria have been provided to ensure its applicability to any other estuary of the world.

Chapter 5

Conclusions and ongoing research

5.1. Summary of contributions

The general objective of this Thesis was to investigate the relationship between hydrodynamics of tide-dominated estuaries and the distribution of plastic debris, emphasizing the hydrodynamics due to the astronomical tide and its asymmetry. Furthermore, this Thesis contributed to the development of a general methodology to identify *hotspots* of plastic debris in estuaries, that allows to assist managers in the definition of prevention and cleanup strategies.

This general objective is achieved through the three specific objectives previously defined in the Chapter 1. The main conclusions drawn from the research associated with each objective are summarized below.

Objective 1. Characterization of tidal asymmetry on a global scale to know its effect in the estuaries as a boundary condition

This specific objective arises from the need to characterize astronomical tide at the mouth of the estuaries. The purpose is to use this information, as a boundary condition, for the study of estuarine processes worldwide. This objective was successfully achieved through the application of clustering and harmonic approaches to the Global Tidal Solution TPXO9-atlas. TPXO9-atlas is the most complete global tidal solution (15 tidal constituents) to date, which has a spatial resolution (1/30°) suitable to describe tidal features in coastal areas. The results were validated with data from 757 tide gauges distributed worldwide, selected from GESLA-2 database. The validation shows that the classification performed characterizes the world's coastal areas well or very well in 97% of the nodes compared and only in the 3% of them shows poor or unacceptable representation.

Below, the key points that summarize the main scientific-technical contributions and the advances in knowledge associated with the first specific objective of the Thesis are shown:

- A graphic guide of astronomical-tide asymmetry and periodicity—both parameters related to the estuarine transport processes—on a global scale were provided. This guide can be used by the scientific community to extract the boundary conditions for studies on the transport of substances, in general, and plastics, in particular, in any estuary of the world.
- The 'tidal elevation time derivative' of astronomical tide ($d\eta/dt$), a variable representative of the rising/falling tidal speed, can describe estuarine flood/ebb currents in absence of additional drivers and thus may be related to estuarine substance transport in both directions.
- Symmetric tides were found to cover about 77.4% of the world's coastal areas, and most of these tides correspond to the mixed semidiurnal

regime (60%), followed by the semidiurnal regime (30%).

- The most asymmetric tides, both positives and negatives (11.3% of coastal areas show positive asymmetries and 11.3% also show negative asymmetries), were found to be concentrated in relatively adjacent areas of the world and mainly correspond to diurnal and mixed diurnal regimes.

- The astronomical triplet O1/K1/M2 dominates in the diurnal and mixed diurnal regimes, whereas the main contribution to the semidiurnal regime comes from the M2/M4 constituents.

Objective 2. Study of the spatial evolution of tidal asymmetry when tide propagates through estuaries of different geometry and its effect in the fate of plastic debris

The second specific objective of this Thesis was achieved by performing hydrodynamic and Lagrangian transport analysis. Different tides—defined at the mouths of the estuaries according to asymmetries—were propagated through a set of estuaries with different geometry. The tides correspond to some of the representative types (identified in the classification carry out in the Chapter 2) that are more different from each other in terms of asymmetry. Some findings of previous studies on the evolution of symmetric tides are confirmed and some novel conclusions on the evolution of asymmetric tides, as well as the effects of both on the accumulations of plastic debris, are provided:

- Symmetric tides evolve to positive asymmetric with tidal propagation as lateral and bottom frictions of channel increase. On the contrary, tidal asymmetry may experience a negative trend if frictions are weak or if the tidal flat area is large enough to counteract the effect of the channel.

- From the propagation of asymmetric tides it is concluded that, in estuarine areas where the main channel shows an important section that favour tidal circulation, the asymmetric tidal character is strongly conditioned by the asymmetry present at the mouth. On the contrary, when there is a clear opposition to the flow or an important intertidal storage area, the relevant role is played by the estuary geometry.

- The tidal-flow opposition imposed by the geometry of the estuaries is also reflected in the accumulation of plastics. The initial asymmetry at the mouths leads to the importation of plastic debris into estuaries the easier the tidal flow through the channel is. In this type of geometries, positive tidal asymmetries show an import capacity 50% higher than those of symmetric and negative asymmetric tides. As opposition to flow through the channel and intertidal storage grow, a clear flood dominance arises, although small influences of the external tidal asymmetry are also appreciated. Thus, probabilities of plastic debris accumulation are around 90% for positive asymmetric tides and range between 70-80% for symmetric or negative asymmetric tides. The fact that these geometries characterize most estuarine systems explains the frequent behavior of estuaries as plastic traps.

- A remarkable and novel aspect that derives from these analyses is the regulatory role of kurtosis in plastic-debris accumulation within tidal estuaries. The kurtosis coefficient increases with the asymmetric nature of the tide. For positive/negative asymmetric tides, this means that the stronger flood/ebb currents are less frequent and consequently the transport capacity induced by the asymmetries is also reduced.

Objective 3. Development of a methodology to assess the probability of plastic debris accumulation in estuaries

Finally, a methodology, that is based on clustering techniques, numerical modelling, and statistical analysis, was developed to address the limitations of the current state-of-the-art techniques—high demand for economic and time resources—for assessing the hotspots of plastic-debris in estuaries. In addition, the general criteria necessary to apply the methodology in any estuary of the world were provided. This methodology was validated through its application to the Santoña Bay, an estuary located in Cantabria (North coast of Spain). The comparison between results and field measurements shows that the implementation of the methodology can provide valuable information for the management of plastic debris in estuarine environments. The following specific conclusions are drawn from the analysis performed:

- The methodology can be applied, with minimal resources, in worldwide estuaries and can provide annual, seasonal, or specific time horizon accumulations. Databases, such as CFS, which provide current predictions over a 6-month time horizon, highlight the power of this methodology.
- Clustering and numerical models were shown to be a good combination for studying the fate of plastic debris on an estuarine scale.
- An innovation has been made in the classification of multiple variables for medium-term periods (15 days). The K-means algorithm was shown to successfully describe biweekly multivariate ocean states which conduct transport processes in estuaries and, therefore, the distribution of plastic debris.
- The physical features of estuaries implemented in numerical transport models were found to influence plastic accumulations.

- According to some results collected in previous studies, it was confirmed that plastic debris in estuarine areas tends to accumulate near litter sources and on adjacent beaches.

5.2. Ongoing research

Research on the transport and fate of plastic debris in estuaries is still in a very early stage and there are many open fronts to address in future research. Throughout the development of this Thesis, some aspects that required further investigation emerged. Furthermore, some results suggested interesting ideas for future analysis.

Regarding the general study of the transport and fate of plastic debris in estuaries:

- To perform some detailed analyses on the individual contribution of other drivers besides the astronomical tide, such as waves, wind, and temperature and salinity gradients, to the transport and fate of plastic debris in estuaries.

- To explore, the influence of the intrinsic physicochemical features of plastic debris that affect its buoyancy (e.g., size, shape, density, etc.) and, therefore, their transport and fate, by mean of physical modelling.

  Regarding these previous issues, on the beaches adjacent to the estuarine mouths, the accumulation of a large amount of plastic debris is frequent (Fok et al., 2017, Heo et al., 2013, Stolte et al., 2015). Isobe et al. (2014) found that larger plastics (macro and mesoplastics) accumulated on the coast of the Seto Inland Sea (Japan) and that microplastics were transported offshore by a combination of Stokes drift and buoyancy of the fragments. Waves play a determinant role in the transport and fate of plastics debris in coastal areas;however, the mechanisms and control factors of onshore and offshore transport remain unclear and require well-designed experiments and numerical models (Critchell & Lambrechts, 2016, Moreira et al., 2016).

- To improve the quality of the plastic debris modelling by studying the following coefficients of the transport modelling framework: the diffusion coefficient (D), the wind drag coefficient (C_D), and the *beaching* parameter. There are published studies that analyse the most appropriate coefficients for other types of substances, such as hydrocarbons. However, there is insufficient knowledge to define appropriate values for plastic debris.

  Taking into account that the diffusion coefficient (D) usually shows higher values in open oceans than in closed or semi-closed areas (estuaries and bays) (Abascal et al., 2017), a potential improvement for the plastic-debris transport modelling would be to study the diffusion coefficient (D) in a spatially variable way for different plastic debris types. Thus, particle transport would be driven by forcings affected by a D coefficient, whose value depends on the position of each particle at each instant.

  Concerning wind drag coefficient (C_D), studies such as Yoon et al. (2010), addressed the relationship between the shape and the buoyancy ratio of floating litter items and the wind effect on the transport at a regional scale. However, not enough information is available to define C_D at an estuarine scale so far. Carrying out laboratory or *in situ* experiments would be important to define the most appropriate C_D values associated with different plastic debris typologies in estuaries.

  Regarding the coastal trapping ability, a parameter known in the literature as *beaching*, new additional in-depth studies are also required. Beaching is one of the key parameters related to modelling the transport of any substance. For certain substances, such as hydrocarbons, there are specific studies that analyse the trapping ability of different coastlines and allow defining these parameters for some oil spill models (TESEO, GNOME, Delft3D-PART, etc.). In the case of plastic debris, there is not enough knowledge about the interaction between different types of debris and different types of coastlines. Therefore, further laboratory or field studies are required

to acquire this knowledge.

- To explore the influence of long-term climatic phenomena (e.g., El Niño, La Niña, or Climate Change) on plastic debris accumulation in estuarine areas by incorporating, in addition to the astronomical component of the tide, the variability and trends of storm surge.

In relation to the methodology developed to identify hotspots of plastic debris in estuaries, a more rigorous validation can be performed by acquiring new field data in:

- The study estuary of this Thesis, the Santoña Bay. Results obtained for the Santoña Bay were compared with field data gathered in October 2017. Results showed an adequate general concordance between both series; however, a dispersion was detected in three of the points located in the innermost areas of the estuary. Further studies using a greater number of sampling areas defined in different seasonal periods could explain this dispersion.
- Other study estuaries with different features. Validating the proposed methodology in estuaries with, for instance, an asymmetric tide at the mouth or where temperature and salinity gradients are the dominant drivers would help ensure its general applicability.

Bibliography

Abascal, A., Castanedo, S., Fernández, V., Medina, R., 2012. Backtracking drifting objects using surface currents from high-frequency (HF) radar technology. Ocean Dynamics 62 (7), 1073–1089.

Abascal, A., Castanedo, S., Gutierrez, A., Comerma, E., Medina, R., Losada, I., 2007. Teseo, an operational system for simulating oil spills trajectories and fate processes. In: The Seventeenth International Offshore and Polar Engineering Conference. International Society of Offshore and Polar Engineers.

Abascal, A., Castanedo, S., Medina, R., Liste, M., 2010. Analysis of the reliability of a statistical oil spill response model. Marine Pollution Bulletin 60 (11), 2099–2110.

Abascal, A., Castanedo, S., Medina, R., Losada, I., Alvarez-Fanjul, E., 2009a. Application of HF radar currents to oil spill modelling. Marine Pollution Bulletin 58 (2), 238–248.

Abascal, A., Castanedo, S., Mendez, F., Medina, R., Losada, I., 2009b. Calibration of a Lagrangian transport model using drifting buoys deployed during the Prestige oil spill. Journal of Coastal Research, 80–90.

Abascal, A., Castanedo, S., Núñez, P., Mellor, A., Clements, A., Pérez, B., Cárdenas, M., Chiri, H., Medina, R., 2017. A high-resolution operational forecast system for oil spill response in Belfast Lough. Marine Pollution Bulletin 114 (1), 302–314.

Acha, E., Mianzan, H., Iribarne, O., Gagliardini, D., Lasta, C., Daleo, P., 2003. The role of the Río de la Plata bottom salinity front in accumulating debris. Marine Pollution Bulletin 46 (2), 197–202.

ASCE, 1996. State-of-the-art review of modeling transport and fate of oil spills. Journal of Hydraulic Engineering 122 (11), 594–609.

Aubrey, D., Friedrichs, C., 1988. Seasonal climatology of tidal non-linearities in a shallow estuary. In: Hydrodynamics and sediment dynamics of tidal inlets. Springer, pp. 103–124.

Aubrey, D., Speer, P., 1985. A study of non-linear tidal propagation in shallow inlet/estuarine systems Part I: Observations. Estuarine, Coastal and Shelf Science 21 (2), 185–205.

Balanda, K., MacGillivray, H., 1988. Kurtosis: a critical review. The American Statistician 42 (2), 111–119.

Ballent, A., Pando, S., Purser, A., Juliano, M., Thomsen, L., 2013. Modelled transport of benthic marine microplastic pollution in the Nazaré Canyon. Biogeosciences 10 (12), 7957–7970.

Ballent, A., Purser, A., de Jesus Mendes, P., Pando, S., Thomsen, L., 2012. Physical transport properties of marine microplastic pollution. Biogeosciences Discussions 9 (12).

Barbier, E., Hacker, S., Kennedy, C., Koch, E., Stier, A., Silliman, B., 2011. The value of estuarine and coastal ecosystem services. Ecological monographs 81 (2), 169–193.

Bárcena, J., Camus, P., García, A., Álvarez, C., 2015. Selecting model scenarios of real hydrodynamic forcings on mesotidal and macrotidal estuaries influenced by river discharges using K-means clustering. Environmental, Modelling & Software 68, 70–82.

Bárcena, J., García-Alba, J., García, A., Álvarez, C., 2016. Analysis of stratification patterns in river-influenced mesotidal and macrotidal

estuaries using 3D hydrodynamic modelling and K-means clustering. Estuarine, Coastal and Shelf Science 181, 1–13.

Barker, C., 2011. A statistical outlook for the Deepwater Horizon oil spill. Geophysical monograph 195, 237–244.

Barker, C., Galt, J., 2000. Analysis of methods used in spill response planning: Trajectory Analysis Planner TAP II. Spill Science & Technology Bulletin 6 (2), 145–152.

Barnes, D., Galgani, F., Thompson, R., Barlaz, M., 2009. Accumulation and fragmentation of plastic debris in global environments. Philosophical Transactions of the Royal Society B: Biological Sciences 364 (1526), 1985–1998.

Blanton, J., Lin, G., Elston, S., 2002. Tidal current asymmetry in shallow estuaries and tidal creeks. Continental Shelf Research 22 (11-13), 1731–1743.

Booij, N., Ris, R., Holthuijsen, L., 1999. A third-generation wave model for coastal regions: 1. Model description and validation. Journal of Geophysical Research: Oceans 104 (C4), 7649–7666.

Boon III, J., Byrne, R., 1981. On basin hyposmetry and the morphodynamic response of coastal inlet systems. Marine Geology 40 (1-2), 27–48.

Brown, J., Davies, A., 2007. Flood/ebb tidal dominance in an estuary: sediment transport and morphology. In: Proceedings of 5th IAHR international symposium on 'river, coastal and estuarine morphodynamics', University of Twente, Enschede, The Netherlands. pp. 17–21.

Browne, M., Crump, P., Niven, S. J., Teuten, E., Tonkin, A., Galloway, T., Thompson, R., 2011. Accumulation of microplastic on shorelines woldwide: sources and sinks. Environmental science & technology 45 (21), 9175–9179.

Browne, M., Galloway, T., Thompson, R., 2010. Spatial patterns of plastic debris along estuarine shorelines. Environmental science & technology 44 (9), 3404–3409.

Bujalesky, G., 1997. Morfodinámica y evolución histórica de la espiga Punta Popper y la boca de mareas del río Grande, Tierra del Fuego. Revista de la Asociación Geológica Argentina 52 (2), 187–201.

Byun, D.-S., Cho, Y.-K., 2006. Double peak-flood current asymmetry in a shallow-water-constituent dominated embayment with a macro-tidal flat. Geophysical Research Letters 33 (16).

Camus, P., Mendez, F., Medina, R., 2011a. A hybrid efficient method to downscale wave climate to coastal areas. Coastal Engineering 58 (9), 851–862.

Camus, P., Mendez, F., Medina, R., Cofiño, A., 2011b. Analysis of clustering and selection algorithms for the study of multivariate wave climate. Coastal Engineering 58 (6), 453–462.

Camus, P., Mendez, F., Medina, R., Cofiño, A., 2011c. Analysis of clustering and selection algorithms for the study of multivariate wave climate. Coastal Engineering 58 (6), 453–462.

Camus, P., Mendez, F., Medina, R., Tomas, A., Izaguirre, C., 2013. High resolution downscaled ocean waves (DOW) reanalysis in coastal areas. Coastal Engineering 72, 56–68.

Carpenter, D., Stone, K., Siren, J., Crystal, T., 1972. Magnetospheric electric fields deduced from drifting whistler paths. Journal of Geophysical Research 77 (16), 2819–2834.

Carson, H., Lamson, M., Nakashima, D., Toloumu, D., Hafner, J., Maximenko, N., McDermid, K., 2013. Tracking the sources and sinks of local marine debris in Hawaii. Marine environmental research 84, 76–83.

Castanedo, S., Medina, R., Losada, I., Vidal, C., Méndez, F., Osorio, A., Juanes, J., Puente, A., 2006. The Prestige oil spill in Cantabria (Bay of Biscay). Part I: operational forecasting system for quick response, risk assessment, and protection of natural resources. Journal of Coastal Research, 1474–1489.

Castanedo, S., Mendez, F. J., Medina, R., Abascal, A., 2007. Long-term tidal level distribution using a wave-by-wave approach. Advances in Water Resources 30 (11), 2271–2282.

Castanedo, S., Nuñez, P., Perez-Diaz, B., Abascal, A., Cardenas, M., Medina, R., 2016. Operational Oceanograhy System for Oil Spill Risk Management at Santander Bay (Spain). In: American Geophysical Union, Ocean Sciences Meeting 2016, abstract# PO14B-2772.

Castanedo, S., Perez-Diaz, B., Abascal, A., Cardenas, M., Olabarrieta, M., Medina, R., Receveur, J., Evrard, E., Guyomarch, J., 2014. A high resolution operational oil spill model at Santander Bay (Spain): implementation and validation. In: International Oil Spill Conference Proceedings. Vol. 2014. American Petroleum Institute, pp. 516–530.

Chan, M., Archer, A., 2003. Extreme depositional environments: Mega end members in geologic time. Vol. 370. Geological Society of America.

Chubarenko, I., Bagaev, A., Zobkov, M., Esiukova, E., 2016. On some physical and dynamical properties of microplastic particles in marine environment. Marine Pollution Bulletin 108 (1-2), 105–112.

Claessens, M., De Meester, S., Van Landuyt, L., De Clerck, K., Janssen, C., 2011. Occurrence and distribution of microplastics in marine sediments along the Belgian coast. Marine Pollution Bulletin 62 (10), 2199–2204.

Costa, M., Silva-Cavalcanti, J., Barbosa, C., Portugal, J., Barletta, M., 2011. Plastics buried in the inter-tidal plain of a tropical estuarine ecosystem. Journal of Coastal Research, 339–343.

Cózar, A., Echevarría, F., González-Gordillo, J., Irigoien, X., Úbeda, B., Hernández-León, S., Palma, A., Navarro, S., García-de Lomas, J., Ruiz, A., et al., 2014. Plastic debris in the open ocean. Proceedings of the National Academy of Sciences 111 (28), 10239–10244.

Critchell, K., Lambrechts, J., 2016. Modelling accumulation of marine plastics in the coastal zone; what are the dominant physical processes? Estuarine, Coastal and Shelf Science 171, 111–122.

Dauvin, J., 2012. Are the eastern and western basins of the English Channel two separate ecosystems? Marine Pollution Bulletin 64 (3), 463–471.

Defant, A., 1961. Physical oceanography. Vol. 1. Pergamon.

Dekiff, J., Remy, D., Klasmeier, J., Fries, E., 2014. Occurrence and spatial distribution of microplastics in sediments from Norderney. Environmental Pollution 186, 248–256.

Derraik, J., 2002. The pollution of the marine environment by plastic debris: a review. Marine Pollution Bulletin 44 (9), 842–852.

Díaz, B., Pavón, A., Gómez-Gesteira, M., 2008. Use of a probabilistic particle tracking model to simulate the Prestige oil spill. Journal of Marine Systems 72 (1-4), 159–166.

Dronkers, J., 1986. Tidal asymmetry and estuarine morphology. Netherlands Journal of Sea Research 20 (2-3), 117–131.

Eerkes-Medrano, D., Thompson, R. C., Aldridge, D. C., 2015. Microplastics in freshwater systems: a review of the emerging threats, identification of knowledge gaps and prioritisation of research needs. Water research 75, 63–82.

Egbert, G., Erofeeva, S., 2002. Efficient inverse modeling of barotropic ocean tides. Journal of Atmospheric and Oceanic Technology 19 (2), 183–204.

Fanshawe, T., Everard, M., 2002. The impacts of marine litter. Marine Pollution Monitoring Management Group, Report of the Marine Litter Task Team (MaLiTT) May.

Faris, J., Hart, K., 1994. Seas of debris: a summary of the third international conference on marine debris. Alaska Fisheries Science Center.

Ferrarin, C., Tomasin, A., Bajo, M., Petrizzo, A., Umgiesser, G., 2015. Tidal changes in a heavily modified coastal wetland. Continental Shelf Research 101, 22–33.

Filella, M., 2015. Questions of size and numbers in environmental research on microplastics: methodological and conceptual aspects. Environmental Chemistry 12 (5), 527–538.

Finotello, A., Canestrelli, A., Carniello, L., Ghinassi, M., D'Alpaos, A., 2019. Tidal flow asymmetry and discharge of lateral tributaries drive the evolution of a microtidal meander in the Venice Lagoon (Italy). Journal of Geophysical Research: Earth Surface 124 (12), 3043–3066.

Fok, L., Cheung, P., Tang, G., Li, W., 2017. Size distribution of stranded small plastic debris on the coast of Guangdong, South China. Environmental Pollution 220, 407–412.

Friedrichs, C., Aubrey, D., 1988. Non-linear tidal distortion in shallow well-mixed estuaries: a synthesis. Estuarine, Coastal and Shelf Science 27 (5), 521–545.

Friedrichs, C., Aubrey, D., 1994. Tidal propagation in strongly convergent channels. Journal of Geophysical Research: Oceans 99 (C2), 3321–3336.

Galgani, F., Hanke, G., Maes, T., 2015. Global distribution, composition and abundance of marine litter. In: Marine anthropogenic litter. Springer, Cham, pp. 29–56.

Galgani, F., Hanke, G., Werner, S., De Vrees, L., 2013. Marine litter within the European marine strategy framework directive. ICES Journal of Marine Science 70 (6), 1055–1064.

Galgani, F., Leaute, J., Moguedet, P., Souplet, A., Verin, Y., Carpentier, A., Goraguer, H., Latrouite, D., Andral, B., Cadiou, Y., et al., 2000. Litter on the sea floor along European coasts. Marine Pollution Bulletin 40 (6), 516–527.

Galgani, F., Souplet, A., Cadiou, Y., 1996. Accumulation of debris on the deep sea floor off the French Mediterranean coast. Marine Ecology Progress Series 142, 225–234.

Gallo, F., Fossi, C., Weber, R., Santillo, D., Sousa, J., Ingram, I., Nadal, A., Romano, D., 2018. Marine litter plastics and microplastics and their toxic chemicals components: the need for urgent preventive measures. Environmental Sciences Europe 30 (1), 13.

Gallo, M., Vinzon, S., 2005. Generation of overtides and compound tides in Amazon estuary. Ocean Dynamics 55 (5-6), 441–448.

Galván, C., Juanes, J., Puente, A., 2010. Ecological classification of European transitional waters in the North-East Atlantic eco-region. Estuarine, coastal and shelf science 87 (3), 442–450.

García, A., Sainz, A., Revilla, J., Álvarez, C., Juanes, J., Puente, A., 2008. Surface water resources assessment in scarcely gauged basins in the north of Spain. Journal of Hydrology 356 (3-4), 312–326.

García Alba, J., García Gómez, A., Tinoco López, R. O., Sámano Celorio, M. L., García Gómez, A., Juanes de la Peña, J. A., et al., 2014. A 3-D model to analyze environmental effects of dredging operations-application to the Port of Marin, Spain.

Guo, L., Wang, Z., Townend, I., He, Q., 2019. Quantification of tidal asymmetry and its nonstationary variations. Journal of Geophysical Research: Oceans 124 (1), 773–787.

Haarr, M., Westerveld, L., Fabres, J., Iversen, K., Busch, K., 2019. A novel GIS-based tool for predicting coastal litter accumulation and optimising coastal cleanup actions. Marine Pollution Bulletin 139, 117–126.

Hall, K., 2000. Impacts of marine debris and oil: economic and social costs to coastal communities. Kommunenes Internasjonale Miljøorganisasjon.

Hardesty, B., Harari, J., Isobe, A., Lebreton, L., Maximenko, N., Potemra, J., van Sebille, E., Vethaak, A., Wilcox, C., 2017. Using numerical model simulations to improve the understanding of micro-plastic distribution and pathways in the marine environment. Frontiers in Marine Science 4, 30.

Hartley, B. L., Thompson, R. C., Pahl, S., 2015. Marine litter education boosts children's understanding and self-reported actions. Marine Pollution Bulletin 90 (1-2), 209–217.

Hastie, T., Tibshirani, R., Friedman, J., 2001. The elements of statistical learning. Vol. 1. Springer series in statistics New York.

Heo, N. W., Hong, S. H., Han, G. M., Hong, S., Lee, J., Song, Y. K., Jang, M., Shim, W. J., 2013. Distribution of small plastic debris in cross-section and high strandline on Heungnam beach, South Korea. Ocean Science Journal 48 (2), 225–233.

Hidalgo-Ruz, V., Gutow, L., Thompson, R., Thiel, M., 2012. Microplastics in the marine environment: a review of the methods used for identification and quantification. Environmental science & technology 46 (6), 3060–3075.

Hinojosa, I., Thiel, M., 2009. Floating marine debris in fjords, gulfs and channels of southern Chile. Marine Pollution Bulletin 58 (3), 341–350.

Hoitink, A., Hoekstra, P., Van Maren, D., 2003. Flow asymmetry associated with astronomical tides: Implications for the residual transport of sediment. Journal of Geophysical Research: Oceans 108 (C10).

Hoitink, A., Hoekstra, P., Van Maren, D., 2006. Comment on "On the role of diurnal tides in contributing to asymmetries in tidal probability distribution functions in areas of predominantly semi-diurnal tide" by PL Woodworth, DL Blackman, DT Pugh and JM Vassie [Estuarine, Coastal and Shelf Science 64 (2005) 235–240]. Estuarine, Coastal and Shelf Science 67 (1-2), 340–341.

Hunter, J., Craig, P., Phillips, H., 1993. On the use of random walk models with spatially variable diffusivity. Journal of Computational Physics 106 (2), 366–376.

Hunter, J., Woodworth, P., Wahl, T., Nicholls, R., 2017. Using global tide gauge data to validate and improve the representation of extreme sea levels in flood impact studies. Global and Planetary Change 156, 34–45.

Hydraulics, W. D., 2018a. Delft3d-FLOW Simulation of multi-dimensional hydrodynamic flows and transport phenomena, including sediments. User Manual, Delft, Holanda.

Hydraulics, W. D., 2018b. Delft3d-PART Simulation of mid-field water quality and oil spills, using particle tracking. User Manual, Delft, Holanda.

Hydraulics, W. D., 2018c. Delft3d-WAVE, Simulation of Short-crested Waves With SWAN. User Manual, Delft, Holanda.

Iglesias, G., Carballo, R., 2010. Effects of high winds on the circulation of the using a mixed open boundary condition: the ría de Muros, Spain. Environmental Modelling & Software 25 (4), 455–466.

Isobe, A., Kako, S., Chang, P.-H., Matsuno, T., 2009. Two-way particle-tracking model for specifying sources of drifting objects: application to the East China Sea Shelf. Journal of Atmospheric and Oceanic Technology 26 (8), 1672–1682.

Isobe, A., Kubo, K., Tamura, Y., Nakashima, E., Fujii, N., 2014. Selective transport of microplastics and mesoplastics by drifting in coastal waters. Marine Pollution Bulletin 89 (1-2), 324–330.

Jambeck, J., Geyer, R., Wilcox, C., Siegler, T., Perryman, M., Andrady, A., Narayan, R., Law, K., 2015. Plastic waste inputs from land into the ocean. Science 347 (6223), 768–771.

Jeon, C.-H., Buijsman, M. C., Wallcraft, A. J., Shriver, J. F., Arbic, B. K., Richman, J. G., Hogan, P. J., 2019. Improving surface tidal accuracy

through two-way nesting in a global ocean model. Ocean Modelling 137, 98–113.

Jiménez, M., Castanedo, S., Zhou, Z., Coco, G., Medina, R., Rodriguez-Iturbe, I., 2014. Scaling properties of tidal networks. Water Resources Research 50 (6), 4585–4602.

Kako, S., Isobe, A., Kataoka, T., Hinata, H., 2014. A decadal prediction of the quantity of plastic marine debris littered on beaches of the East Asian marginal seas. Marine Pollution Bulletin 81 (1), 174–184.

Kako, S., Isobe, A., Magome, S., Hinata, H., Seino, S., Kojima, A., 2011. Establishment of numerical beach-litter hindcast/forecast models: An application to Goto Islands, Japan. Marine Pollution Bulletin 62 (2), 293–302.

Karsten, R., McMillan, J., Lickley, M., Haynes, R., 2008. Assessment of tidal current energy in the Minas Passage, Bay of Fundy. Proceedings of the Institution of Mechanical Engineers, Part A: Journal of Power and Energy 222 (5), 493–507.

Klein, S., Worch, E., Knepper, T., 2015. Occurrence and spatial distribution of microplastics in river shore sediments of the Rhine-Main area in Germany. Environmental science & technology 49 (10), 6070–6076.

Kowalski, N., Reichardt, A., Waniek, J., 2016. Sinking rates of microplastics and potential implications of their alteration by physical, biological, and chemical factors. Marine Pollution Bulletin 109 (1), 310–319.

Kubota, M., 1994. A mechanism for the accumulation of floating marine debris north of Hawaii. Journal of Physical Oceanography 24 (5), 1059–1064.

Law, K., Morét-Ferguson, S., Maximenko, N., Proskurowski, G., Peacock, E., Hafner, J., Reddy, C., 2010. Plastic accumulation in the North Atlantic subtropical gyre. Science 329 (5996), 1185–1188.

Lebreton, L.-M., Greer, S., Borrero, J., 2012. Numerical modelling of floating debris in the world's oceans. Marine Pollution Bulletin 64 (3), 653–661.

Lesser, G., 2009. An approach to medium-term coastal morphological modelling. IHE Delft Institute for Water Education.

Lesser, G., Roelvink, J. v., Van Kester, J., Stelling, G., 2004. Development and validation of a three-dimensional morphological model. Coastal Engineering 51 (8-9), 883–915.

Li, W., Tse, H., Fok, L., 2016. Plastic waste in the marine environment: A review of sources, occurrence and effects. Science of the Total Environment 566, 333–349.

Liebezeit, G., Dubaish, F., 2012. Microplastics in beaches of the East Frisian islands Spiekeroog and Kachelotplate. Bulletin of Environmental Contamination and Toxicology 89 (1), 213–217.

Lima, A., Barletta, M., Costa, M., 2015. Seasonal distribution and interactions between plankton and microplastics in a tropical estuary. Estuarine, Coastal and Shelf Science 165, 213–225.

Liubartseva, S., Coppini, G., Lecci, R., Creti, S., 2016. Regional approach to modeling the transport of floating plastic debris in the Adriatic Sea. Marine Pollution Bulletin 103 (1-2), 115–127.

Lomónaco, P., 1999. Propagación de la onda de marea en estuarios someros. Ph.D. thesis, Universidad de Cantabria.

Maier-Reimer, E., Sündermann, J., 1982. On tracer methods in computational hydrodynamics. In: Engineering applications of computational hydraulics. pp. 198–216.

Mathalon, A., Hill, P., 2014. Microplastic fibers in the intertidal ecosystem surrounding Halifax Harbor, Nova Scotia. Marine Pollution Bulletin 81 (1), 69–79.

Maximenko, N., Hafner, J., Niiler, P., 2012. Pathways of marine debris derived from trajectories of Lagrangian drifters. Marine Pollution Bulletin 65 (1-3), 51–62.

Mazarrasa, I., Puente, A., Núñez, P., García, A., Abascal, A., Juanes, J., 2019. Assessing the risk of marine litter accumulation in estuarine habitats. Marine Pollution Bulletin 144, 117–128.

Méndez, F., Menéndez, M., Luceño, A., Losada, I., 2006. Estimation of the long-term variability of extreme significant wave height using a time-dependent peak over threshold (POT) model. Journal of Geophysical Research: Oceans 111 (C7).

Menendez, M., Tomás, A., Camus, P., Garcia-Diez, M., Fita, L., Fernandez, J., Méndez, F., Losada, I., 2011. A methodology to evaluate regional-scale offshore wind energy resources. In: OCEANS 2011 IEEE-Spain. IEEE, pp. 1–8.

Menéndez, M., Woodworth, P., 2010. Changes in extreme high water levels based on a quasi-global tide-gauge data set. Journal of Geophysical Research: Oceans 115 (C10).

Minguez, R., Abascal, A., Castanedo, S., Medina, R., 2012. Stochastic Lagrangian trajectory model for drifting objects in the ocean. Stochastic environmental research and risk assessment 26 (8), 1081–1093.

Monsen, N., Cloern, J., Lucas, L., Monismith, S., 2002. A comment on the use of flushing time, residence time, and age as transport time scales. Limnology and oceanography 47 (5), 1545–1553.

Moore, C., Lattin, G., Zellers, A., 2011. Quantity and type of plastic debris flowing from two urban rivers to coastal waters and beaches of Southern California. Revista de Gestão Costeira Integrada-Journal of Integrated Coastal Zone Management 11 (1), 65–73.

Moore, R., Wolf, J., Souza, A., Flint, S., 2009. Morphological evolution of the Dee Estuary, Eastern Irish Sea, UK: a tidal asymmetry approach. Geomorphology 103 (4), 588–596.

Moreira, F., Balthazar-Silva, D., Barbosa, L., Turra, A., 2016. Revealing accumulation zones of plastic pellets in sandy beaches. Environmental Pollution 218, 313–321.

Nash, J., Sutcliffe, J., 1970. River flow forecasting through conceptual models part I—A discussion of principles. Journal of Hydrology 10 (3), 282–290.

Navedo, J., Masero, J., Juanes, J., 2007. Updating waterbird population estimates within the East Atlantic Flyway: status and trends of migratory waterbirds in Santoña marshes. Ardeola 54 (2), 237–249.

Navedo, J., Orizaola, G., Masero, J., Overdijk, O., Sánchez-Guzmán, J., 2010. Long-distance travellers stopover for longer: a case study with spoonbills staying in North Iberia. Journal of Ornithology 151 (4), 915–921.

NGA, N. G.-I. A., 2017. Pub. 146, Sailing Directions (Enroute) Newfoundland, Labrador, and Hudson Bay. Springfield, Virginia.

Nidzieko, N., 2010. Tidal asymmetry in estuaries with mixed semidiurnal/diurnal tides. Journal of Geophysical Research: Oceans 115 (C8).

Nidzieko, N., Ralston, D., 2012. Tidal asymmetry and velocity skew over tidal flats and shallow channels within a macrotidal river delta. Journal of Geophysical Research: Oceans 117 (C3).

Núñez, P., Castanedo, S., Medina, R., 2020. A Global Classification of Astronomical Tide Asymmetry and Periodicity Using Statistical and Cluster Analysis. Journal of Geophysical Research: Oceans 125 (8), e2020JC016143.

Oigman-Pszczol, S., Creed, J., 2007. Quantification and classification of marine litter on beaches along Armação dos búzios, Rio de Janeiro, Brazil. Journal of Coastal Research, 421–428.

OSPAR, 2009. Marine litter in the North-East Atlantic Region: Assessment and priorities for response. London, United Kingdom, 127.

OSPAR, 2010. Guideline for monitoring marine litter on the beaches in the OSPAR maritime area. OSPAR Commission: London, UK 84.

Pawlowicz, R., Beardsley, B., Lentz, S., 2002. Classical tidal harmonic analysis including error estimates in MATLAB using T_TIDE. Computers & Geosciences 28 (8), 929–937.

Pereiro, D., Souto, C., Gago, J., 2018. Calibration of a marine floating litter transport model. Journal of Operational Oceanography 11 (2), 125–133.

Porter-Smith, R., Harris, P., Andersen, O., Coleman, R., Greenslade, D., Jenkins, C., 2004. Classification of the Australian continental shelf based on predicted sediment threshold exceedance from tidal currents and swell waves. Marine Geology 211 (1-2), 1–20.

Ranasinghe, R., Pattiaratchi, C., 2000. Tidal inlet velocity asymmetry in diurnal regimes. Continental Shelf Research 20 (17), 2347–2366.

Rech, S., Macaya-Caquilpán, V., Pantoja, J., Rivadeneira, M., Madariaga, D. J., Thiel, M., 2014. Rivers as a source of marine litter. A study from the SE Pacific. Marine Pollution Bulletin 82 (1-2), 66–75.

Roelvink, J., Van Banning, G., 1995. Design and development of DELFT3D and application to coastal morphodynamics. Oceanographic Literature Review 11 (42), 925.

Rubinstein, R. Y., Kroese, D. P., 1981. Simulation and the Monte Carlo method. Vol. 10. John Wiley & Sons.

Sadri, S., Thompson, R., 2014. On the quantity and composition of floating plastic debris entering and leaving the Tamar Estuary, Southwest England. Marine Pollution Bulletin 81 (1), 55–60.

Saha, S., Moorthi, S., Wu, X., Wang, J., Nadiga, S., Tripp, P., Behringer, D., Hou, Y., Chuang, H.-y., Iredell, M., et al., 2011. NCEP climate forecast

system version 2 (CFSv2) 6-hourly products. Research Data Archive at the National Center for Atmospheric Research, Computational and Information Systems Laboratory.

Song, D., Wang, X., Kiss, A., Bao, X., 2011. The contribution to tidal asymmetry by different combinations of tidal constituents. Journal of Geophysical Research: Oceans 116 (C12).

Spearman, C., 1961. The proof and measurement of association between two things.

Speer, P., Aubrey, D., 1985. A study of non-linear tidal propagation in shallow inlet/estuarine systems Part II: Theory. Estuarine, Coastal and Shelf Science 21 (2), 207–224.

Stolte, A., Forster, S., Gerdts, G., Schubert, H., 2015. Microplastic concentrations in beach sediments along the German Baltic coast. Marine Pollution Bulletin 99 (1-2), 216–229.

Thornton, L., Jackson, N., 1998. Spatial and temporal variations in debris accumulation and composition on an estuarine shoreline, Cliffwood Beach, New Jersey, USA. Marine Pollution Bulletin 36 (9), 705–711.

UNEP, 2005. Marine Litter: An Analytical Overview. UNEP.

Van Sebille, E., England, M., Froyland, G., 2012. Origin, dynamics and evolution of ocean garbage patches from observed surface drifters. Environmental Research Letters 7 (4), 044040.

van Utenhove, E., 2019. Modelling the transport and fate of buoyant macroplastics in coastal waters. Ph.D. thesis, Delft University of Technology.

Vermeiren, P., Muñoz, C., Ikejima, K., 2016. Sources and sinks of plastic debris in estuaries: a conceptual model integrating biological, physical and chemical distribution mechanisms. Marine Pollution Bulletin 113 (1-2), 7–16.

Viehman, S., Vander P, J. L., Schellinger, J., 2011. Characterization of marine debris in North Carolina salt marshes. Marine Pollution Bulletin 62 (12), 2771–2779.

Viikmäe, B., Torsvik, T., Soomere, T., 2013. Impact of horizontal eddy diffusivity on Lagrangian statistics for coastal pollution from a major marine fairway. Ocean Dynamics 63 (5), 589–597.

Wahl, T., Haigh, I., Nicholls, R., Arns, A., Dangendorf, S., Hinkel, J., Slangen, A., 2017. Understanding extreme sea levels for broad-scale coastal impact and adaptation analysis. Nature communications 8 (1), 1–12.

Westfall, P., 2014. Kurtosis as peakedness, 1905–2014. rip. The American Statistician 68 (3), 191–195.

Willmott, C., 1981. On the validation of models. Physical Geography 2 (2), 184–194.

Woodworth, P., Blackman, D., Pugh, D., Vassie, J., 2005. On the role of diurnal tides in contributing to asymmetries in tidal probability distribution functions in areas of predominantly semi-diurnal tide. Estuarine, Coastal and Shelf Science 64 (2-3), 235–240.

Woodworth, P., Hunter, J., Marcos, M., Caldwell, P., Menéndez, M., Haigh, I., 2017. Towards a global higher-frequency sea level dataset. Geoscience Data Journal 3 (2), 50–59.

Yonkos, L., Friedel, E., Perez-Reyes, A., Ghosal, S., Arthur, C., 2014. Microplastics in four estuarine rivers in the Chesapeake Bay, USA. Environmental science & technology 48 (24), 14195–14202.

Yoo, C.-I., Yoon, H.-S., Kim, G.-T., 2007. The behavior of floating debris in the Nakdong River Estuary using a simple numerical particle model. Journal of the Korean Society of Marine Environment & Safety 13 (4), 9–14.

Yoon, J.-H., Kawano, S., Igawa, S., 2010. Modeling of marine litter drift and beaching in the Japan Sea. Marine Pollution Bulletin 60 (3), 448–463.

Zambianchi, E., Iermano, I., Suaria, G., Aliani, S., 2014. Marine litter in the Mediterranean Sea: an oceanographic perspective. In: CIESM Workshop Monograph 46: Marine litter in the Mediterranean and Black Seas. CIESM Publisher Monaco, pp. 31–41.

Zambianchi, E., Trani, M., Falco, P., 2017. Lagrangian transport of marine litter in the Mediterranean Sea. Frontiers in Environmental Science 5, 5.

Zhang, H., 2017. Transport of microplastics in coastal seas. Estuarine, Coastal and Shelf Science 199, 74–86.

Zhou, Z., Coco, G., Townend, I., Gong, Z., Wang, Z., Zhang, C., 2018. On the stability relationships between tidal asymmetry and morphologies of tidal basins and estuaries. Earth Surface Processes and Landforms 43 (9), 1943–1959.

Zhou, Z., Olabarrieta, M., Stefanon, L., D'Alpaos, A., Carniello, L., Coco, G., 2014. A comparative study of physical and numerical modeling of tidal network ontogeny. Journal of Geophysical Research: Earth Surface 119 (4), 892–912.